UCLouvain

UNIVERSITÉ CATHOLIQUE DE LOUVAIN
INSTITUTE OF NEUROSCIENCE
INSTITUTE OF INFORMATION AND COMMUNICATION TECHNOLOGIES, ELECTRONICS AND APPLIED MATHEMATICS

# Fingerpad mechanics and grip force adaptation to friction during object manipulation

Félicien Schiltz

Ph.D. dissertation submitted in line with the requirements for the degree of
*Docteur en sciences de l'ingénieur*

Dissertation committee:

Prof. Jean-Louis Thonnard (UCL, advisor)
Prof. Philippe Lefèvre (UCL, advisor)
Dr. Benoit Delhaye (UCLouvain)
Prof. Frédéric Crevecoeur (UCLouvain)
Prof. Thomas Pardoen (UCLouvain)
Prof. Stephen Redmond (University College Dublin)
Prof. Ilana Nisky (Ben-Gurion University of the Negev)
Prof. Pierre-Antoine Absil (UCLouvain, chairman)

March 2022

# Remerciements

Au moment d'écrire ces lignes, je me rends compte cela fait presque 4 ans et demi que j'ai commencé cette thèse. En 4 ans et demi, on peut dire que j'ai eu le temps de vivre bien des émotions. Je suis passé par l'euphorie lors de la publication de mes articles, la joie lors des conférences au Japon, en Californie ou en Italie, mais aussi la frustration lorsque je me battais avec mes données ou le doute lorsque la tâche me paraissait insurmontable. Au final, les émotions vont et viennent avec le temps et ce que j'emporte avec moi, c'est la fierté d'avoir bravé les moments difficiles, d'avoir apporté une contribution à la science et d'être arrivé au bout de cette épreuve, sans aucun doute la plus difficile de ma vie. J'ai un jour entendu une citation qui disait que pour s'améliorer, il faut sortir de sa zone de confort. Eh bien, je pense avoir vécu cette citation lors de ces 4 dernières années et demi, car je n'ai pas passé beaucoup de temps dans ma zone de confort et j'ai l'impression de ne plus être la même personne. Durant cette thèse, j'ai appris à analyser des données, lire des articles scientifiques, synthétiser pour répondre à des questions de recherche, présenter des résultats de manière claire et bien trop d'autres choses pour toutes les citer ici. Si je suis arrivé au bout, je sais que c'est aussi grâce à toutes les personnes qui m'entourent et m'ont soutenu lors de ce projet, c'est pourquoi j'aimerais prendre le temps de les remercier ici.

Philippe et Jean-Louis, merci de m'avoir fait confiance et de m'avoir offert cette superbe opportunité. Merci à tous les deux pour votre encadrement et votre implication dans tous mes projets, qui ont tout simplement été impeccables. Tous les doctorants n'ont pas des réunions (presque) hebdomadaires comme ce fut le cas pour moi. Philippe, merci pour ta disponibilité et tes conseils toujours plus que pertinents. Je me souviendrai toujours que tu as une fois consacré une après-midi à m'aider à analyser des données afin de préparer une présentation que j'avais à faire lors de ma première conférence. Jean-Louis, merci pour ta vision très « straight to the

point », qui nous a souvent permis de gagner du temps sur bien des projets, ainsi que ton attitude « work hard, party hard », que j'espère imiter dans la suite de ma vie. Je te remercie pour cela, puisque ça m'a permis de passer plein de bons moments pendant ma thèse (karaokés à Tokyo, restaurants à Kyoto, en Allemagne, verres du vendredi au Ad Hoc et j'en passe).

Benoît, je ne saurai jamais assez te remercier pour les heures que tu as consacrées à m'aider. Grâce à ton expertise, j'ai appris énormément. Je sais que sans ta présence, la qualité de cette thèse serait bien moins bonne que ce qu'elle est maintenant, si elle avait seulement vu le jour. Y a-t-il un seul graphe (hors introduction et conclusion) que nous n'avons pas passé plusieurs heures à discuter ? Un seul paragraphe auquel tu n'as pas participé, au minimum par tes relectures ? Pour tout cela, je te suis énormément reconnaissant.

Allan, je te remercie aussi pour l'excellente formation et les conseils dont j'ai pu bénéficier à tes côtés lors des premiers mois de cette thèse. Lorsque je suis arrivé, j'ai eu droit à ActiveTouch, un device unique au monde avec lequel je pouvais obtenir de magnifiques données. J'ai eu droit à un code clair et des exemples de comment l'utiliser pour analyser des données, des formations sur la littérature scientifique que je devais connaitre pour m'attaquer à cette thèse, des discussions très enrichissantes avec toi, et bien d'autres choses encore. En tout, j'ai eu droit à une véritable formation qui m'a permis de comprendre comment aborder la tâche monumentale qu'est une thèse dans ce domaine. Merci pour tout, je n'aurais pu rêver d'un meilleur accueil.

Je tiens à remercier également les membres de mon comité d'encadrement et de mon jury, Fred, Thomas, Ilana, Stephen et Pierre-Antoine. Les discussions que nous avons eues ont été très intéressantes et constructives et la qualité de ce document s'en est considérablement améliorée.

Merci également à Antoine et Laurent, qui avez été à mes côtés pendant l'intégralité de ma thèse et avez partagé avec moi certains des meilleurs moments (notre voyage de 10 jours en Californie est pour moi un excellent souvenir). Merci pour les conseils lorsque j'avais besoin d'un regard extérieur sur mes données et merci pour les blagues du vendredi, les soirées (parfois passées à bosser), etc. Je vous souhaite le meilleur dans vos carrières respectives et je suis sûr que nous garderons le contact par la suite.

Merci aussi à tous les membres de l'équipe de recherche, ceux qui sont partis et ceux qui restent : Ghady, Anne, David C., David G., Nicolas, Florence, Irene, Florence, Donatien, Omer, Benjamin, Clémence, James, Hari, Lise et Simon. J'ai toujours apprécié l'ambiance presque familiale qui régnait dans l'équipe, sans aucun doute grâce aux gens qui la composaient.

Merci également à toutes les personnes qui m'ont aidé pour le côté technique, les « vrais » ingénieurs. François, Julien, Cécile, Benoît H., Massimo, Thierry, CATL et Arsalis. Votre aide m'a été très précieuse et c'était toujours avec bonne humeur et intérêt que vous me donniez les coups de main dont j'avais besoin.

Même si vous n'étiez pas directement impliqués dans mes recherches, je remercie aussi mes amis pour votre soutien moral et les bons moments passés ensemble durant toutes ces années. Entre l'équipe de city-trips européens, les gros du Queyras, la team « vacances Sud-Ouest », les ASBO, les anciens du CI, les habitants du manoir et les rôlistes de D&D, j'ai été plus que bien entouré pendant ces années, ce qui a contribué à m'améliorer mentalement et à traverser ces années de thèse plus facilement. Je remercie en particulier ceux qui se sont portés volontaires pour venir à Woluwé participer à mes expériences à la fin de la première vague du Covid, me permettant de récolter des données cruciales pour cette thèse.

Merci à mes parents, qui avez toujours été à mon écoute. Vos conseils, vos encouragements et votre confiance en moi m'ont toujours été très chers et ce depuis que je suis né. Merci Irène d'avoir toujours été à l'écoute, merci Adam et Mélusine, les frangins, chaque moment passé avec vous est toujours excellent. Merci aussi à tous mes grands-parents, qui êtes tous des exemples pour moi, merci aux oncles, tantes, cousins et à la famille au sens large.

Pour terminer, merci Céline. Tu es avec moi depuis maintenant plus de 9 ans. Tu m'as toujours soutenu dans les moments difficiles. Merci pour tout. Je sais qu'en ta compagnie, ces prochaines années seront aussi exceptionnelles que les 9 qui se sont écoulées.

# Contents

CHAPTER 1

# Introduction and background

*"It's a magical world, Hobbes, ol' buddy… Let's go exploring!"*

*Calvin & Hobbes – Bill Watterson*

Object manipulation in everyday life is omnipresent. From the child playing with its toys to the surgeon holding its scalpel, dexterous manipulation of objects is a skill that humans learn to master from a very young age and end up performing in a way that is very precise and more versatile than any robot or animal. This skill relies on collecting information on the state of the manipulated object using our senses, with touch being of first importance. Using this information, the central nervous system sends commands to our muscles to perform movements that take into account how slippery an object is, its shape, the characteristics of the desired movement and more. This entire procedure, although very complex, is usually performed without even being consciously planned by the human performing it. In the first chapter of this thesis, we will give context for how touch and motor control work together. First, we will describe the anatomy of the fingers and the skin. Then, we will present the mechanoreceptors located in the skin, muscles and joints, how they work and the information that they provide. After, we will give the mechanical properties of the skin and explore its tribology. Next, we will explore the way touch is used during object manipulation and its relationship with friction. Finally, we will present this thesis' content and what it brings to our knowledge of touch and to the processes involved in object manipulation.

## 1.1. Finger and skin structure

The fingers are used for most object manipulation that humans perform in everyday life, from simple ones such as pushing a door to complex ones such as knitting or tying a knot. They are indispensable in everyday life to sense the world through touch and also to manipulate objects. In this section, we will first review the finger structure, with a particular emphasis on the skin, since it is the interface between the outside world and the human body, hence essential for the sense of touch.

### 1.1.1. General anatomy of the fingers

Humans usually have ten fingers, five per hand. The index, middle, ring, and little fingers are divided into three phalanges (distal, intermediate, and proximal phalanges), while the thumb only has two (distal and proximal). The opposability of the thumb with respect to the other fingers allows humans to exert great forces when holding objects and great dexterity when manipulating them.

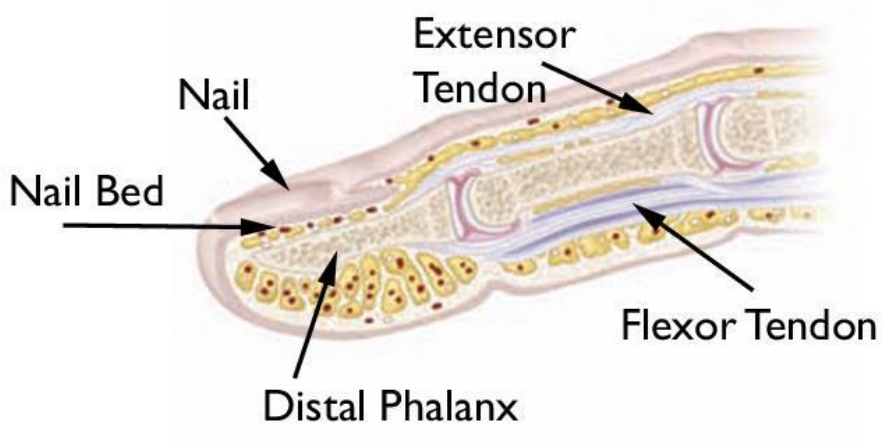


**Fig. 1.1. Anatomy of the finger.** Longitudinal cut with the bones, tendons, skin, and articulations visible. Adapted from (Sarwak, 2010).

The bones are positioned close to the central axis of the fingers and support their general structure. They are linked by joints around which angular movements of the phalanges can be performed. The extensor and flexor tendons are connected to the bones and are pulled upon by muscles in the hands and arms to produce those movements. The bones are surrounded by skin, whose roles include protection of the interior of the

body from external threats and sensing the world via touch. The skin's complex structure will be presented in more detail in the next section. Finally, nails are located at the end of the dorsal side of the fingers. They are made of a plate of hard keratin that continuously grows from the nail bed. They are present in most primates and have evolved from the claws of earlier animals. Among other functions, they protect the distal phalanges from injuries.

### 1.1.2. Anatomy of the skin[1]

The skin is often considered as our largest organ, weighing 5-6kg and thus representing approximately 6% of our body weight (Goldsmith, 1990). It has a surface area of 2 square meters and a thickness that varies from 0.5mm on the eyelids to 4mm on the heels of the feet. It is our interface with the external world and it serves several purposes. First, it constitutes a barrier that protects our internal organs from external threats, such as mechanical shocks, harmful bacteria, UV radiation from the sun (Dale Wilson et al., 2012), etc. More importantly in the context of this thesis, it also serves as an important mean to sense the external world, as it is essential to our sense of touch, pain, temperature, etc. Other functions of the skin include thermoregulation (Romanovsky, 2014) and metabolic functions such as the production of vitamin D.

In humans, the skin can be separated into two categories. The glabrous skin is present on the palmar side of the hands and feet, lips, and part of the sexual organs. The hairy skin is present on most of the rest of the body. In general, glabrous skin is thicker, more resistant, and also a lot more sensitive to mechanical deformations and pain than hairy skin (Mancini et al., 2014). The glabrous skin of the hands is usually the one in contact with objects during manipulation and contains four types of tactile afferent neurons (see *1.2 Perceiving the world via touch)*.

The skin is divided into three layers. In the interior, the **hypodermis** (yellow part in Fig 1.2) is mainly composed of fatty tissues that connect the skin to the underlying bones and muscles. The **dermis** (green part in Fig 1.2) merges with the hypodermis in the inner portion of the skin. It contains nerves, blood vessels, sweat glands, and most tactile afferents. It provides the skin with support and elasticity through the proteins collagen and elastin. It also protects from pathogenic microbes and toxic substances through

[1] The content of this section is based on (Hertenstein and Weiss, 2011; Peckham et al., 2017; Gould, 2018)

different specialized cells used by the immune system (mast cells, T cells, dendritic cells, and macrophages). More information on the role of the skin in the immune system can be found in (Quaresma, 2019) but are out of the scope of this thesis. The dermis also contains sweat glands, which are linked to the surface of the skin through sweat ducts.

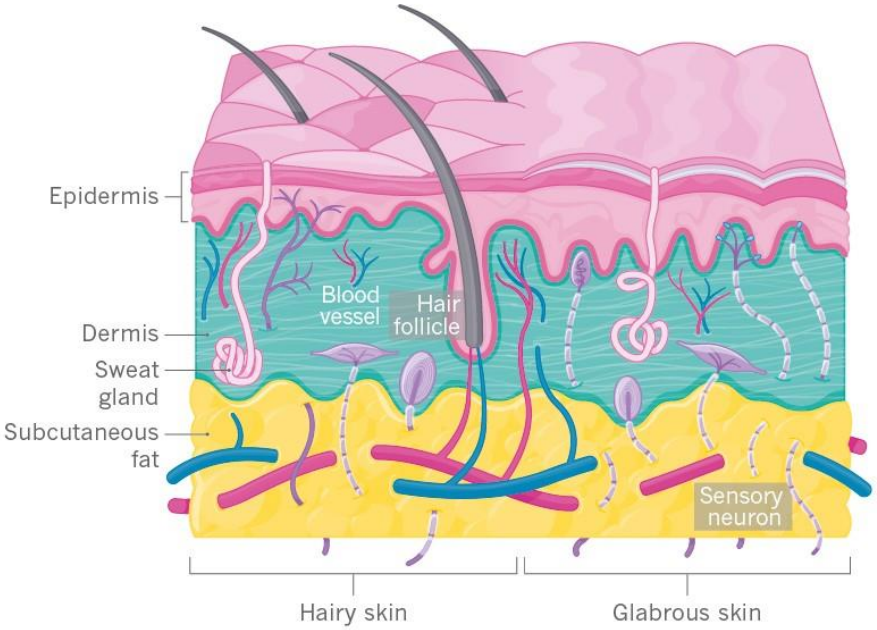


**Fig. 1.2. Structure of the hairy and glabrous skin.** The skin is divided into three layers, first the hypodermis in the interior, mainly composed of fat, then the dermis in the middle, and finally the epidermis in the exterior. Adapted from (Gould, 2018).

The **epidermis** (pink part in Fig 1.2), which is the outer part in contact with objects during manipulation is itself composed of different parts. At the most inner part of the epidermis, marking the frontier with the dermis is the stratum basale (see Fig 1.3 for a more detailed view of the structure of the epidermis). It is a layer of continuously dividing cells that travel through the epidermis towards the exterior of the skin. This layer also contains melanocytes, which create melanin, a pigment responsible for our skin color. It also contains Merkel cells, associated with SA1 afferent fibers (see *1.2 Perceiving the world via touch).* The time required by a basal cell to go from the stratum basale to the top of the epidermis is approximately a month. The next layer is the stratum spinosum, or squamous cell layer, which contains the keratinocytes. The latter produce the keratin, a tough and protective

protein that makes up the majority of the structure of the skin, hair and nails. The mature basal cells travel through this layer to reach the stratum granulosum, also called the granule cell layer. There, they lose their nuclei and become more keratinized, making this layer waterproof. In the glabrous skin, a thin additional layer is then found, called the stratum lucidum (next-to-last layer, in grey in Fig 1.2). During their travel through the stratum lucidum and stratum granulosum, the cells get flatter, and adhere together as they get dehydrated and eventually die. This process results in layers of tough, durable material, which continues to migrate up the surface of the skin to the stratum corneum, where they finally detach from the rest of the skin when they get too fragile.

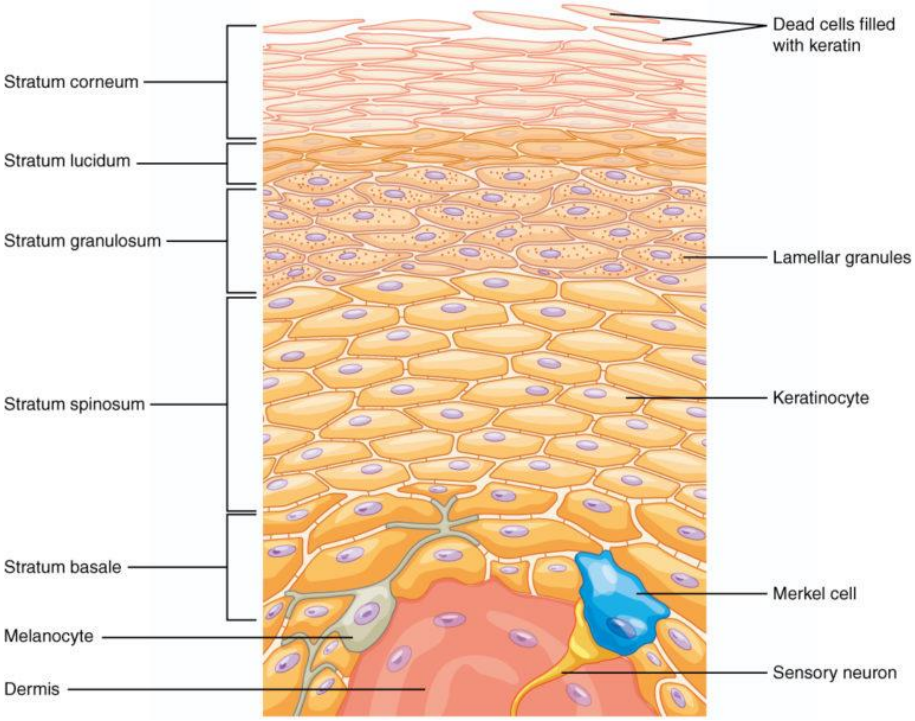


**Fig. 1.3. Structure of epidermis of the glabrous skin.** The skin cells continuously divide in the stratum basale and travel toward the exterior of the epidermis. Adapted from (Betts et al., 2013).

In the fingertip skin and the glabrous skin in general, the skin is arranged in ridges and valleys forming what we call the fingerprints. The periodicity of the ridges was measured at 458±71µm and the depth of the valleys relative to the top of the ridges at 102±26µm (Cornuault et al., 2015) (see Fig 1.4). Sweat pores are found at the top of the ridges. They are the termination of

the sweat ducts, which carry the moisture content from the sweat glands. The patterns formed by the fingerprint ridges are unique across all individuals, even between identical twins. This is because the pressure of the amniotic fluid across the surface of the hands and the growth rate of fingers both influence the patterns of the fingerprints.

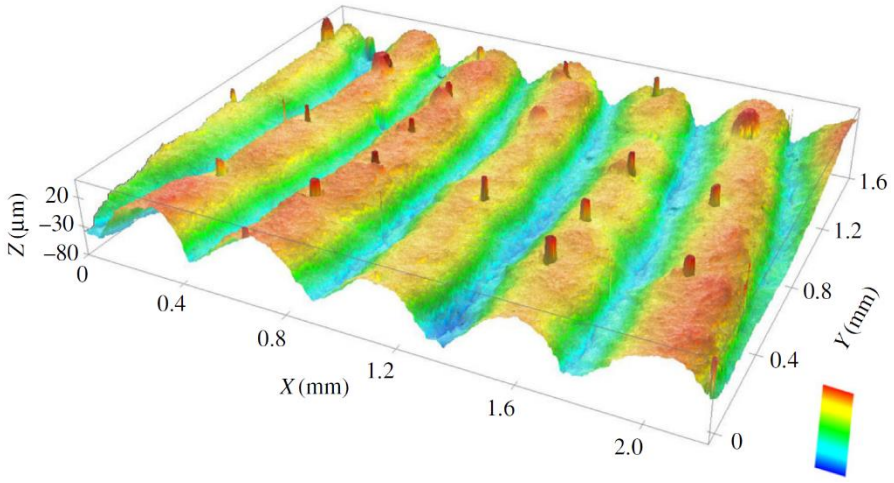


**Fig. 1.4. Three-dimensional rendering of the fingerprint geometry.** A silicone elastomer was used to obtain a negative replica of the fingerprint geometry. Surface texture imaging was carried out using a three-dimensional optical profiler. The curvature of the fingerpad has been removed. Adapted from (Dzidek et al., 2017).

## 1.2. Perceiving the world via touch[2]

Our sense of touch is of the uttermost importance when perceiving the world. Right now, without even having to think about it, you might be feeling the floor under your feet, a light breeze coming from an open door, or the pages of this thesis as you hold it in your hands. All this information comes from receptors located in your skin and connected to your nervous system. It is conducted to your brain and used to make conscious and unconscious decisions, such as closing the door or changing the position of your legs. What we usually call "touch" can include the perception of different kinds of stimuli by the body, all grouped under the umbrella of somatosensation (perception of sensory stimuli over the whole body). Those can include thermoreception (feeling of temperature), proprioception (position of the body), nociception (pain), and touch in the mechanoreceptive sense. The

[2] The content of this section is based on (Hertenstein and Weiss, 2011; Delhaye et al., 2018; Tuthill and Azim, 2018; Handler and Ginty, 2021)

following sections focus on the glabrous skin, as it is the one involved in object manipulation and thus the most relevant in the context of this thesis.

Mechanoreception relies on a myriad of sensory organs located in the dermis and epidermis of the skin, called mechanoreceptors. Those that mediate innocuous touch are called “low-threshold mechanoreceptors” (LTMRs), while those that mediate pain are called “high-threshold mechanoreceptors” (HTMRs).

LTMRs are very sensitive and can detect forces as low as 0.5mN (Johansson et al., 1980). They convert mechanical deformations of the skin into neural signals - also called spikes or action potentials - which are conducted by nerve fibers - also called afferents - which innervate the mechanoreceptors and conduct the signals to the central nervous system. These afferents can be classified according to their preferred mechanical stimulus type or their response to a static indentation of the skin. There are four main types of afferents dedicated to mechanical touch: (i) fast adapting afferents of type I, (ii) slow adapting afferents of type I, (iii) fast adapting afferents of type II and finally (iv) slow afferents of type II. The fibers of those afferents are Aβ fibers, that conduct signals at a speed of 30-75m/s (Gasser, 1941).

In this section, we will first present the four types of cutaneous mechanoreceptive afferents. We will then briefly give an overview of proprioception in section 1.2.2. and nociception in section 1.2.3.

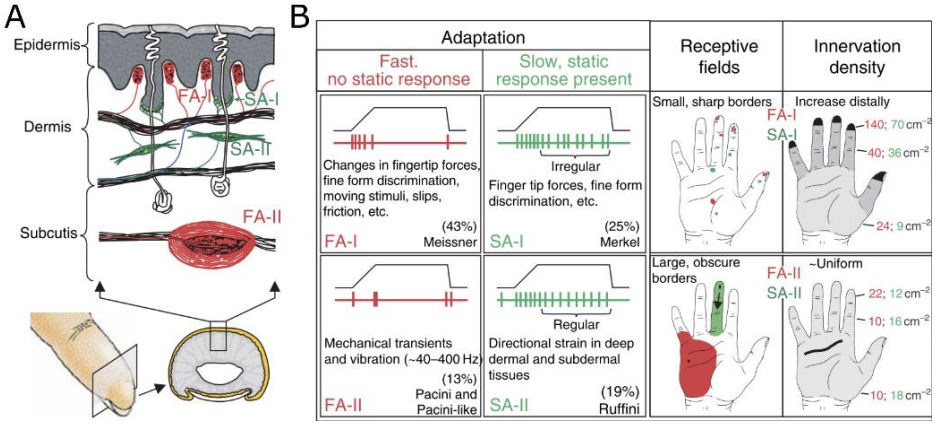


**Fig. 1.5. Types of tactile mechanoreceptive sensors in the glabrous skin of the human hand.** A| Location of the mechanoreceptors in the skin and their shape. B| Characteristics of the mechanoreceptive afferents. Adapted from (Johansson and Flanagan, 2008).

### 1.2.1. Mechanoreceptive afferents

*FA-I and Meissner corpuscles*

The type 1 fast adapting afferents - also called FA-I or RA-I - are characterized by bursts of action potential during the onset and offset of touch stimuli (Knibestöl, 1973) and have small and sharp receptive fields (see Fig 1.4 B). When a single FA-I is excited using intraneural microstimulation[3], participants report the sensation of a point of tingling vibration (O'Neill et al., 2019). The mechanoreceptors associated with FA-I are called Meissner corpuscles and are found in dermal papillae, which are extensions of the dermis into the epidermis. This makes them very close to the contact between the skin and objects and allows for very high sensitivity. The proximity to the exterior of the skin is also the cause for the small receptive fields.

There are about 140 FA-I per cm² in the fingertips, which is more than for any other mechanoreceptor. The receptive field of a single Meissner corpuscle is about the dimension of a skin ridge (about 0.4mm) and a single FA-I afferent is branched to several Meissner corpuscles, resulting in a

[3] Intraneural microstimulation, or INMS, is a technique in which the experimenter uses a thin metal needle to excite neurons and to generate sensations at individual afferents (Torebjörk and Ochoa, 1980). This technique is based on microneurography, a process in which the activity of individual afferents is recorded using a thin metal needle (Vallbo and Hagbarth, 1968).

receptive field composed of distinct subfields across multiple ridges (Fig 1.5). It is possible, although not yet demonstrated, that spatial details at the scale of a single fingerprint ridge are resolved at the population level. Although all afferents are sensitive to slip events, FA-I are particularly sensitive to the compressive skin strains associated with those slips (Delhaye et al., 2021a). The sensitivity to changes in dynamic forces of FA-I afferents and their very high number in the glabrous skin imply an important role in the control of grip force during object manipulation (Macefield et al., 1996; Johnson, 2001).

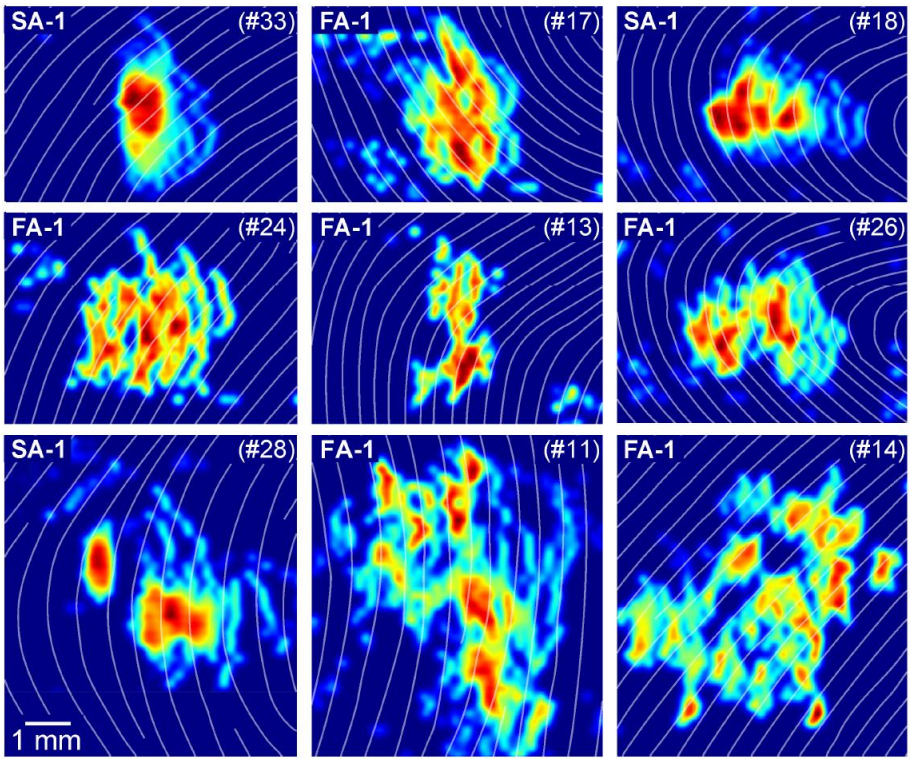


**Fig. 1.6. Receptive fields of FA-I and SA-I single afferents.** Examples of receptive sensitivity maps of neurons obtained by scans of a small probe at 30 mm/s. The white lines indicate the grooves between papillary ridges. Adapted from (Jarocka et al., 2021).

*SA-I and Merkel cells*

The type 1 slowly adapting afferents or SA-I make use of Merkel cells and are also located in the dermis, at the frontier with the epidermis, but not in the papillary dermal papillae. They are thus a little bit further from the surface of the skin than the Meissner corpuscles while remaining closer than the other afferent types (Fig 1.4 A). They are sensitive to static indentations

and present an irregular firing rate that decreases over time (Knibestöl, 1975). When a single SA-I is activated using INMS, participants report sensing a single point of positive or negative pressure (O'Neill et al., 2019). As for FA-I, afferent Aβ fibers split into multiple branches and connect to multiple Merkel cells, resulting in heterogeneous and disjointed but small and sharp receptive fields (Fig 1.5). There are 70 SA-I per cm² in the fingertips, making them the second most represented afferents. At the population level, they convey a neural image of spatially patterned skin indentations, with a spatial resolution of about 1mm at the fingertip (Phillips and Johnson, 1981).

*FA-II and Pacinian corpuscles*

The type 2 fast adapting afferents -also called FA-II or PC – use Pacinian corpuscles and other cells of the same class that are located deep in the dermis (Fig 1.4 A). They are thought to innervate a single Pacinian corpuscle. However, those are deeper in the skin than Merkel cells and Meissner Corpuscles, resulting in larger and more diffuse receptive fields. There is also a smaller number of them, with approximately 22 per cm² in the fingertips. They are activated at the onset and offset of skin indentations (Bell et al., 1994) and during high-frequency vibrations with amplitudes as small as 10nm (Brisben et al., 1999). They are thought to be responsible for the detection and perception of distant events using vibrations transmitted through objects, probes, and tools held in the hand (Johnson et al., 2000). When activated using INMS, participants report sensing vibrations that are not located at a single point, but over a larger area instead (O'Neill et al., 2019).

*SA-II and Ruffini corpuscles*

The type 2 slowly adapting afferents, also called SA-II, are assumed to terminate in Ruffini corpuscles (Fig 1.4 A). They are the least numerous in the fingertips, with approximately 12/cm². They react to skin indentation with a regular spike train preceded by a period of adaptation (Fig 1.4 B) (Harrington and Merzenich, 1970). They are the only LTMR to be often observed firing in the absence of a stimulus (Chambers et al., 1972). As for FA-II, they have large and diffuse receptive fields. They are six times less sensitive to skin indentation than SA-I but are more sensitive to skin stretch (Edin, 1992). They have been observed to be directionally sensitive, sending the most spikes when the skin was stretched in one direction and being silenced when it was stretched at a 90° angle relative to that direction, suggesting a role in the perception of hand and finger orientation (Johnson, 2001; Fleming and Luo, 2013). As mentioned earlier, their termination in Ruffini corpuscles is only

hypothesized. A study has suggested that it was the case with cats (Chambers et al., 1972), but studies have failed to show similar findings with humans (Handler and Ginty, 2021). Moreover, anatomical studies have been unable to confirm that SA-II afferents end in Ruffini corpuscles (Paré et al., 2003). SA-II do not produce a clear and identifiable sensation when excited using INMS (O'Neill et al., 2019).

### 1.2.2. Proprioception

Proprioception is the sense of self-movement and body position (Tuthill and Azim, 2018). Along with mechanoreception, it has an important role in dexterous object manipulation. It is mediated via mechanosensory neurons located within muscles, tendons, and joints. Those neurons and their functions are briefly described in this section.

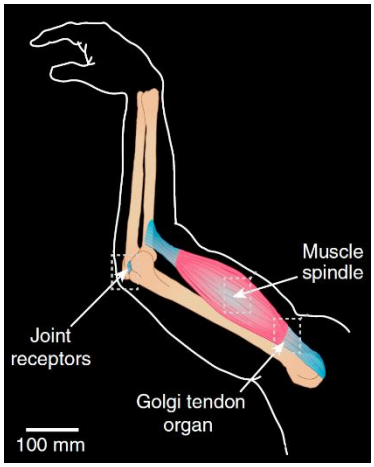


**Fig. 1.7. Location of proprioceptive organs in a human limb.** Adapted from (Tuthill and Azim, 2018).

**Muscle spindles** are located deep inside the muscles (see Fig 1.6). They are capsules of connective tissues that contain specialized intrafusal muscle fibers positioned in parallel with the muscles. Some afferents spiral around the central portion of those intrafusal muscle fibers and respond to muscle stretch. They are known as "Group Ia afferents" and encode a muscle's length and its rate of change. Other afferents are located at the edge of the spindle. They are known as "Group II afferents" and they encode only muscle length.

**Golgi tendon organs** are located at the interface between the muscles and tendons (see Fig 1.6). Each contains the sensory endings of a single

mechanosensory neuron wrapped around strands of collagen which are attached to individual muscle fibers. The corresponding afferents are known as “Group Ib afferents”. They encode muscle tension, as their firing frequency increases with in parallel with it and as they are silent at rest.

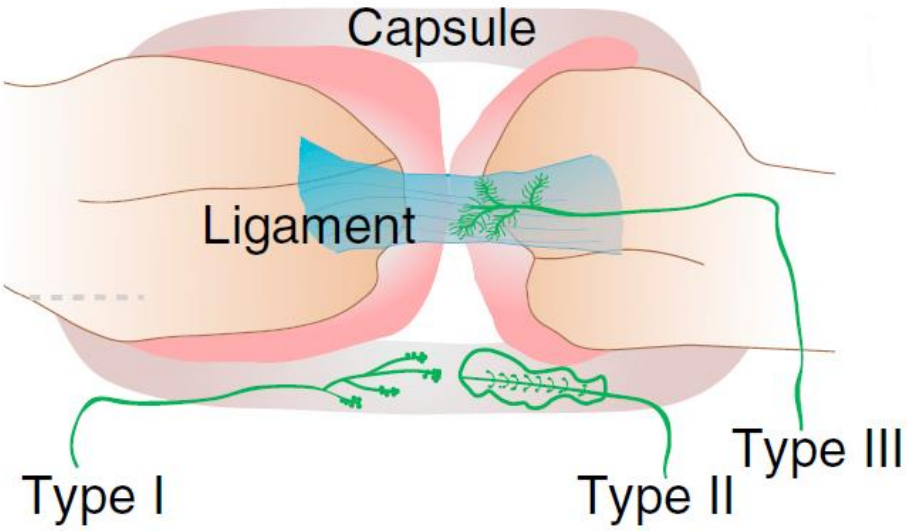


**Fig. 1.8. Schematic of receptor types in the joint capsule that convey proprioceptive information.** Adapted from (Tuthill and Azim, 2018).

**Joint receptors** are located inside the joint capsule, a fibrous membrane that envelops the joints (see Fig 1.6 and Fig 1.7). They consist of sensory neurons typically associated with the mechanoreceptors of the tactile system (see sections 1.2.1 to 1.2.4). Type I are slowly-adapting receptors in the outer layer of the fibrous joint capsule, type II are rapidly-adapting receptors in the deeper layers of the joint capsule and type III are slowly-adapting receptors embedded in the ligaments and terminal regions of the tendons. These receptors' responses have been experimentally shown to peak when the joint angle reaches its minimum and maximum values (Burke et al., 1988). Thus, they are thought to have the role of limit detector or to signal potential joint damage.

Altogether, the receptors of proprioception provide information about limb position and velocity, muscle tension, and the angle rate of change of the angle of the joints. Thus, proprioception plays an important role in

stability, locomotion movement planning and execution, as well as dexterous manipulation.

### 1.2.3. Nociception

In the skin are also located afferents known as nociceptors, which are sensitive to high-intensity stimulation of several energy forms (mechanical, thermal, chemical, etc.). As they have little to no role at all in the context of this thesis, the interested reader is invited to consult good references on the subject, such as (Yam et al., 2018).

## 1.3. Tribology and mechanical properties of the fingerpad skin

When grasping and manipulating objects, the skin deforms at and around the contact interface. Those deformations play important roles. First they allow a more secure grip of the object being manipulated by conforming the skin to the contact surface. Second they are the source of the activation of the mechanoreceptors, which give humans information about the object being manipulated and the state of the contact interface. The volar side of the fingers' distal phalanges is of particular importance, as it is the most sensitive part of the hand which is in contact with held objects during fine manipulation. The following sections will thus focus on the description of their mechanical properties.

### 1.3.1. Mechanical properties of the fingerpad

The mechanical properties of the fingerpad are complex, as it consists of a bone, a nail, and different layers of skins, which themselves have their own mechanical properties, and are arranged in a specific geometry. Moreover, the mechanical properties of those elements as well as their geometry vary from one person to another. Several general parameters about the mechanics are known and will be briefly described here.

An important parameter to describe the mechanical properties of a material is the **Young's modulus** or elastic modulus. It quantifies the relationship between the tensile, compressive, or shearing stress σ and the strain ε of elastic materials. It is determined using the formula below:

$$E = \frac{\sigma}{\varepsilon}$$

Intuitively, it is a constant that measures how much force a material requires to be deformed by a corresponding amount. It is only valid in the

range of forces in which the material is elastic, as too much force will permanently deform the material. The fingerpad skin is not a perfectly elastic material even at low normal forces, as it presents elements of viscoelasticity and other non-linearities. Approximations of the Young's modulus of the fingerpad as measured in vivo by stretching and shearing the skin can be found in Fig 1.6. As shown, it varies a lot according to the person, but also if measured along or across the ridges.

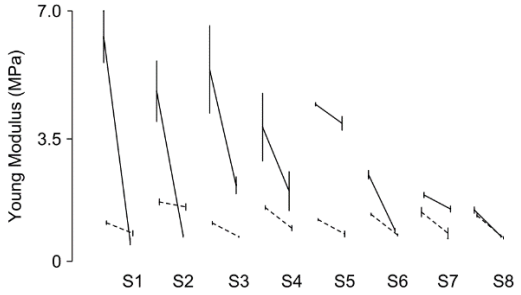


**Fig. 1.9. Young's moduli of eight human participants.** Solid lines show the effective Young's moduli measured by stretching the skin, and the dashed line by shearing the skin. For each participant, left: effective Young's moduli of the skin along the ridges; right: across the ridges. Adapted from (Wang and Hayward, 2007).

Note that these values are obtained by stretching the skin at a scale of 0.3mm with strain values reaching up to 80%. As for Young's modulus when measured with normal indentation of the skin, it is highly dependent on the scale (see Fig 1.7), since different layers of the skin have different Young's moduli, with the stratum corneum being much stiffer than deeper tissues. It is also dependent on the area of the indentor. At an indentation depth of 10µm, the Young modulus was shown to decrease from 0.15 to 0.015MPa when the radius of a spherical indentor increased from 10µm to 10 mm (van Kuilenburg et al., 2012).

As mentioned previously, the fingerpad skin is not perfectly elastic and presents elements of damping and inertia. At frequencies lower than 100Hz and for small enough amplitudes, the skin behaves elastically. Damping dominates above this value. Inertial values can be neglected up to 500Hz (Wiertlewski and Hayward, 2012). Interestingly, the damping behavior at high values of frequency is used to generate changes in friction by using vibrating glass plates (Wiertlewski et al., 2016; Vardar et al., 2017; Monnoyer et al., 2018). Indeed, when a glass plate is excited with high frequency waves, the damping behavior of the skin creates an air cushion between the skin and

the glass, diminishing the area of contact and thus the friction between the surfaces. This can be used to give the illusion of touching different textures when touching screens (Bau et al., 2010).

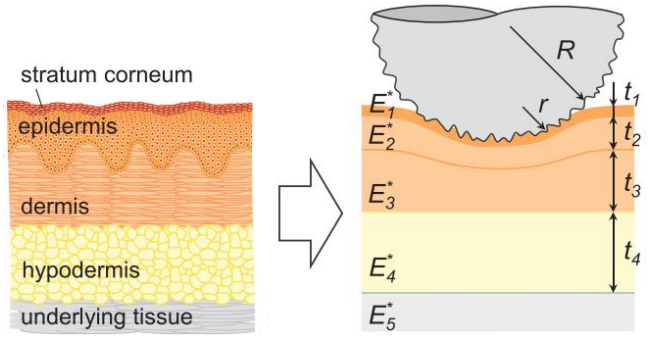


**Fig. 1.10. Schematic overview of the contact between an indenter and the skin.** Each layer of the skin has its own Young modulus. Adapted from (van Kuilenburg et al., 2012).

Quantifying and describing the deformations of the whole fingerpad is interesting, but requires estimations and computer modeling, as in (Wu et al., 2006; Tada and Pai, 2008). Techniques such as optical coherence tomography (OCT) allow direct observation of the interior of the fingerpad skin (Liu et al., 2013, 2017), but only up to a depth of about 1mm. Quantifying the deformations in the depths of the skin in three dimensions is more complex than the surface strains, which can be done by observation as described in the next section.

### 1.3.2. Observing the surface deformations of the fingerpad

Describing the shear deformations of the surface of the fingerpad is much easier than describing deformations in 3 dimensions in the sub-layers of the skin. Moreover, the deformations in the sublayers are linked to the surface deformations even if the precise relationship between the two has not been described yet. Describing the fingerpad surface strains is possible because diverse optical techniques allow direct observation of the skin when in contact with transparent smooth materials such as glass. These techniques use a light source and a camera. When light from the light source goes through the material, it is mostly absorbed by the fingerpad where it touches the glass and it is mostly reflected back to the camera where the skin does not touch the glass. This results in dark fingerprints (Fig 1.8), which allow to measure deformations by tracking their displacement.

**Fig. 1.11. Typical image of the fingerpad.** Note that the ridges are black as they are in contact with the glass. The sweat pores are also visible (white points on the ridges).

The surface fingerpad deformations have been described in different studies and conditions and will be further described in section *1.3.6 Tangential loading* and in the following chapters of this thesis.

### 1.3.3. Contact area

When the fingerpad enters in contact with a smooth material such as glass, the skin flattens against it and the contour of the contact area forms approximately an ellipsoid. A good approximation for the contact area is the Hertz equation (Johnson, 1985) of a deformable ellipsoid being pressed on a flat and rigid surface (Adams et al., 2013):

$$A_{gross} = \pi \left[\frac{3R(1-\nu)^2}{4E}\right]^{\frac{2}{3}} (NF)^{\frac{2}{3}}$$

where $NF$ is the force applied by the fingertip normally to the surface, $E$ is the fingertip's Young modulus, ν is its Poisson ratio[4] and $R$ is equal to $(R'R'')^{\frac{1}{2}}$, with $R'$ and $R''$ being the fingertips radii of curvature of the approximating ellipsoid. We can observe with the experimental data in Fig 1.9 that the area of contact seems to increase logarithmically with the normal

[4] The Poisson ratio is the measure of the deformation of a material in a direction perpendicular to the direction of loading. For the fingerpad skin, it is usually considered to be 0.5 or slightly smaller as it is largely incompressible (Srinivasan and Dandekar, 1996; Wang and Hayward, 2007).

force, which is consistent with this equation as both functions are similar over this interval.

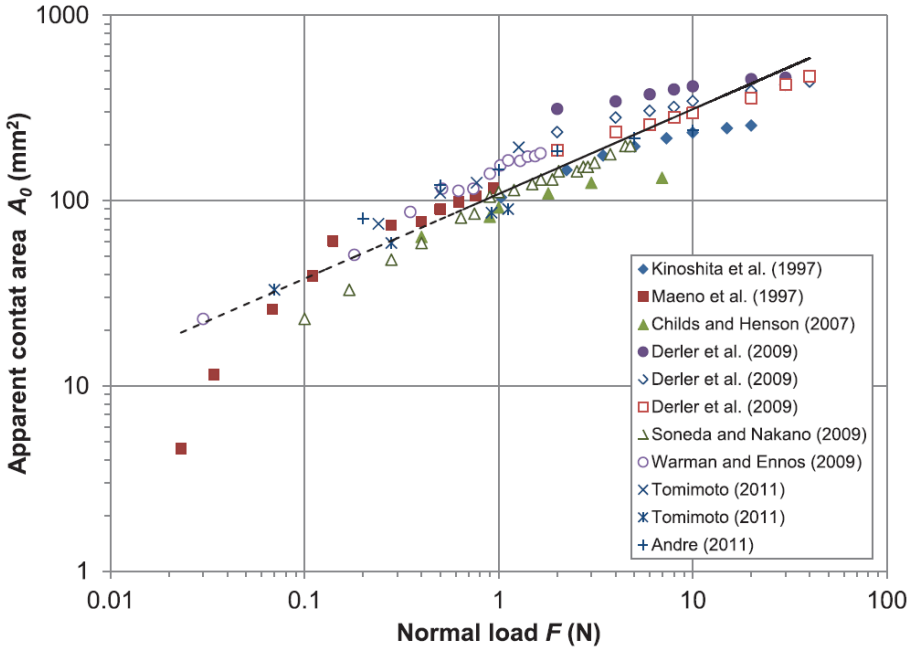


**Fig. 1.12. Gross contact area of the index fingertip in contact with a smooth rigid surface as a function of the normal force.** Data were taken from (Kinoshita et al., 1997; Kobayashi and Maeno, 1998; Childs and Henson, 2007; Derler et al., 2009; Warman and Ennos, 2009; Soneda and Nakano, 2010; André et al., 2011; Tomimoto, 2011). Figure adapted from (van Kuilenburg et al., 2013).

The contact as measured in Fig 1.9 is called the gross contact area and is defined as the total area contained within the overall contact boundary. However, as it can be observed in Fig 1.8, when the finger is pressed against a smooth surface, the skin located in the valleys between the ridges is not in contact with the material. Moreover, the skin of the ridges is not in perfect contact with the material either. We can thus define the contact area in two additional different ways. $A_{ridge}$ is the apparent area encompassed by the fingerprint ridges and $A_{real}$ is the actual area of contact. Those three definitions follow the inequalities $A_{gross} > A_{ridge} \geq A_{real}$. An estimation for the value of $A_{ridge}$ is the following equation (Dzidek et al., 2017):

$$A_{ridge} = k_r \left[ \frac{NF^{5/6}}{(1 + (\beta)(NF))^{1/3}} \right]$$

$A_{real}$ is much more complicated to calculate and is dependent on the scale of the observation. Moreover, it is highly dependent on the moisture content of the fingertip, which changes over time, as explained in section *1.3.5. Moisture*.

### 1.3.4. Friction

Whether the fingerpad is used to explore a surface or to hold an object, an important parameter is the frictional force. The frictional force is a vector parallel to the plane of the contact between the finger and the material, whose direction is opposite to that of the movement of the finger or the object. According to the two-term non-interacting model, it can be approximated with the following expression (Bowden and Tabor, 1954; Johnson et al., 1993; Adams et al., 2007):

$$F_{\mu} = F_{\mu,adh} + F_{\mu,def}$$

where $F_{\mu,adh}$ is due to the molecular bonds formed at the interface of the contact between the skin and the object and $F_{\mu,def}$ is due to the work stored and dissipated by deformations of either the skin or the contacted material. However, $F_{\mu,def}$ is negligible if the finger is in contact with a smooth and rigid surface or in the case of static friction (which is more important than dynamic friction during object manipulation). For organic polymers in rubbery state, $F_{\mu,adh}$ can be expressed as (Schallamach, 1952):

$$F_{\mu,adh} = \tau_{real} A_{real}$$

where $\tau_{real}$ is the average interfacial shear strength, which can vary according to the location inside the contact. We can also write:

$$F_{\mu,adh} = \tau_{gross} A_{gross}$$

where $\tau_{gross}$ is the average interfacial shear strength over the gross contact area. It has been found to increase linearly with the average pressure. It can thus be expressed as:

$$\tau_{gross} = \tau_0 + \alpha p$$

where $\tau_0$ is an intrinsic interfacial strength, $\alpha$ is the linearity coefficient and p is the average pressure, given by $NF/A_{gross}$. These last two equations can be combined with the equation of the relationship between the area of contact between the area of the sphere and rigid plane of section 1.3.3 to obtain the following equation:

$$F_\mu = \pi\tau_0 \left[\frac{3R(1-\nu)^2}{4E}\right]^{\frac{2}{3}} NF^{\frac{2}{3}} + \alpha NF$$

It is common to write in the simplified following form (Adams et al., 1997):

$$F_\mu = k * NF^n$$

where $k$ is a load-dependent coefficient of friction and $n$ is known as the frictional load index. Both values are dependent on the mechanical properties of particular human fingers. This last expression is a valid approximation because both follow a similar trend over normal forces values applied by the fingertips in everyday life (1-15N). The coefficient of friction itself can be expressed as:

$$\mu = \frac{F_\mu}{NF} = \frac{k}{NF^{1-n}}$$

This dependency of the coefficient of friction on the normal force has been observed in many papers, including in the context of this thesis (André et al. 2009, Barrea et al. 2016, Supp. Fig. 1 & 2 of chapter 3). An example of this relationship is provided in Fig 1.10.

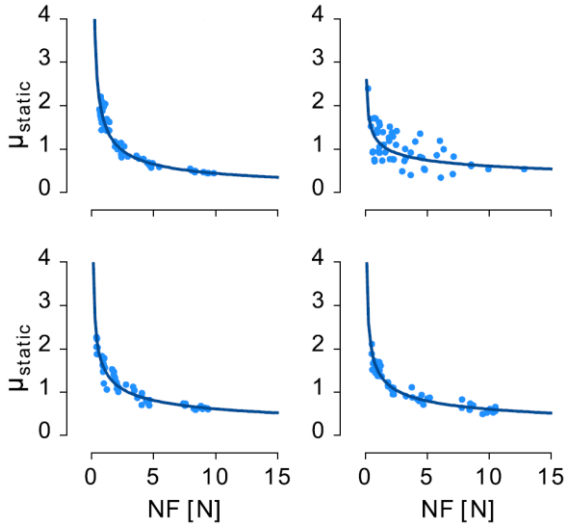


**Fig. 1.13. Static coefficient of friction as a function of normal force for 4 different human volunteers.** Volunteers were asked to rub their finger against a rigid surface equipped with a force sensor. The coefficient of friction and normal force were

measured at the moment of slip (data points). The curves are functions fitted to data point according to the relationship $\mu = \frac{k}{NF^{1-n}}$. Adapted from (Barrea et al. 2016).

This inverse dependency of the coefficient of friction relative to the normal force is counter-intuitive, as it could be expected that Amonton's law of friction would apply[5]. However, as shown theoretically and experimentally, the relationship between the frictional force and the normal force is much more complex. This relationship plays an important in dexterous manipulation. When manipulating light objects, humans can apply very small forces, as the coefficient of friction is especially large at low values of normal forces. However, when manipulating heavier objects, humans have to take into account this relationship between the normal force and the coefficient of friction, as the higher the squeezing force, the lower the coefficient of friction.

### 1.3.5. Moisture

Moisture level on the glabrous skin varies from person to person and can change rapidly. It has an important impact on the tribology of the skin and has to be taken into account during dexterous object manipulation. Sweat pores can be found on the ridges of the fingertips with a density of approximately 220-550/cm² (Baker, 2019). They moisturize the skin by transporting sweat secreted by the sweat glands below the skin surface through the sweat ducts[6]. Their roles include temperature control of the skin as well as excretion of toxicants. They respond to emotional and thermal stimuli. As we will explain, they also have a role in dexterous objects manipulation.

Moisture influences the tribology of the fingertip skin. The effects of water on skin mechanical properties have been described in several studies (Comaish and Bottoms, 1971; Buchholz et al., 1988). In particular, it has been observed that the coefficient of friction increases with the moisture content of the skin, for both the glabrous and hairy skin (Adams et al., 2007; Derler et al., 2007). Later, this result has been refined and the relationship between

[5] Amonton's law of friction states that the force of friction is directly proportional to the applied load, with a constant coefficient of friction as factor of proportionality.

[6] It is worth noting that only eccrine sweat glands are present in the glabrous skin of the hands. The sweat they produce is mostly water and NaCl, unlike the sebum produced by the sebaceous glands, which can be found in the hairy skin. The interested reader is invited to consult (Baker, 2019) for more information.

the coefficient of friction and moisture has been shown to follow a bell-shaped curve, with the coefficient of friction decreasing when moisture increases above an ideal level (see Fig 1.11) (André et al., 2009). Moreover, it has been shown that, during active manipulation of objects, the grip force was adjusted according to the particular level of friction obtained with the moisture content. And, even more surprisingly, that the moisture content tended towards the value for which the corresponding coefficient of friction was optimal (see Fig 1.12).

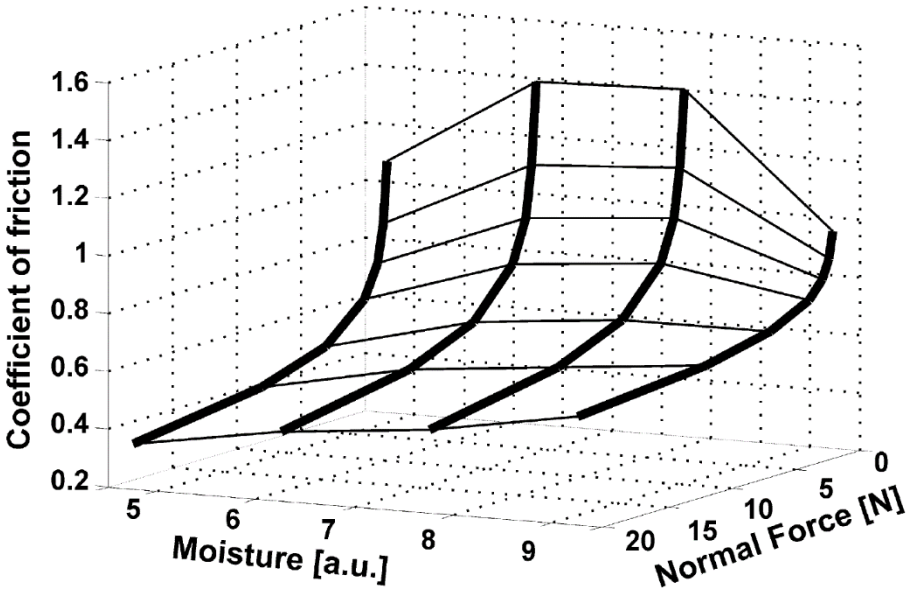


**Fig. 1.14. Estimation of the coefficient of friction of the thumb as a function of the moisture and normal force for 10 healthy human volunteers.** Volunteers were instructed to hold an object in a precision grip at a constant level of normal force, while slippage was produced by moving the object. Adapted from (André et al. 2009).

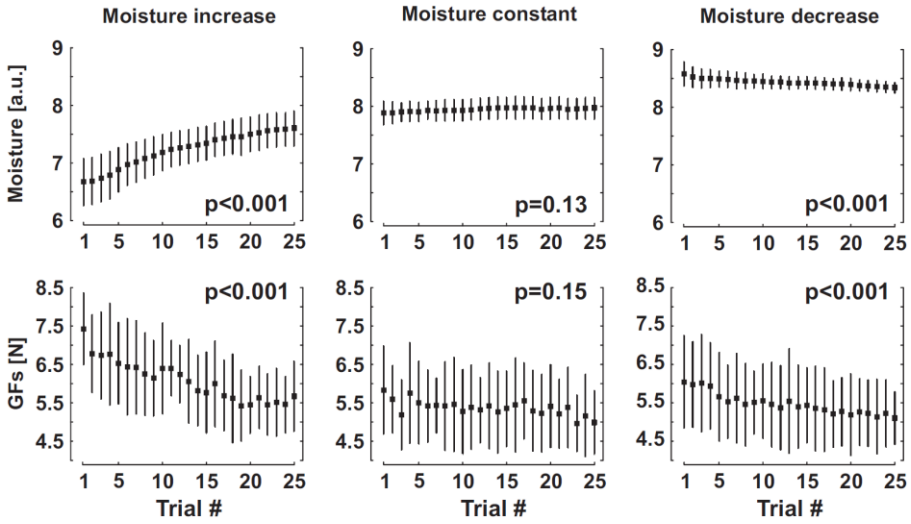


**Fig. 1.15. Representative changes in moisture level and grip force (GF) with trial numbers for a single volunteer.** The volunteer performed point-to-point movements during each trial. The trials were separated into blocks of 25 with longer pauses between blocks. The blocks were then separated into three categories, according to the change in moisture. Each data point corresponds to the mean moisture level for each trial across all blocks and the vertical bars are the associated standard deviations. The p-values of the linear regression fitting the data are given for each relationship. Adapted from (André et al. 2010).

Direct observation of the fingerpad skin in contact with smooth materials has explained these results. Using high-resolution imaging, the real area of contact $A_{real}$ has been shown to increase over time following a first-order kinetics relationship when the fingerpad was pressed against a smooth surface such as glass (Dzidek et al., 2017). This evolution is the result of microscopic junctions made between the keratin of the stratum corneum and the glass surface. This process is itself driven by the increase of moisture level thanks to the secretion of sweat from the sweat glands. Indeed, increased hydration causes the skin to become softer. Saturation was typically reached within 20 seconds of contact, regardless of the initial moisture state of the finger and the normal force applied (see Fig 1.13). The surprisingly slow speed of this process is important for dexterous manipulation of smooth, rigid objects, because since the coefficient of friction is proportional to $A_{real}$, it can be low at the time of contact and take several seconds to increase. For this reason, tools often have a rubbery handle, as for those materials, close contact is instantaneous, because the material follows the shape of the skin.

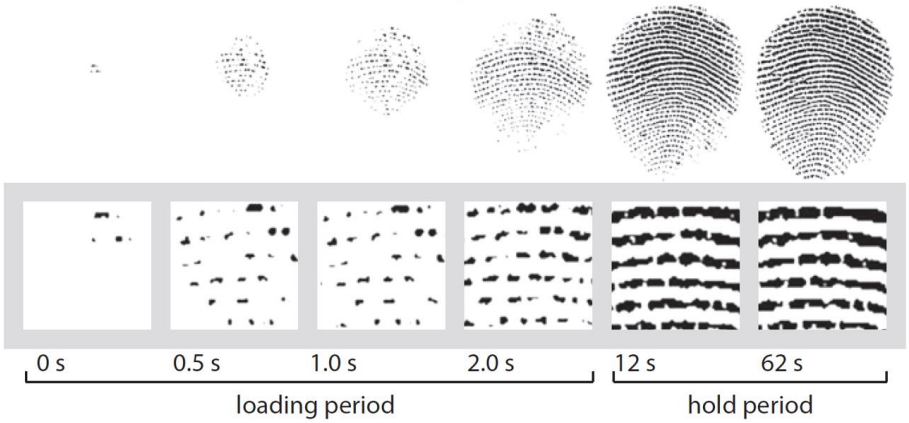


**Fig. 1.16. Temporal evolution of the contact area of the index fingertip on a glass surface.** Adapted from (Dzidek et al., 2017).

Recently, the precise mechanisms that allow the moisture content to reach the level that maximizes friction have been described by a study that combined spectroscopic imaging and infrared coherence tomography to observe how moisture behaves in a fingertip at the scale of individual ridges (Yum et al., 2020). When the fingertip comes into contact with a smooth rigid material, the sweat pores secrete sweat on the ridges, creating a close contact as described above. The excess sweat present in the valleys does not help to increase this close contact since they do not contribute to the plasticization of the skin in contact with the material. In fact, too much moisture in the area of contact can decrease the coefficient of friction by creating a slippery layer of water. The excess sweat thus evaporates and leaves the area of contact thanks to capillary evaporation (see Fig 1.14).

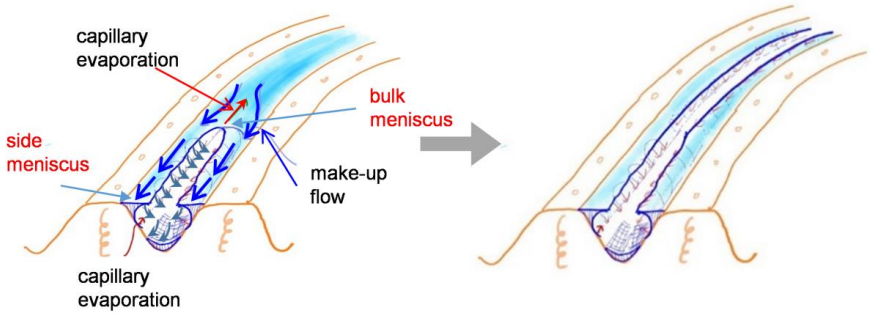


**Fig. 1.17. Schematic diagram of the process of capillary evaporation for an initially wet fingerpad.** The excess sweat evaporates, leaving only water in close contact with the skin. Adapted from the supplementary figures of (Yum et al., 2020).

### 1.3.6. Tangential loading

The index fingerpad can undergo tangential loading during object manipulation or during tactile exploration. Understanding how the finger deforms when loaded tangentially is important to understand the fingerpad tribology and has been extensively studied. Because of the curvature of the fingertip, the pressure is higher in the center of the area of contact between the finger and the contacted material than on the edge (see Fig 1.15) (Tada et al., 2002). The traction profile is different in the slip and stick zones and is at its largest at the frontier between the stick and slip zone. When the tangential force increases, the slip zone increases in size and takes in more traction.

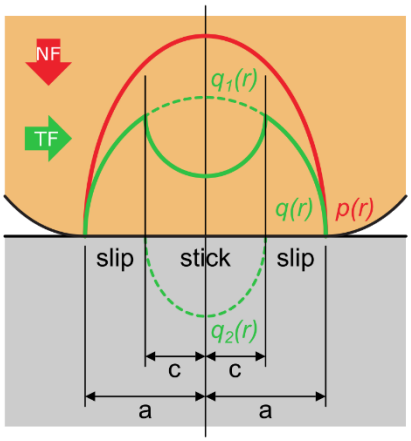


**Fig. 1.18. Schematic illustration of force profiles under tangential loading during partial slip.** Pressure (p, red) and traction (q, green) profiles under normal (NF, red) and tangential (TF, green) loading of an elastic sphere in contact with a rigid surface. The radii of the contact and no-slip areas are denoted by *a* and *c* respectively. Reproduced from (Barrea, 2017), itself adapted from (Johnson, 1985) with material from (Tada et al., 2006a).

This means that when the tangential force is increased continuously, the slippage will progress from the exterior to the interior of the contact area (see Fig 1.16), until full slip if the ratio of tangential force over normal force exceeds the coefficient of friction (André et al., 2011). The transition period between no-slip and full slip is commonly known as partial slip. The stick ratio is the ratio between the area that has not undergone slippage and the total area of contact between the skin and the object. It is a value that starts at 1 before the finger starts to slip and reaches 0 at full slip, with values in between indicating the presence of partial slip (Tada et al., 2002).

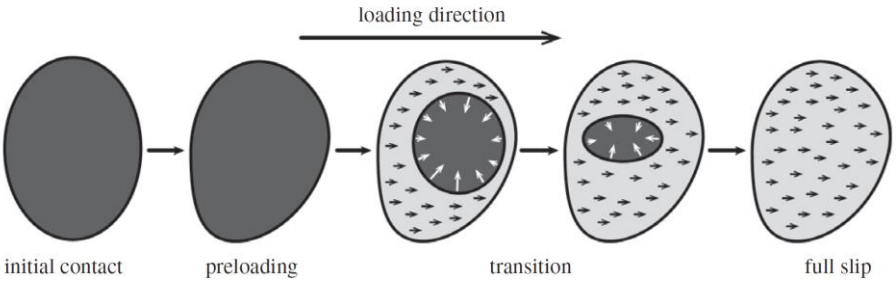


**Fig. 1.19. Course evolution of the dynamics of finger contact from the initial contact to full slip.** From left to right: initial stuck contact (dark grey), preloading, slip onset starting at the trailing edge, growth of the slip region (light grey), full slip. Adapted from (André et al., 2011).

Direct observation showed that the gross contact area diminishes during tangential loading and that the deformations are dependent on the direction of the loading. However they seem to be highly patterned and reproducible and could thus be a potential source of information for the central nervous system (Delhaye et al., 2014). The slipping part of the fingertip undergoes strains (compression, stretch, and shear) that can reach up to 50% and are dependent on fingertip geometry (Delhaye et al., 2016). These strains are very important in the detection of partial slip, as demonstrated by the observation that diminishing the level of strains by reducing the friction impedes the detection of the partial slip (Barrea et al., 2018).

## 1.4. Touch and friction during object manipulation

### 1.4.1. The precision grip paradigm

When manipulating objects, different positions of the hand and fingers on the object are possible. An interesting paradigm that has been studied for approximately 40 years is the precision grip (see Fig 1.16). The precision grip consists in holding an object between the index and the thumb of one hand. In this paradigm, the grip force is defined as the mean of the norm of the forces normal to the surface of the object exerted by the finger. The load force results from the frictional forces at the interface between the object and the fingers and is defined as the norm of the sum of the forces applied tangentially to both surfaces by each finger. When the object is accelerating vertically, significant inertial forces will be induced. The resultant Load Force

can thus be calculated as the vectorial sum of those forces and the weight of the object:

$$\overrightarrow{LF} = m(\vec{a} - \vec{g})$$

where *m* is the mass of the object, $\vec{g}$ is the acceleration due to gravity and $\vec{a}$ is the vertical component of the acceleration of the object.

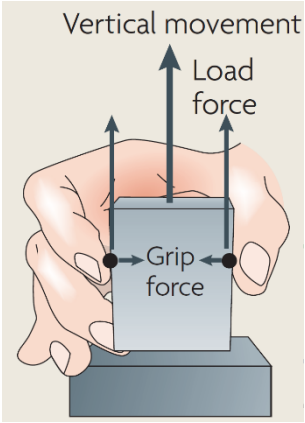


**Fig. 1.20. Forces at play during precision grip.** Adapted from (Johansson and Flanagan, 2009).

### 1.4.2. Grip Force and Load Force coupling during dexterous manipulation

When performing vertical movements with an object held in a precision grip, the Load Force is used to accelerate the object. The maximal value of the Load Force that the fingers can apply to the object is determined by the coefficient of friction and the Grip Force following this inequality:

$$\left\|\overrightarrow{LF}\right\| \leq \mu \left\|\overrightarrow{GF}\right\|$$

If it is not respected, this means that the level of Grip Force is not high enough and that the object will slip[7]. During the vertical acceleration of an object, the Load Force will change and the Grip Force will be scaled according to the value of the coefficient of friction to avoid slippage. Strikingly, the Grip Force changes in parallel with the Load Force (Johansson and Westling, 1984; Westling and Johansson, 1984). The minimum value of the Grip Force to

[7] To be more precise, this inequality must be respected for both the index and the thumb independently. But as the coefficient of friction and the forces applied by both fingers are very close, the presented simplification is a good approximation.

avoid slippage is commonly known as the Slip Force and the difference between the Grip Force and the Slip Force is the Safety Margin. The safety margin prevents slippage and is scaled to the uncertainty about the acting Load Force (Hadjiosif and Smith, 2015).

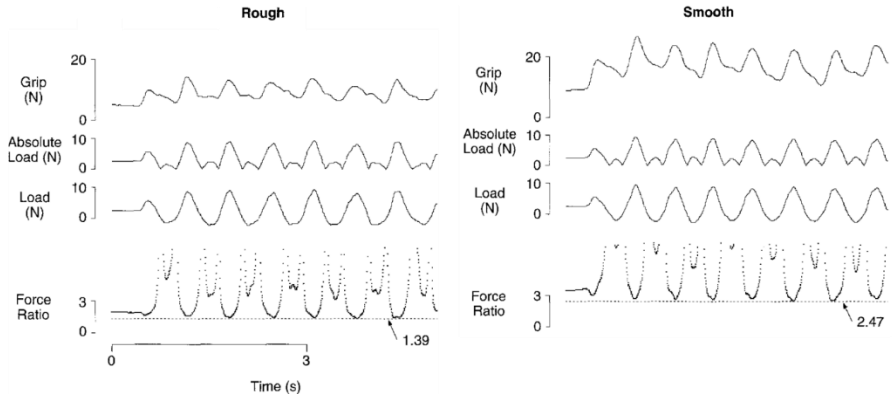


**Fig. 1.21. Grip Force and Load Force during vertical cyclic movements.** The surface of contact was either rough (left) or smooth (right) and thus more slippery. The Grip Force is synchronously adapted to the Load Force. The Grip Force is consistently higher in the case of the smooth object. The dotted line at the bottom of the graphs indicates the minimum value of the Grip Force over Load Force ratio observed for each trial. Adapted from (Flanagan and Wing, 1995).

The change in parallel of the Grip Force with the Load Force indicates that an anticipatory mechanism is at play. This is confirmed by the influence of the friction (Westling and Johansson, 1984) or the weight (Johansson and Westling, 1988) experienced during the previous trial on the Grip Force applied. Moreover, factors such as the size of the lifted object also influence the Grip Force, showing the impact of vision on the grip-load force coupling (Ellis and Lederman, 1993; Buckingham and Goodale, 2010; Plaisier and Smeets, 2012; van Polanen and Davare, 2015).

We can infer that control during manipulation depends on a process of prediction of the object's dynamics, called *feedforward control*, and also on the sensory information sent to the central nervous system, called *feedback control*. Those two processes seem to function in parallel and to be scaled to the performed movement according to their reliability (Körding and Wolpert, 2004; Crevecoeur et al., 2010).

In summary, the precision grip and the associated coupling of the Grip Force and Load Force is an excellent paradigm to study the mechanisms used

to perform dexterous manipulation. This is demonstrated by the numerous studies that brought some understanding to the sensorimotor control of movement and that have been carried out using this paradigm. Those studies performed all kinds of movements and in various environments such as grip-lifting tasks (Johansson and Westling, 1984), point-to-point movements (Flanagan and Wing, 1993), cyclic arm movements (Flanagan and Wing, 1995), collisions (White et al., 2011), in different gravity conditions during parabolic flights (White et al., 2005; Opsomer et al., 2018) or upside-down (Opsomer et al., 2021), with an off-centered mass that resulted in a significant torque (Kinoshita et al., 1997; Crevecoeur et al., 2011; Giard et al., 2015), with artificial inertial and viscous loads (Flanagan and Wing, 1997) and with distraction of the volunteer using high-level cognitive tasks (Guillery et al., 2013, 2017).

### 1.4.3. The importance of afferent feedback for dexterous manipulation

Proprioception and touch have an important role during dexterous manipulation. This is proven by the difficulty of deafferented patients to perform simple tasks in everyday life such as walking, writing, or even lifting a glass of water (Rothwell et al., 1982; Blouin et al., 1993; Sainburg et al., 1993; Sarlegna et al., 2006; Miall et al., 2019). It has been further demonstrated by disrupting the tactile feedback of healthy subjects with local anesthesia of the fingers, which led to a disturbed control of the Grip Force during manipulation with the precision grip (Johansson and Westling, 1984; Augurelle et al., 2003).

Both cutaneous and muscle afferents provide the central nervous system with relevant information during dexterous manipulation. Their different positions imply that they should respond in different ways to different stimuli (e.g. only cutaneous afferents will be able to relay information about a partial slip of the finger skin, and proprioceptive afferents will be sensitive to tensions and vibrations in the muscles and joints due to changes of the Load Force). Isolating their contributions is difficult but necessary to understand their role during dexterous object manipulation. Several ingenious solutions have been found.

A first solution was to record the different types of afferent responses while perturbations were applied on an object held in a precision grip. On one hand, it was found that muscles and joint afferents could not be awarded a significant role in automatic Grip Force changes due to the perturbations,

but that they might provide information related to the reactive force produced by the subject (Macefield and Johansson, 1996). On the other hand, cutaneous afferents from all classes except FAII responded to the perturbation. The FAI in particular tended to respond early enough to explain the automatic Grip Force reaction (Macefield et al., 1996).

Another solution was to instruct human volunteers to put their index fingertip on a glass plate and to increase their normal force to keep it from moving when a perturbation in the form of a sudden tangential force was applied (Crevecoeur et al., 2017). The finger was either restrained to suppress the feedback from muscular and joint afferents or it was anesthetized to suppress the feedback from cutaneous afferents. Results show that proprioception is involved in more rapid automatic responses (observable ~60ms after the perturbation) and that touch is involved in slower responses adapted to the perturbation ( ~90ms after the perturbation).

Yet another solution was to trick human participants by generating artificial skin stretch on the area of contact with a manipulated object. Those skin stretches are only perceived by cutaneous afferents. They have the effect of increasing the perceived stiffness of the object (Quek et al., 2014). Interestingly, when the object is manipulated in a precision grip, the artificial skin-stretch increases the Grip Force modulation to the Load Force immediately upon first contact with the object (Farajian et al., 2020). These results show that indeed, proprioceptive and cutaneous afferents play different roles in dexterous manipulation. The precise way in which the central nervous system uses information from both of these sources as well as that collected by the other senses is complex and remains to be explained.

## 1.5. Thesis content

### 1.5.1. Overview

In this thesis, we will expand our understanding of the role of touch during dexterous manipulation. In particular, we will answer research questions such as: How does the skin of the index deform when manipulating objects and how is it influenced by the Grip Force applied? When lifting objects with different frictions, what are the cues that allow humans to adapt their Grip Force to the coefficient of friction? When manipulating those objects with different friction, are the amplitude of deformations of the fingerpad skin similar across friction conditions? We have addressed those questions by conducting experiments using a novel device called “the Active

Touch", that allows recording fingerpad deformation in parallel with the Grip and Load Force while using the precision grip.

In this first chapter, we introduced the background for this thesis. We gave an overview of the anatomy of the finger and the skin, the sense of touch, the mechanical properties of the skin, and their role in object manipulation. In the second chapter, we will present and validate the Active Touch device and describe how the fingerpad deforms during object manipulation. In the third chapter, we will show how localized fingerpad strains allow to quickly adapt the grip force when lifting objects. In the fourth chapter, we describe how the grip force is adjusted so that the upper bound of the amount of partial slip and finger skin deformation remains similar across friction conditions. Finally, in the fifth chapter, we summarize the contributions of the thesis and discuss them. We will also present the remaining open questions, give possible future directions, and present potential applications.

### 1.5.2. Publications and communications

*Journal paper*

**Measuring fingerpad deformation during active object manipulation.** Schiltz* F., Delhaye* B. P., Barrea A., Thonnard J.-L., and Lefèvre P. Journal of Neurophysology (2021) 126(4): 1455-1464. https://doi.org/10.1152/jn.00358.2021

(*) equal contribution.

This paper is presented in Chapter 2.

**Grip force is adjusted at a level that maintains an upper bound on partial slip across friction conditions during object manipulation.** Schiltz* F., Delhaye* B. P., Thonnard J.-L., and Lefèvre P. IEEE Transactions on Haptics. doi: 10.1109/TOH.2021.3137969

(*) equal contribution.

This paper is presented in Chapter 4.

*Submitted papers*

**Fast grip force adaptation to friction relies on localized fingerpad strains.** Schiltz* F., Delhaye* B. P., Crevecoeur F., Thonnard J.-L., and Lefèvre P.
(*) equal contribution.

This paper is presented in Chapter 3.

*Conference communications*

**Finger pad mechanics during object lifting.** Schiltz F., Barrea A., Thonnard J.-L., and Lefèvre P. Eurohaptics 2018, Pisa, Italy (2018). Work-in-progress poster presentation. **Best work-in-progress poster award**

**Finger pad mechanics during object lifting.** Schiltz F., Barrea A., Delhaye B.P., Thonnard J.-L., and Lefèvre P. 48th Annual Meeting of the Society for Neuroscience, San Diego, CA (2018). Poster presentation.

**Finger pad mechanics during object lifting.** Schiltz F., Barrea A., Delhaye B.P., Thonnard J.-L., and Lefèvre P. Materials science and haptics, Saarbrucken, Germany (2019). Poster presentation.

**Adaptation to friction during object manipulation.** Schiltz F., Delhaye B.P., Thonnard J.-L., and Lefèvre P. Materials science and haptics, Saarbrucken, Germany (2019). Eurohaptics 2020, Leiden, The Netherlands (2020). Work-in-progress poster presentation.

CHAPTER 2

# Measuring fingerpad deformation during active object manipulations

*"That's the whole problem with science. You've got a bunch of empiricists trying to describe things of unimaginable wonder."*

*Calvin & Hobbes - Bill Watterson*

Published as: Benoît P. Delhaye*, Félicien Schiltz*, Allan Barrea, Philippe Lefèvre and Jean-Louis Thonnard, "Measuring fingerpad deformation during active object manipulation", in Journal of Neurophysiology, vol. 126, no. 4, pp. 1455-1464, October 2021. (*) equal contribution.

During active object manipulation, the finger-object interactions give rise to complex fingertip skin deformations. These deformations are in turn encoded by the local tactile afferents and provide rich and behaviorally relevant information to the central nervous system. Most of the work studying the mechanical response of the finger to dynamic loading has been performed under a passive setup, thereby precisely controlling the kinematics or the dynamics of the loading. However, to identify aspects of the deformations that are relevant to online control during object manipulation, it is desirable to measure the skin response in an active setup. To that end, we developed a device that allows us to monitor finger forces, skin deformations, and kinematics during fine manipulation. We describe the

device in detail and test it to precisely describe how the fingertip skin in contact with the object deforms during a simple vertical oscillation task. We show that the level of grip force directly influences the fingerpad skin strains and that the strain rates are substantial during active manipulation (norm up to 100%/s). The developed setup will enable us to causally relate sensory information, i.e. skin deformation, to online control, i.e. grip force adjustment, in future studies.

## 2.1. Introduction

Humans are exquisitely skillful at dexterous manipulation of objects with their fingers. This dexterity partly relies on optimally adjusting the grip force (GF), the force exerted normally to the object surface, to the load force (LF) due to the object weight and inertia, and the fingertip-object contact friction (Johansson and Flanagan, 2009). Indeed, an excessive amount of force is undesirable as it leads to excessive expenditure of energy and could potentially crush the object. However, an insufficient grip force will let the object slip from the hands. Accordingly, we usually exert a grip force just above the minimum, thereby continuously varying GF according to LF and the level of friction (Johansson and Westling, 1984; Westling and Johansson, 1984; Cadoret and Smith, 1996; Flanagan and Wing, 1997). Deformations and vibrations produced in the skin during object manipulation are faithfully encoded by the numerous tactile afferents innervating the hand and fingers. These afferents in turn provide the central nervous system with rich and behaviorally relevant tactile information content (Macefield and Johansson, 1996; Jenmalm et al., 2003; Goodwin and Wheat, 2004; Delhaye et al., 2018, 2021a). This, for instance, allows the central nervous system to adjust the grip force exerted on a manipulated object to the grip conditions (Johansson and Flanagan, 2009). Without tactile afferent feedback, we fail to react to unexpected perturbations in object load or surface friction and to maintain a stable grip force to load force ratio, hence highlighting the critical role played by tactile feedback during object manipulation (Nowak et al., 2001; Augurelle et al., 2003; Witney et al., 2004).

In vivo biomechanics of the fingerpad has been extensively studied in passive conditions, highlighting the systematic occurrence of partial slips at the periphery of the fingertip-object contact during the tangential loading of the fingerpad (Tada and Kanade, 2004; Tada et al., 2006a; André et al., 2011; Delhaye et al., 2014, 2016). Indeed, we have shown that slip is not instantaneous and that the transition from a stable to a slipping contact

develops progressively with partial slips initiating at the periphery and progressing towards the center of contact until the point of a full slip. As a consequence of the relative movements between the non-slipping regions and the slipping regions, partial slip is associated with substantial (up to 25%) surface-tangential skin strains (Delhaye et al., 2016). Furthermore, we have shown that those skin strains caused by partial slips are readily encoded by human afferents (Delhaye et al., 2021a). Besides, we have also demonstrated that human subjects can consciously perceive incipient slip, before full slip is reached, given that the surface-tangential skin strains are sufficient (Barrea et al., 2018). Taken together, those results have essential implications for object manipulation: indeed, the systematic occurrence of partial slips during tangential loading implies that partial slips will take place during active manipulation. Because partial slips provide a measure of how far from fully slipping the contact is, they might be used by the central nervous system to adjust GF to the object properties during active manipulation.

It remains unclear, however, how much partial slips spread inside the contact area during active object manipulation and how they will be affected by the gripping conditions, including the biomechanical properties of the fingertips. Indeed, for a given object load, the amount of partial slips depends on how much grip force is exerted on the object and also on the frictional properties of the fingertip-object contact (André et al., 2011).

To investigate this, we developed a new instrumented device that enables synchronously recording the forces exerted by the fingers together with the fingertip skin deformation at the finger-object contact with a high spatial and temporal resolution during active manipulation. The device was tested in an experiment involving 18 subjects who were requested to perform vertical oscillatory movements. We describe the typical strain patterns taking place in the contact in parallel with the kinematic and dynamic parameters of the task.

## 2.2. Methods

### 2.2.1. Apparatus

To characterize the deformations taking place at the contact between the fingerpad and an actively manipulated object, we developed a manipulandum equipped with force sensors as well as an imaging system.

This system can capture images of the skin in contact with the object through a flat and optically transparent plate of glass (Figure 2.1).

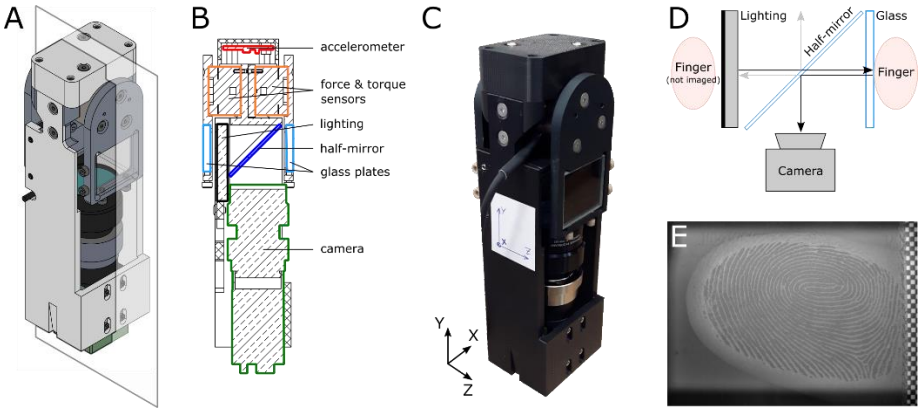


**Fig. 2.1. Detailed description of the device. A|** Assembly sketch of the device. **B|** Cut of the device along the plane in panel A with its key elements and sensors highlighted. **C|** Photograph of the manipulandum along with the definition of the reference frame used in the context of this study. **D|** Custom optical system to image fingerprints. Arrows show the trajectory of the light emitted by the "Lighting" and reflected at optical interfaces. In this study, the index finger was imaged, and the thumb was not. **E|** Typical image obtained with the system. The checkerboard pattern on the right of the image is used to measure very small movements of the glass relative to the camera.

The device is designed to be handled using a precision grip (Westling and Johansson, 1984), i.e. pinched between thumb and index. Its aluminum core supports two force sensors, one on each side of the manipulandum, to measure the forces exerted by each finger (Fig 2.1B, orange, ATI Mini27 Ti, ATI-IA). On the outer side of each force sensor, an aluminum piece supports a transparent plate of glass, where the object is contacted to be manipulated. The rest of the device, including its top hat and diverse small parts, is 3D printed using PLA to be lightweight and customized at will (Fig 2.1A-C). Only one finger can be imaged, but the outer plate design is symmetric so that the contacting surfaces are the same for both fingers. Both surfaces can be removed and swapped quickly, allowing the experimenter to test materials of different properties (e.g. friction or texture) during one experiment. An accelerometer (Fig 2.1B, red, LIS344ALH, STMicroelectronics) is included in the top hat of the device. All signals are acquired using an ADC acquisition system (NI6225, National Instruments).

Fingerprints in contact with the glass plate are imaged using a custom optical system based on the principle of frustrated total internal reflection, with a coaxial light source and camera (Fig 2.1D). The light source (Fig 2.1B, black, LFL-1012-SW2, CCS Inc.) is placed on the opposite side of the imaged finger. The light passes through a half-mirror to illuminate the finger. Part of the light is reflected by the contacting glass and part of it is transmitted. The light transmission index is increased where the fingerprints contact the glass, causing less reflection and therefore dark fingerprints in the captured images (Fig 2.1E). The light is then collected by a small and lightweight monochrome camera equipped with a macro lens (Fig 2.1B, green, camera: GO-5000M-PMCL, JAI, monochrome, 2560 x 2048 full pixel resolution; macro lens: Cinegon 1.8/16, Schneider Optics). The setup enables us to image the entire fingerprint at a high spatial (1696 x 1248 pixels) and temporal (100 Hz) resolution. Note that only a subset of the camera field of view was recorded because of constraints related to the architecture of the device, in particular the size of the area illuminated by the light source. Optical tracking allows us to measure partial slips from fingerprint images and to derive the skin strains (Delhaye et al., 2014, 2016). A checkerboard pattern is glued on the glass on the side of the field of view to track very small glass movements relative to the camera caused by the elastic deformation of the device. The squares of the checkerboard, whose dimensions are 0.5 x 0.5 mm, enable us to measure the image resolution (64 pixels/mm) and to verify that the effects of optical distortion and elastic deformation of the manipulandum are minimal. The width of the device, i.e. the distance between both fingers gripping the object, is 50 mm. The total mass of the device is 540 g.

### 2.2.2. Participants

Eighteen healthy subjects (9 women, ages 20-34 years) participated in the experiment. Each subject provided written informed consent to the procedures and the study was approved by the local ethics committee at the host institution (Institute of Neuroscience, Université catholique de Louvain, Brussels, Belgium).

### 2.2.3. Experimental procedure

For this experiment, the device was held by a system of pulleys and a counter-weight with the same mass as the device, such that the net weight of the whole system was close to zero, but its inertia was twice that of the device alone. The goal was to isolate the forces and deformations related to dynamic interactions (inertial forces) as opposed to static weight. Moreover,

an optical distance sensor (DT20-P224B, SICK Sensor Intelligence) was placed above the device and measured its vertical position continuously.

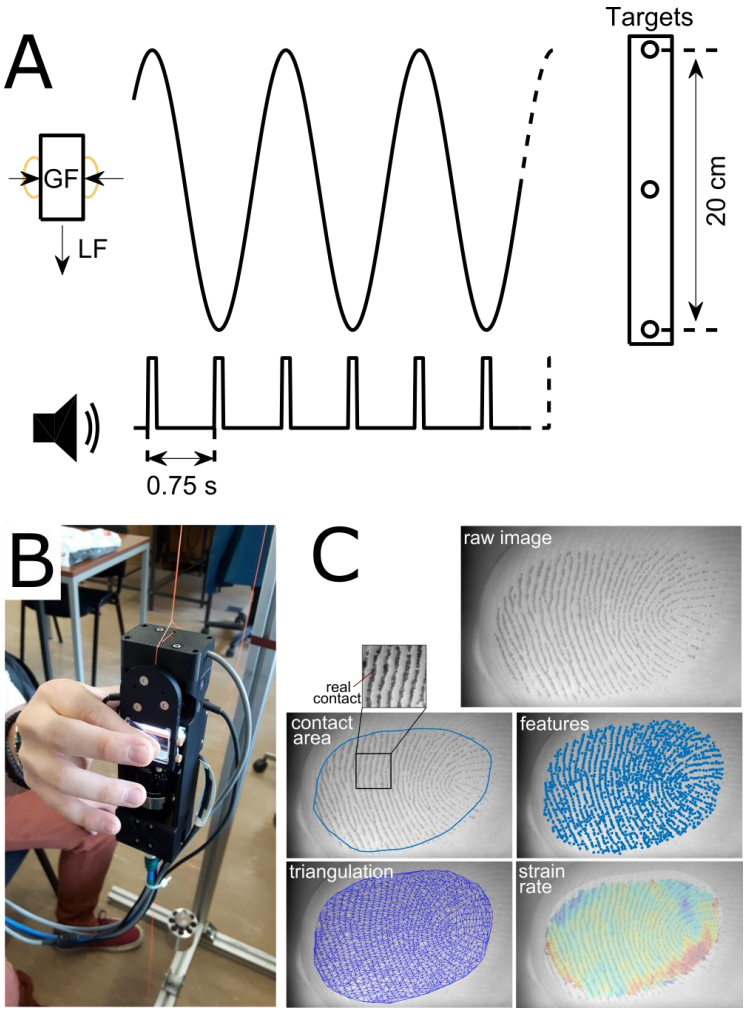


**Fig. 2.2. Experimental protocol and image processing. A|** Subjects performed vertical oscillations with a peak-to-peak amplitude of 20 cm, delimited by visual targets and rhythmed by auditory cues every 0.75 s (at each peak of the movement). **B|** The device was held in a precision grip. A system of pulleys and a counter-weight completely compensated the weight of the device. **C|** Image processing pipeline. From the raw images, the contact area is extracted. Feature points are then detected inside this contact area and tracked from frame to frame. A Delaunay triangulation is computed from the first frame and the strain rate tensor of each triangle can be computed for each pair of images.

Subjects were asked to grab the device with their index and thumb at the center of the glass plates such that the fingerprints were centered in the field of view of the camera (Fig 2.1C-E). Then, they were instructed to move the device up and down producing an oscillatory movement between two targets spaced by 20 cm for 30 seconds (Figure 2.2). The period was set to 1.5 seconds, therefore generating 20 oscillations for each block (Fig 2.2A). A short tone was played every 750 ms to indicate the instant when they were supposed to reach one of the targets. A higher-pitched tone indicated the end of the block when the subjects were asked to release the object and prepare for the next trial. The same procedure was repeated for 15 blocks. Because we observed that subjects tended to apply an excessive level of grip force, a subset of them (6) were explicitly asked to try to minimize the grip force.

Moreover, at the end of the experiment, the subjects were asked to rub their index finger against the glass surface repeatedly using a published procedure (Barrea et al., 2016) to evaluate the coefficient of friction as a function of the normal force. A power function was fit to the data ($\mu = k(NF)^{n-1}$, where $\mu$ is the coefficient of friction). It was used to predict the slip force.

The forces, torques, position, and acceleration were acquired at 200 Hz. The images were captured at 100 frames per second at a resolution of 1696 by 1248 pixels.

### 2.2.4. Data analysis

Force, torque, and position signals were low-pass filtered (4$^{th}$ order Butterworth, zero phase-lag, cutoff 40Hz). The grip force (GF) was obtained by computing the average of the force normal to the surface from the two force sensors (along the z-axis, see Fig 2.1C). The load force (LF) is the sum of the vertical component of the tangential force from the two force sensors (along the y-axis, see Fig 2.1C). The object velocity was obtained by numerical differentiation, and the positive velocity peaks were used to split the data into individual oscillations during which different parameters were computed (mean GF, max LF, …). The vertical position of the center of pressure (COP) was obtained using $COP_y = \left(T_x - F_y . z_0\right)/F_z$, where T is torque along a given axis, F is force and $z_0$ is the normal distance between the contact surface and the sensor's surface. It measures the vertical position of the resultant force exerted by the index finger normally to the glass. The slip force (SF) is the minimum normal (grip) force needed to avoid slip. It was

obtained from the power function fit for each subject as a function of the tangential force ($TF = \mu.SF = k(SF)^n$). The GF and LF modulations were obtained for each oscillation by subtracting the minimum value from the maximum value of the specific oscillation.

### 2.2.5. Image processing

We used an image processing pipeline already described in previous work to detect the slipping regions and evaluate the surface skin strains inside the contact area (Delhaye et al., 2014, 2016). It is summarized here (see Fig 2.2C). First, the gross contact area was extracted from the background using a two-stage procedure. The first stage consists in manually depicting the contact area contour for a small subset of frames (typically 10 to 20 frames per subject). In the second stage, features relevant for the segmentation (Sankaran et al., 2017) are computed and fed to a machine learning algorithm (classification tree, *fitctree* function in Matlab) that is trained on the manually segmented data to extract the contact area and then used to extract the contact area on the whole sequence of frames.

Second, for each oscillation, three sets of features having good gradient properties for tracking (Shi and Tomasi, 1994) were sampled at the first, the middle, and the last frame of each oscillation respectively. Indeed, the contact area varies during the movement due to rolling of the fingertip, i.e. some skin parts are coming into contact and other parts are leaving contact during the active movement. It is therefore essential to re-sample features at different times to cover the contact area with features during the whole oscillation. The minimum spacing between features for feature detection was set to 17 pixels. Then, those features were tracked from frame to frame using a classical algorithm implemented in OpenCV (Lucas and Kanade, 1981; Bradski, 2008). Depending on the initial frame (first, middle or last), the features were either tracked forward or backward in time (or both). Finally, the 3 sets of features (first, middle and last) were merged, and those overlapping were suppressed. The very small glass movements that occurred due to the compliance of the force sensors and the plates (of the order of a couple of pixels) were monitored by tracking features located on a checkerboard attached to the glass. The velocity of the glass movement was subtracted from the velocity of the fingerprint movement before further analyses.

Third, a Delaunay triangulation was performed on the features from their location in the first frame. And the triangle strain rate from frame to frame

was computed as described earlier (Delhaye et al., 2016), to yield a 2-by-2 strain rate tensor for each triangle and each pair of consecutive frames (Fig 2.2C). The strain rate norm was obtained by computing the norm of the strain rate tensor for each triangle and each pair of consecutive frames. Moreover, if the triangle's center moved by more than 1/2 of a pixel between 2 consecutive frames, it was considered as slipping whereas if the movement was smaller than 1/2 pixel, it was considered non-slipping or stuck to the glass. The *stick ratio*, the ratio of non-slipping area to the total contact area, was obtained for each pair of consecutive frames.

### 2.2.6. Statistical analysis

All statistical analyses were performed in MATLAB, using the functions *corr* (for Pearson correlation), *ttest* (for paired t-tests) and *regress* (for linear regression). The power-law fits were obtained by computing the coefficients of a linear regression on the logarithmic transformation of the data.

## 2.3. Results

We asked subjects to perform paced vertical oscillations holding the manipulandum in precision grip, i.e. with the thumb and index finger (Fig 2.2B). Figure 2.3 shows the evolution of the recorded variables during a typical experimental block. A video of the fingerpad during a typical trial is also provided on Figshare[8]. The manipulandum weight was fully compensated by a counterweight, and therefore LF was only due to the object acceleration and was zero when the object was still. Thus, as expected, the manipulandum movement (Fig 2.3A) generated cyclic fluctuations in LF due to the inertial forces, and we observed two peaks of load force that were very similar in amplitude, one in the upper and one in the lower part of the trajectory. The load force variations were accompanied by variations of the grip force applied by the subjects (median correlation across oscillations, r=0.61±0.17, mean±std across subjects, n=18, see also here below and Figure 2.6), and LF peaks gave rise to synchronized grip force peaks (Fig 2.3B). These GF peaks were such that the GF/LF ratio was kept above the friction limit in most cases (in red, Fig 2.3C), and therefore the object did not slip. However, even though full slip was avoided during most oscillations, the zone of stable contact also fluctuated, as partial slip was observed and was quantified by the stick ratio (SR, Fig 2.3D), which typically reached a minimum when the constraints were maximal, that is at the maximum of LF or the minimum GF

[8] https://doi.org/10.6084/m9.figshare.15142071.v1

to LF ratio. As described earlier in a passive context (Delhaye et al., 2016), partial slip is accompanied by significant strain patterns in the slipping regions. The heatmaps provided in the bottom part of Figure 2.3 show the evolution of the three independent components of the strain rate tensor at each point of the contact area during one oscillation (Fig 2.3E). The last line shows the norm of the strain rate tensor (Fig 2.3F, see *Methods*). While it does not bear any physical meaning, the strain rate norm provides a clear picture of the distribution of the strains and their intensities inside the contact area, irrespective of the type of deformation and invariant to rotation. As expected from previous reports, the strains take place at the periphery of the contact and propagate further toward the center as the SR decreases, i.e. when the GF to LF ratio comes closer to the friction limit. As shown in a typical trace in Figure 2.3, each oscillation was isolated based on its trajectory (Fig 2.3A, see *Methods*) and analyzed separately.

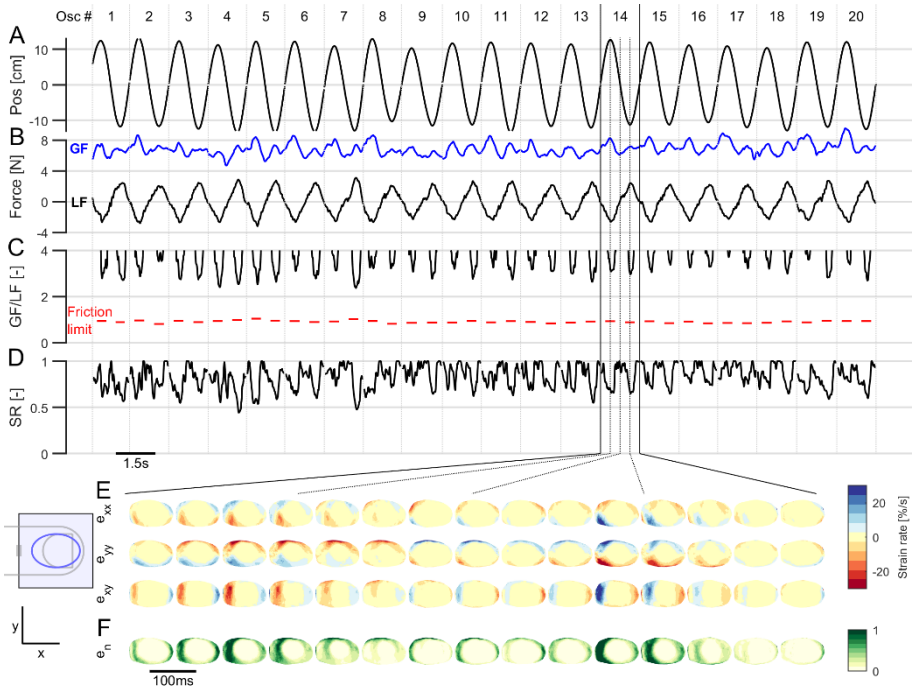


**Fig. 2.3. Typical trace. A,B,C,D|** Evolution of the manipulandum vertical position (**A|**), fingertip forces (grip force, in blue, and load force, in black, **B|**), slip margins (grip force to load force ratio, in black, and friction limit at the load force peak, in red, **C|**) and stick ratio (**D|**) as a function of time during a typical experimental block. The oscillations are delimited with vertical lines at the times of positive velocity peaks. **E,F|** Evolution of the strain rate tensors, shown as three heatmaps for e_xx, e_yy, and e_xy (**E|**), and the strain rate norm (normalized by the 90$^{th}$ percentile, **F|**)

as a function of time during a typical oscillation. The sketch of the finger on the left shows the orientation of the finger with respect to the heatmaps (strains are shown as if viewed through the finger). The red parts are negative and show compression, and the blue parts are positive and show stretch. Consecutive heat maps are separated by 100 ms.

### 2.3.1. Forces and strain patterns during oscillations

Since all signals followed a stereotyped pattern for each oscillation, we looked at the averaged evolution of the traces during all oscillations (Figure 2.4). The GF, LF, and SR patterns follow the behavior described earlier (Fig 2.4A-B, see also Figure 2.3). That is, the maximum GF and the minimum SR were observed on average at the time of the maximum LF. We also looked at the vertical displacement of the center of pressure (COP, Fig 2.4C), which is mainly caused by a redistribution of the pressure inside the contact area and the rolling of the finger. We observed that the COP moved significantly downward during the first half of the oscillation and upward during the second half of the oscillation. Even though each oscillation showed a slightly different pattern of deformation and widely different levels of minimum SR across subjects (see below), the general shape follows a trend that is expected from previous work (Delhaye et al 2016). The strain rate amplitude, as measured by the $90^{th}$ percentile of the strain rate norm across the entire contact, typically followed a trajectory similar to the variation of LF, or LF rate. Fig 2.4E shows the averaged pattern of strain rate during one oscillation for a typical subject. Since the central stuck zone is pulled up by the glass during the upper part of the trajectory (and pulled down during the lower part of the trajectory), the vertical strains (e_yy) were tensile in the lower regions of the contact area and compressive in the upper region of the contact area (Fig 2.4E). As a consequence of the elastic properties of the skin, horizontal strains (e_xx) appeared following the same pattern as the vertical ones, except that they were tensile where the vertical strains were compressive and vice versa. They were also smaller in amplitude. Finally, shear strains were substantial on the proximal (left) and distal (right) parts of the contact area. The norm of the strain rate (e_n) shows the areas of the skin where the strains are the largest, irrespective of the direction of the strains. It can be observed from those that a wave of strains progresses from the exterior of the contact area towards its center as the stick ratio decreases. In Figure 2.3, the wave of strains doesn't reach the center of the fingertip as the stick ratio doesn't reach zero.

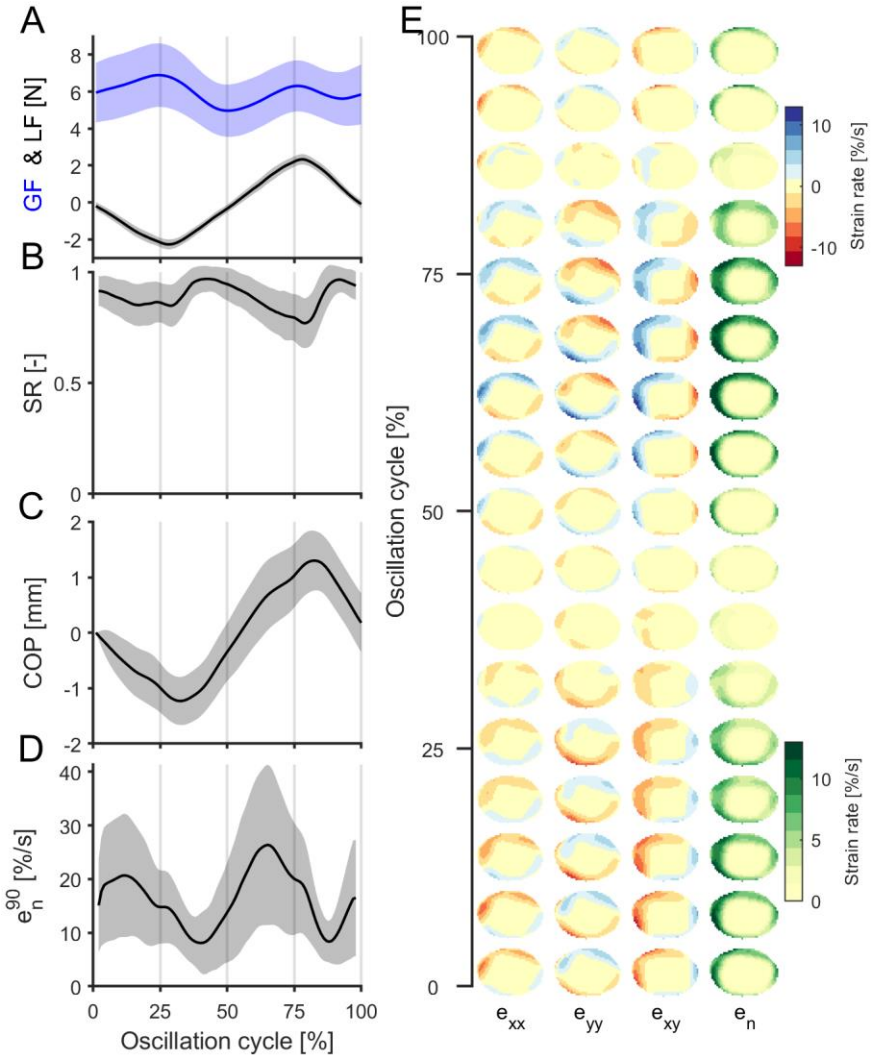


**Fig. 2.4. Oscillation averaged traces and strain rate patterns for a typical subject. A,B,C,D|** Average traces across all oscillations expressed as a function of oscillation cycle progress (in percent) for a typical subject. The forces (grip force, in blue, and load force, in black, **A|**), stick ratio (SR, **B|**), the center of pressure (COP, **C|**), and 90$^{th}$ percentile of the strain rate norm (**D|**) are shown. The shaded areas represent the standard deviations. The oscillations are cut using the positive velocity peaks and the signals are synchronized by expressing their evolutions in terms of percentage of time inside the oscillation cycle. **E|** Average strain rate patterns for a typical subject. Consecutive heat maps go from the bottom up and each column shows strain rates along a dimension. Strains were synchronized in the same way as the traces in A,B,C,D. Each strain heatmap is presented the same way as in Fig 2.3E-F.

### 2.3.2. Different levels of grip force during manipulation

Looking at subjects' gripping behavior (Figure 2.5), as described by the average GF value during one oscillation, we found that it was consistent across the entire experiment (Fig 2.5A). Indeed, even though the average grip force was on average slightly higher in the first block, this difference was not significant when compared to the last block (Fig 5B, paired t-test, $t(17) = -1.14$, $p = 0.272$). Within a block, there was a clear tendency of subjects to progressively decrease their grip force (Fig 2.5A). This was not related to a change in the movement kinematics, which should affect the load force. Indeed, even though the first two oscillations of each block seemed to sometimes generate a higher load force (i.e. faster movement), the average load force of the third movement was already at the same level as the last movement (paired t-test, $t(17) = -1.59$, $p = 0.130$). Interestingly, GF progressively decreased during the experimental block and the difference between the grip force of the third and the last movement was highly significant (Fig 2.5C, paired t-test, $t(17) = -3.67$, $p = 0.002$), as previously observed during similar experiments (Augurelle et al., 2003).

While the skin deformation patterns were similar across subjects and the grip force levels were constant across the experiment, we observed that different subjects used very different levels of grip force leading to very different amplitudes of deformations. Indeed, we found that the subjects that were instructed to use a minimum GF tended to apply an amount of GF just above the minimum required by friction, as shown by the peak in GF being just above the slip force estimated thanks to the friction measurements (Fig 2.5D). However, other subjects applied an excessive amount of GF. This is not resulting from the subject not coordinating their GF with the LF, as the subjects applying excessive GF also showed a high level of GF modulation, thereby taking into account the LF modulation (Fig 2.5E). It was rather explained by a high level of mean GF.

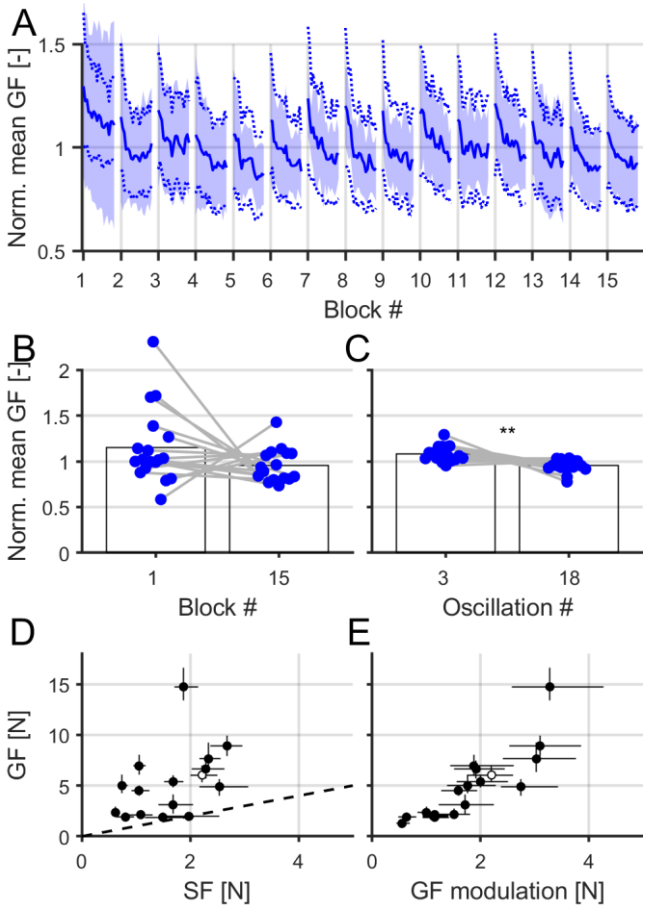


**Fig. 2.5. Gripping behavior. A|** Evolution of the mean grip force (GF) across oscillations, blocks, and subjects (n=18). For each subject, the forces were normalized by the mean across all blocks and oscillations. Lines are mean across subjects and shaded areas show standard deviation. Dashed lines show means of minimum and maximum grip forces. **B|** Comparison of grip force at the first and last block (averaged across oscillations from those blocks). **C|** Comparison of grip force at the third and 18$^{th}$ oscillation (averaged across blocks). Pairs in B and C were t-tested, significant results are marked with stars (**: p<0.01). **D|** Grip force (GF) as a function of slip force (SF) at the instant of minimum GF to LF ratio. The slip force is the minimum grip force required to avoid slipping. The dashed line is the identity line. **E|** Grip force (GF, same as in D) as a function of the grip force modulation. In **D** and **E,** one point corresponds to the median value for one subject, the vertical and horizontal whiskers show the interquartile, the empty dot corresponds to the subject shown in Figure 2.4.

### 2.3.3. Mechanical parameters related to different grip force levels

The different levels of GF that individual subjects used to perform the oscillations led to different observations about the parameters of the manipulation (Figure 2.6). First, the vertical displacement of the COP (see *Methods*) tended to strongly decrease with the grip force level (Fig 2.6A). This decrease was observed across subjects, with a relationship that followed a negative power law (Fig 2.6A left, $R^2$=0.91, F(1,16)=165.65, p<0.001, $f(x) = a.x^b$, with a=10.93 and b=-0.84). It was also observed within-subjects, with a negative correlation that was significant at the group level (Fig 2.6A, right, paired t-test, t(17) = -4.45, p<0.001). This trend was not followed for the two subjects with the lower GF values, probably because of the very small range of GF (as shown by the very small horizontal whiskers for the two blue dots in Fig 2.6A right). The skin displacement range was also quantified. It measures the maximal vertical range of motion of a fingerprint feature inside the contact area and therefore quantifies how much the skin moves within the slipping regions (Fig 2.6B, left). This variable is strongly correlated with the maximum level of skin strain rate (shown in Fig 2.6C, correlation r=0.88). Both variables decreased with the grip force, according to a power-law (Fig 2.6B, left, displacement range: $R^2$=0.63, F(1,16)=26.99, p<0.001, $f(x) = a.x^b$, with a=1.79 and b=-1.27 ; Fig 2.6C, left, strain rate norm: $R^2$=0.61, F(1,16)=25.50, p<0.001, $f(x) = a.x^b$, with a=84.37 and b=-1.04), and the negative correlation within subjects was also observed (Fig 2.6B, right, displacement range: paired t-test, t(17) = -3.55, p = 0.002; Fig 2.6C, right, strain rate norm: paired t-test, t(17) = -3.32, p = 0.004). Again, the within-subjects correlation was lower for some subjects having small variations of GF across trials.

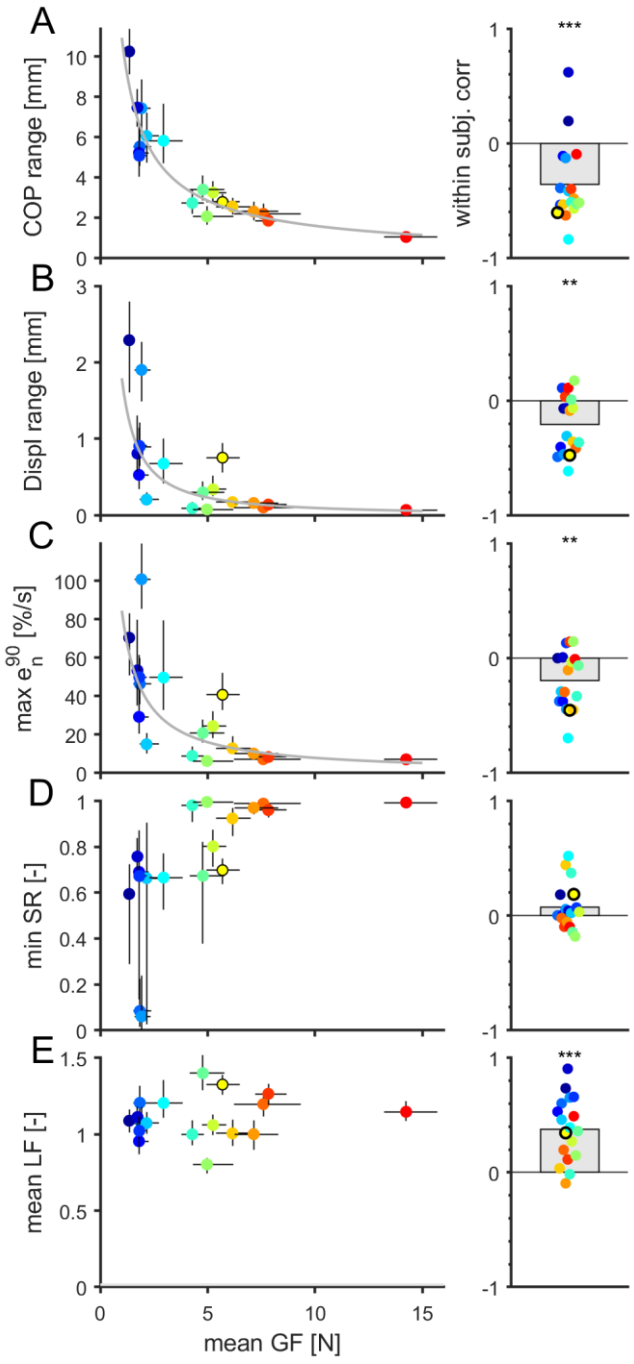


**<u>Fig. 2.6. Mechanical parameters related to behavior.</u> A, B, C, D, E|** Relationship between different mechanical parameters and the grip force (GF), namely center of pressure range of motion (**A|**), fingerprint maximal range of motion (**B|**), maximal value of the 90$^{th}$ percentile of the strain rate norm (**C|**), minimum of stick ratio (SR,

**D|**), and mean load force (LF, **E|**). Left panels show the median across all oscillations of the different parameters as a function of mean grip force (GF) across oscillations for each subject. Dots are medians, vertical and horizontal whiskers show interquartile. Right panels show the intra-subject correlation of the parameters with the grip force, with the grey box indicating the average correlation across subjects. A t-test was performed for each variable and the stars depict the result of the test (nothing, $p>0.05$; *, $p<0.05$; **, $p<0.01$;***, $p<0.001$; n=18). Colors were attributed to each subject according to the mean GF level and correspond across panels. The yellow dot with a black contour corresponds to the subject shown in Figure 2.4.

The maximal strain rates were substantial, and ranged from 6%/s to 100%/s (Fig 2.6C, left). Obviously, the maximal strain rates strongly correlated with the maximal strain values observed during an oscillation (r=0.99), which ranged from 1% to 17% depending on the subject's GF level. Finally, as could be expected, the minimum value of the stick ratio within an oscillation was low for low levels of grip force and tended to 1 for very high levels of grip force (Fig 2.6D, left). We did not observe any significant tendency at the group level in the within-subjects correlation (Fig2. 6D, right, paired t-test, $t(17) = 1.60$, $p = 0.128$). As a control, we verified that the use of a high level of grip force was not related to the level of load force, but rather to an inappropriate adjustment to friction. We found that indeed, while there were some variations in the level of load force across subjects, related to variations in the movement acceleration from trial to trial, the correlation with the grip force was low (r=0.17, Fig 2.6E, left). However, within-subjects, we observed a clear positive correlation at the group level, meaning that the subjects adapted their level of grip force to the movement kinematics (Fig 2.6E, right, paired t-test, $t(17) = 5.74$, $p<0.001$). As could be expected, this tendency was strongest for the low GF values, for which the risk of slip is higher, and therefore a tight coupling between LF and GF is required.

In summary, we showed that higher levels of GF yielded less fingertip rolling (as measured with the vertical displacement of the center of pressure), fewer skin strains (as measured with the strain rate norm) and a higher proportion of the skin remaining stuck on the glass (as measured with the stick ratio).

## 2.4. Discussion

### 2.4.1. General discussion

In this paper, we described a novel device that enables synchronous monitoring of strains in the fingertip skin in contact with a manipulated

object and the forces exerted by the fingers on the object. The device was tested in an experiment involving 18 subjects and permitted to describe and quantify the strain patterns emerging from active object manipulation. This is the first study showing that substantial skin strain rates (>50%/s) take place inside the contact area during active manipulation, even though the object is in a stable, non-fully slipping contact and the object never dropped from the hand of the subjects.

The development of this device was inspired by a previous publication presenting a much simpler apparatus (Tada et al., 2002). This equipment was also manipulated in a precision grip and comprised force sensors under each finger and a camera to monitor the stick ratio, which relied on 167 manually drawn points on the fingertip to monitor skin displacement from frame to frame. Importantly, our setup has a much higher resolution (64 pixels per mm) and therefore enables an accurate measurement of local skin strains, which was not possible earlier.

Given the substantial amplitude of the strain rates measured in this study, it is reasonable to assume that those strains can be faithfully captured by the tactile afferents, and in particular the FA-I afferents (fast adapting type I afferents). Indeed, we recently demonstrated, in a passive setup, that FA-I afferents are sensitive to the compressive strain rates related to partial slip, comparable in scale to those observed here (Delhaye et al., 2021a). Those strains therefore likely provide tactile feedback about grip safety (Khamis et al., 2014).

There was a wide range of mean grip force levels used by different subjects observed in this study. Some subjects tended to apply a grip force level just above the friction limit while some others exerted a much higher grip force. Those behaviors lead to very different feedback. The “safe” strategy – exerting a high level of grip force – leads to a very limited amount of partial slip and a low level of deformation. Therefore, it also provides a limited amount of information related to contact stability. The “risky” strategy – using a grip force level just above the friction limit – leads to a large fraction of the contact area in partial slip and substantial strain rates inside the contact. Therefore, this strategy enables rich tactile feedback about the contact state at each oscillation.

While there was a clear relationship between the level of grip force and the amount of skin strains (Fig 2.6C), there was also a large variability. This variability can be explained by individual differences in skin properties.

Indeed, the fingerpad can have very different mechanical and geometrical properties: stiffness (Wang and Hayward, 2007), humidity (André et al., 2010), size (Peters et al., 2009), and all of those likely influence deformation and perception (Peters et al., 2009; Gueorguiev et al., 2016).

### 2.4.2. Limitations

The developed device has some limitations. First, for a device that is intended to be used in precision grip, that is pinched between the thumb and index finger, its mass is rather large (around 500 grams). This limitation can be compensated by a counterweight, as done in this work, but it modified the weight/inertia relationship of the object, which makes it more remote from natural object manipulation. The manipulation of an object with no weight but high inertia, as done in the present study, is comparable to object manipulation in weightlessness in terms of contact forces with the object. Furthermore, due to the counterweight setup, we are limited to vertical movements. In addition, we used smooth transparent glass. While this is a very convenient material for imaging the skin-object contact, the flat contact with a glass surface is very different from the rough contact experienced with most natural objects.

As summarized above, some subjects tended to use a high level of grip force, much higher than the friction limit. This contrasts with previous work showing that, under normal sensory feedback, people tend to manipulate objects with a grip force close to the slip limit (Augurelle et al., 2003). This might be explained by three factors. First, the instrumented object might look fragile and subjects tended to apply excessive GF levels to make sure not to drop it. Second, by compensating the weight of the object with a counterweight (see *Methods*), the experienced weight is much lower than the one expected from the object appearance and size, which may surprise the subjects. As a result, it is likely that an excessive GF is exerted by caution. Moreover, there is a discrepancy between the perceived weight of the object, which is zero, and the interaction force resulting from the doubled inertia. Therefore, it cannot be excluded that the motor system might have determined the object weight through its inertial parameters and attempted to set the grip force accordingly. Finally, glass remains a material having particular frictional properties, with a coefficient of friction that can vary by up to one order of magnitude depending on several factors (Pasumarty et al., 2011; Adams et al., 2013; Delhaye et al., 2014), and might therefore encourage higher safety margin even if not needed.

## 2.5. Conclusion

The device developed in this study will enable the monitoring of fingertip skin strains at the finger-object contact and provide a window into the feedback from tactile afferents inside the contact area during manipulation. Future work will test if unexpected changes in the object parameters, such as a change in friction, can be quickly detected and accounted for thanks to the feedback provided by partial slip.

CHAPTER 3

# Fast grip force adaptation to friction relies on localized fingerpad strains

*"To invent your own life's meaning is not easy, but it's still allowed, and I think you'll be happier for the trouble."*

*Bill Waterson*

Humans can quickly adjust their grip force to a change in friction at the object-skin interface during dexterous manipulation in a precision grip. To perform this adjustment, they rely on the feedback of the mechanoreceptive afferents innervating the fingertip skin. Because these tactile afferents encode information related to skin strain, the nature of the feedback signaling a change in friction must somehow originate from a difference in the way the skin deforms when manipulating objects of different frictions. To better characterize the origin of the underlying sensory events, we asked human participants to perform a grip-lifting task with a manipulandum equipped with an optical imaging system. This system enabled to monitor fingertip skin strains through transparent plates of glass that had different levels of friction. We observed that, following an unexpected change in friction across trials, participants adapted their grip force within 370ms after contact with the surface. By comparing the strain patterns when unexpectedly switching from a high to a low friction condition, we found a significant increase in skin strain inside the contact area arising over 100ms before the motor response, during the loading phase, suggesting that local and partial strain patterns before lift-off are used in the nervous system to adjust the grip force as a function of the frictional condition.

## 3.1. Introduction

In a seminal paper in the 80s, Johansson and Westling described how efficiently human participants handle objects of different textures and friction (Johansson and Westling, 1984). They observed that when lifting objects, humans scaled their grip force (GF) to the frictional properties of the surface, such that an object with a slippery surface was gripped more firmly than one with a sticky surface. Moreover, it was found that a change in the frictional properties of the object from one trial to the next elicited a GF adaptation that was observable only 100ms after contact with the surface. Such adaptation was canceled under local anesthesia, underlining the essential role of afferent feedback (Westling and Johansson, 1987; Nowak et al., 2001; Augurelle et al., 2003; Witney et al., 2004). A rapid feedback loop is thus able to take into account tactile afferent information about the surface efficiently (Johansson and Flanagan, 2009; Delhaye et al., 2018).

However, the mechanisms underlying such a feedback loop remain unknown. Indeed, since the surfaces used in the aforementioned paper (Johansson and Westling, 1984) had very different textures, it is not clear whether the feedback provided by the afferents was related to the topography of the material, thereby quickly eliciting the recall of a motor memory related to the surface, or if the feedback was directly related to friction, such that the motor system could scale the GF accordingly. Notably, it was later demonstrated that humans can adapt to changes in friction (Birznieks et al., 1998), even those that are not directly associated with a change in texture (Cadoret and Smith, 1996). In this study, different textures and coatings were used to show that humans adjust the level of GF to the coefficient of friction and not to the texture when lifting objects. These results suggest that the skin strain during each lifting movement can be used to scale the grip force without necessarily requiring a full slip event.

The possibility that humans adjust their grip force quickly based on an estimate of friction is supported by recent imaging studies of fingertip strain during loading. We and others have shown that localized partial slips take place at the object-finger interface during tangential loading (Levesque, 2002; Tada et al., 2006a; André et al., 2011; Delhaye et al., 2014). Partial slips are associated with substantial skin strains in the contact area (Delhaye et al., 2016) that trigger strong afferent responses (Delhaye et al., 2021a), and may therefore signal an impending slip. Importantly, reducing friction accelerates the progress of partial slips and leads to an earlier discharge of the tactile afferents, which can potentially inform the central nervous system

about the upcoming contact instability (Khamis et al., 2014; Delhaye et al., 2021a). Moreover, the perception of tactile slip seems to be induced by skin strains associated with partial slip, since it is perceived before full slippage and is impeded when the amount of strains is diminished by applying a coating that reduces friction (Barrea et al., 2018). Furthermore, generating artificial skin strains at the contact interface with the object during lifting also leads to an increase in GF (Farajian et al., 2020).

Taken together, the aforementioned findings lead us to hypothesize that partial slip, or the associated skin strains, are a sufficient sensory signal to adjust the GF to the friction condition during active manipulation. To test this hypothesis, we sought to describe and quantify where and when skin strains associated with partial slip take place following an unexpected change of friction, and if those allow participants to adapt their GF to a change in friction that is not associated with a change in texture. To this end, we used a validated custom-made manipulandum able to record interaction force and skin deformation at the contact area between the object and the finger (Delhaye et al., 2021b). We asked human participants to repeatedly grip and lift a manipulandum, while the friction was changed unbeknownst to the participant (Fig 3.1B). We found that participants adjusted the GF to a change in friction only 114ms after liftoff (370ms after contact was made with the surface), suggesting that most of the sensory information about the friction change was available before the object started moving. To further understand the mechanisms underlying such adjustments, we imaged, at the same time, the contact area between the index finger and the object. We used those images to track the skin strains resulting from partial slip (Fig 3.1F-G), and reveal a localized strain contrast after friction changes very early in the trial, i.e. before liftoff. Our findings thus support the hypothesis that humans make use of localized strain patterns to adjust the GF to unexpected changes in friction.

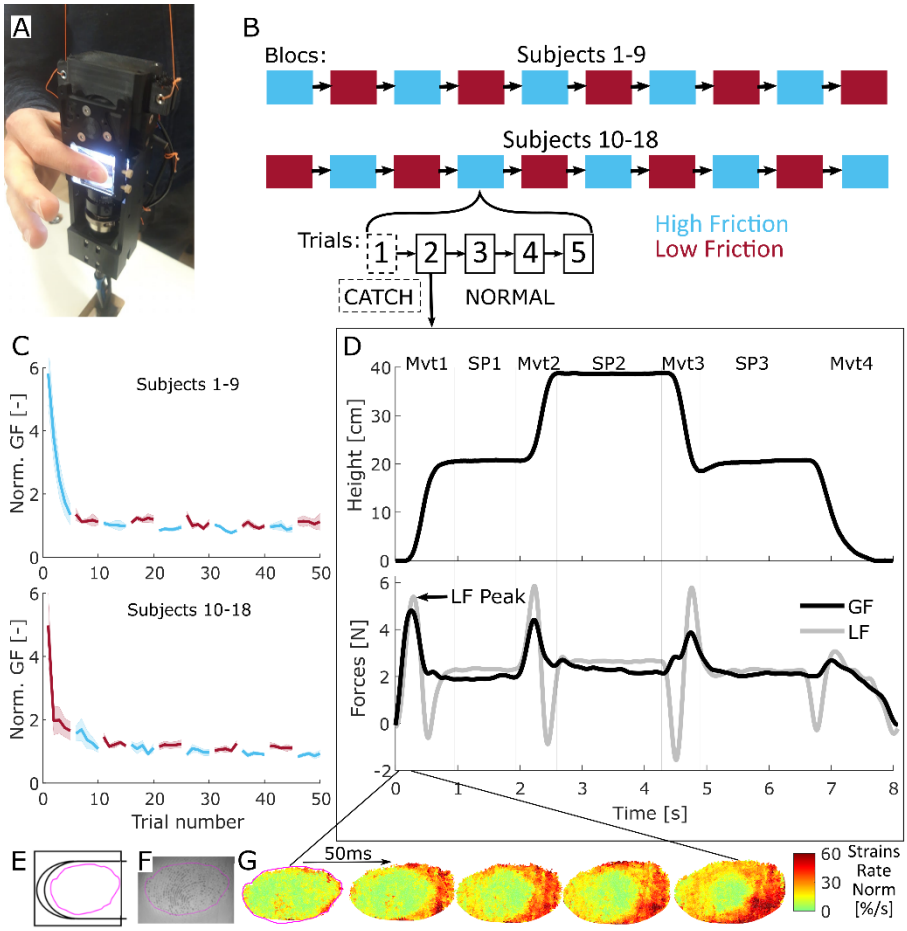


**Fig 3.1. Experimental setup, experimental procedure, and typical trial. A|** Participants held the manipulandum in a precision grip with both fingers applied on transparent glass plates. The device includes sensors allowing the measurement of the forces applied by both fingers as well as an imaging system allowing the recording of the index fingertip skin. **B|** Participants performed ten blocks of five trials. Transparent plates with high and low friction properties were interchanged between each block. Half of the participants started with the high friction material. The first trial of each block is called "CATCH" trial, as opposed to "NORMAL" trials. **C|** Group mean of the GF of the first SP for participants who started with the high friction material for the top graph and for participants who started with the low friction material for the bottom one. GF is normalized according to the procedure described in *Methods*. The shaded areas show the standard error of the mean. **D|** Evolution of the vertical position of the manipulandum and the forces applied during a typical trial. It consists of four fast movements (**Mvt**) with static phases (**SP**) in-between. Note that the second LF peak of each movement is due to the participant having to slow down the manipulandum because of the inertia of the system. The LF

during the second static phase is slightly higher due to a larger portion of the cable being positioned under the device at this height. **E|** Position of the index finger and area of contact with the glass. All strains in this study are displayed as if they were observed through the glass during the manipulation. The distal side is on the left. The pink curve delimits the contact area. **F|** Typical image. Only the index finger was monitored. **G|** Heat maps of the norm of the skin strain rates obtained from a pair of consecutive images, as described in (Delhaye et al. 2016). This sequence shows strains during the first 200ms of a typical first movement (Mvt1 in panel C). Strains are observed at the periphery of the contact area. The central stuck zone remains undeformed.

## 3.1. Methods

### 3.1.1. Participants

Eighteen volunteers (5 females; ages 20-65) participated in the experiment. All of them provided written informed consent to the procedures and the study was approved by the ethics committee at the host institution (UCLouvain, Brussels, Belgium).

### 3.1.2. Apparatus

At rest, the device was standing on a table with a hole to allow the passage of the cables coming from the bottom of the device. Its weight (540g) was partially compensated by a counterweight (320g) attached to a system of pulleys. The device is described at length in a recent publication(Delhaye et al., 2021b). Succinctly, forces were measured under each fingertip using two six-axis force and torque sensors (ATI Mini27 Ti, ATI-IA, Apex, NC, USA). From those measurements, the GF and LF were computed, as described in *Data Analysis*. The position was measured using an optical distance sensor (DT20-P224B, SICK Sensor Intelligence). The position and forces were sampled at 200 Hertz with a NI-DAQ card (NI6225, National Instruments).

A custom optical system allowed to image the index fingerprints in contact with the glass (Fig 3.1F). Because of constraints in the design of the manipulandum, it was only possible to monitor one side, as the light is emitted by an array from the side where the thumb is, blocking its observation. This system is based on the principle of Frustrated Total Internal Reflection and enables a high contrast between the point in contact with the glass and those that are not. Images are recorded at 100 fps with a camera (GO-5000M-PMCL, JAI, monochrome, 2560 x 2048 full pixel resolution).

Image size is 1696 x 1248 pixels with a resolution of 4096 pixels/mm², which corresponds to an area of 26.5 x 19.5mm.

Two kinds of glass plates were used to generate different levels of friction. The first set of plates are simple transparent optically flat plates of glass. They are referred to as "high friction". A process called "glass frosting" was used to alter friction in the second set of plates. In brief, a chemical process was used to imprint a nanoscale pattern on the surface of the glass. With the right set of parameters (height and roughness), this decreased the real area of contact between the finger and the plate and thus the coefficient of friction (Derler et al., 2009; Skedung et al., 2010, 2011; Adams et al., 2013; Wiertlewski et al., 2016; Inamoto and Tomeno, 2019). This nano-structured glass was referred to as the "low-friction" surface. The transparent plates are indistinguishable to the naked eye.

### 3.1.3. Experimental procedures

Participants stood in front of a table on which the device was positioned. After an auditory cue, they were instructed to grip and lift the device to a height of about 20cm within 0.8s, and then hold it still for 1.5s. They then performed three fast point-to-point movements (0.8s) with pauses (1.5s) in-between. Auditory cues were used to pace each movement. We observed that participants' movements were slightly slower than what was instructed, resulting in slightly longer movements and shorter static phases. The participants were requested (and often reminded during the experiment) to use a minimal amount of GF. Indeed, we observed in a preliminary study that participants tended to use an excessive amount of GF naturally, probably because this device composed of a camera and sensors seems fragile and looks heavy. The glass plates were cleaned with alcohol after each trial. This served the purpose of getting images as clean as possible. Also, this procedure removed sweat that could alter the topography of the glass plates at a microscopic level and thus the level of friction. After each block of five trials, participants were instructed to take a break on the other side of the room, from a location where they could not see the experimenter manipulating the device. During that break, the experimenter interchanged the plates such that the friction was changed from high to low or from low to high. This procedure was quick and took a maximum of 2 minutes. Half of the participants started with the high friction condition and the other half with the low friction. This caused no difference in their adaptation to friction, as measured by the difference in GF between conditions during the first static phase of normal trials (t-test, $t(15)=0.36, p=0.72$). The coefficient of friction

was measured for each material at the end of the experiment (see *Friction Measurement*). In total, the experiment lasted between one and a half and two hours for each participant.

Friction measurements. We measured the coefficient of friction between the participants' fingers and both materials at the end of the experiment using the method described in (Barrea et al., 2016). Briefly, participants were instructed to rub their index finger and thumb on the glass plates for three periods of fifteen seconds at different levels of normal forces. The approximate range of normal forces for each period was 0 to 2.5N for the first, 2.5 to 6N for the second, and 6 to 10N for the third. The moment of slippage was detected by finding the maximum of the ratio of tangential force over normal force at the start of each rubbing motion. This ratio was measured and was our estimation for the static coefficient of friction corresponding to the normal force applied at that moment. The data were obtained for both fingers of all participants (see Supp Fig 3.1-2) and fit with a negative power law (André et al., 2009). From the fits, we computed a single coefficient of friction value for each participant and each material for the 1-5N range that corresponded to the approximate range that the participants used for manipulation. The friction was averaged across both fingers. The measurement of the friction was always performed first on the material with which the participant finished the experiment.

### 3.1.4. Data analysis

Forces and position data were filtered with a fourth-order low-pass Butterworth filter with a cut-off frequency of 40Hz. The GF is defined as the mean of the norm of the forces normal to the surface of the object exerted by each finger. The LF is defined as the norm of the sum of the forces applied tangentially to both surfaces by each finger. When comparing dynamics or kinematics between participants as in Fig 3.3, 3.4 and 3.5, an average curve was first computed for each participant by first synchronizing all trials on the maximum of LF for each separate movement. Then, statistics such as the inter-subject mean or standard error of the mean were computed based on these average curves.

GF normalization. As participants typically used different levels of GF, a normalization procedure was used when comparing the GF signals across conditions and participants. A GF normalization value was obtained for each participant by taking the mean of GF during the first static phases of all

normal trials (except the first two blocks that were excluded because of the learning period). They are shown in Supp Fig 3.3.

Image processing. A previously described image processing pipeline was used to evaluate the skin strains from the raw images (see Delhaye et al, 2014, 2016). This pipeline is only summarized here. First, a custom-made machine learning algorithm was used to detect the area of contact between the finger and the glass plate for each image. This algorithm was trained for each participant separately with manually detected areas of contact for randomly selected images. Then, feature points were selected automatically from several frames of the sequences of images (at the beginning, during, and at the end of each movement). Their position was tracked forward and backward in time from frame to frame using an algorithm of optical flow (Lucas and Kanade, 1981; Shi and Tomasi, 1994). A Delaunay triangulation was then computed and the evolution of the shape of the triangles allowed to measure the local strain rate along three dimensions (vertical, horizontal, and shear strain rate). The norm of the strain rate was calculated as follows:

$$\varepsilon_n = \left\| \begin{matrix} \varepsilon_{xx} & \varepsilon_{xy} \\ \varepsilon_{xy} & \varepsilon_{yy} \end{matrix} \right\| = \sqrt{\varepsilon_{xx}^2 + \varepsilon_{yy}^2 + 2\varepsilon_{xy}^2} \quad (1)$$

where $\varepsilon_{xx}$, $\varepsilon_{yy}$ and $\varepsilon_{xy}$ are the horizontal, vertical, and shear strains rates components respectively. This gave a quantitative measure of how the different parts of the fingertips were being deformed, irrespective of the type and directions of these strains. In this study, we were mostly interested in comparing the amount of strain rate according to the condition of friction and the adaptation of GF rather than the specific description of these strains(Delhaye et al., 2021b).

As different participants showed markedly different levels of strains, we normalized the strain rate norm of each participant by the mean value of the strain rate norm across the entire area of contact and trials at the time of maximum LF. The normalization values of the strain rate norm are given together with the normalization value of the GF for each participant in Supp Fig 3.3.

The first images of the contact were difficult to interpret. Indeed, the fingertip skin can be rough and stiff on a small scale, depending on the moisture content of the individual's skin. When it enters in contact with a stiff surface such as glass, the initial real area of contact is low. However, during the first tens of milliseconds of the contact, moisture secreted by the sweat pores hydrates the skin, rendering it softer and elasticizing it. The skin

then enters in closer contact with the surface and the real area of contact increases (Pasumarty et al., 2011; B. Dzidek et al., 2017; Bochereau et al., 2017). As a rapidly changing real contact area not associated with skin strains was problematic for the interpretation of the results of our image-processing pipeline, we decided to discard the images directly following the time of contact between the skin and the surface from our analysis. We used the first image of the loading phase, defined as the moment when a participant starts applying tangential force to lift the object after the pre-loading phase (Westling and Johansson, 1984) as the first image in our image processing pipeline. This guaranteed that the apparition of moisture would only play a negligible role in our measurement of strains and that the strains caused by the vertical lifting of the object would be included in our analysis.

Strain rate summary across participants. To get a summary of strain rates across trials and participants, we first had to project the values from the triangulation used to compute the strains to a standardized structured grid common for all participants. To that end, we first created a reference ellipse with a major to minor axes radii ratio of 3/2. A gridded mesh of size 91x61 was attached to this reference ellipse. Then a least-square procedure was used to fit ellipses on the coordinates of the fingerprint contact area contour for all individual images (Fitzgibbon et al., 1999). Finally, we computed the projection (offset, scaling, and rotation) from the ellipse obtained from the image at the instant of the LF peak to the reference ellipse for each trial and movement. This projection, obtained for each trial and movement, was applied to the center of each triangle for all images to obtain strains on the reference ellipse. The maximum of LF was chosen to compute the projection because this timestamp is used to synchronize the trials. At that instant, the area of contact between the finger and the glass has already plateaued. After having applied this projection, the strain rate norm was averaged for each participant and each condition (i.e. catch/normal and low/high friction). An example of such data for a typical participant is presented in Supp Fig 3.4. Subsequent statistics on strains across participants were performed on the projected data.

Inspection and sorting of trials. As mentioned in *Results,* the first two blocks were considered to be "training blocks" as the participants' GFs decreased significantly during those for all participants and were thus excluded from the data analysis (Fig 3.1C). The third block was the first included in our analysis because it was the first for which (1) the grip forces were on average smaller than in the next one in the high friction condition

and (2) the grip forces were larger than in the next one in the low friction condition. For some trials, participants placed their index finger outside of the field of the camera or displaced it outside of the field during the trial due to slipping or rolling. Some trials were therefore not included in the analysis. Only the parts of the trials where the finger got out of the field of the camera were removed. After a close inspection of each trial, 99 out of 720 were at least partly removed because the images were unusable during some part of the trial. Those trials were still used for the kinematics and dynamics analysis of Fig 3.2-4. Also, 15 participants were used for the image and forces analyses of Fig 3.5 because two participants had very dry skin and the image quality was insufficient to obtain reliable strain data.

Full slip trials. To get a different look at our data, we counted the proportion of trials for which a full slip occurred during the first movement, which yielded the following results: a full slip occurred in 11.33% of the high friction normal trials, 12.75% of the low friction normal trials, 11.77% of high friction catch trials, and 31.03% of low friction catch trials. A full slip is said to occur when all the feature points whose positions are tracked from frame to frame are measured as moving with respect to the glass. This result is consistent with the differences in strain that are shown in Fig 3.5 B and C. That is, in some cases, the strain wave reached the central point of the contact. Note that even if full slip occurred for some trials, the extent of slippage was small and was quickly stopped by a corrective GF (slipping distance of the central part of the contact area of 0.19±0.25mm, mean±std, for trials in which the full slip was reached). The full slip trials were included in the strain analysis like all other trials. Full slips were reached before the minimal interval of time needed for the sensory feedback to reach the central nervous system defined by the grey box of Fig 3.5A a smaller number of times: in 3.52% of the high friction normal trials, 4.02% of the low friction normal trials, 7.46% of the high friction catch trials and 14.04% of low friction catch trial.

### 3.1.5. Statistical analyses

All statistical analyses were performed with MATLAB, using the functions *corr* (for Pearson correlation), *ttest* (for paired t-tests), and *tinv* (inverse of Student's T cumulative distribution function). The test performed, the number of degrees of freedom, and the T-statistics are always mentioned with the p-value.

## 3.2. Results

Participants performed a series of grip and lift trials using a custom-made manipulandum held in a precision grip (Fig 3.1A). Following an auditory cue, they were instructed to grip and lift the object vertically to reach a target (movement, "Mvt1" in Fig 3.1D), and then hold it stationary for one and a half second (static phase, "SP1"). This task was followed by three up and down movements that are not analyzed in this study (Mvt2- 4, and SP2-3, also paced by auditory cues, not analyzed here). After each experimental block consisting of five trials, the participants were asked to sit on a chair with their back turned away to the experimental set-up, and the experimenter quickly interchanged the surfaces without the participants noticing (Fig 3.1B). Two sets of glass plates having different levels of friction were used (see *Methods*). We defined the first trial following a surface change as a "catch trial", since it included an unexpected change in friction, and the other four trials were called "normal trials". The first two blocks were considered to be "training blocks" as the participants' GFs decreased significantly during those for all participants and were thus excluded from the data analysis (Fig 3.1C).

The manipulandum was equipped with force sensors that allowed us to monitor the GF and the load force (LF, acting vertically and due to the object weight and inertia). A typical point-to-point movement was accompanied by two LF peaks, related to the acceleration and deceleration phases of the movement (Fig 3.1D). Note that each upward LF peak was paired with a GF peak. We synchronized all trials at the instant of the first LF peak. During the static phases, LF remained fairly constant (2.2N, the object's weight) as did GF.

The index fingertip contact with the object's surface was monitored through the glass plates using a high-speed, high-resolution camera (Fig 3.1E-F). Image processing techniques allowed us to track fingerprint movements and evaluate surface skin strains during the lift movement (Fig 3.1G, (Delhaye et al., 2014, 2016), see *Methods*). The rate of change of skin strains resulting from LF increase during the lift of the manipulandum was observed at the periphery of the contact area (Fig 3.1G). In most trials, the center of the fingertip remained stuck and non-deformed, except when full slip was reached (87 times out of 633, or equivalently 14% of trials). The contact area was an approximately ellipsoidal shape and increased over time following a logarithmic increase consistent with previous observations (André et al., 2011). On average, the contact area reached 85% of its maximum value

200ms after the time of contact and had usually reached its maximum value 340ms after initial contact (value reached: 94.4±5% of the maximum value, mean±std). This time corresponded to an average of 30ms before liftoff.

### 3.2.1. Consistent difference in friction between smooth transparent materials

First, we verified that the two materials showed a consistent difference in their coefficient of friction. To that end, the friction between the fingertips, index and thumb, and the two sets of plates was measured at the end of the experiment to reduce potential cues about the different materials that could have been used during the manipulation task. Note that all participants except three reported that they did not notice that different materials were used. Following ((Barrea et al., 2016), see *Methods*), we characterized the coefficient of friction over a range of GFs relevant to our experiment (see Fig 3.2). The data were obtained for both fingers of all participants (and are reported in Supp Fig 3.1 for the index and Supp Fig 3.2 for the thumb) and fit with a negative power law. We observed that the coefficient of friction of the low friction glass remained lower than the one of the high friction glass across all levels of normal force tested, as shown in Fig 3.2A for a typical participant. From the fits obtained for each participant, we summarized the coefficient of friction by a single value, being the average coefficient of friction over the range of 1 to 5N (which spans the levels of GF used in this study, see e. g. Fig 3.1D), and across fingers. Overall, the friction was always higher in the case of the high friction material and the average relative difference was larger than 20% (paired t-test, $t(17)=10.0696$, $p<0.001$) (Fig 3.2B-C). Given that we aimed to observe behavioral adaption to changes in friction, we required a sufficient difference between materials and set a lower bound to a relative difference of 10%. Accordingly, one participant was removed from all subsequent analyses because the relative friction difference was too low (only 2%, less than the 10% required, see the unfilled dot in Fig 3.2B-C, participant S1 from Supp Fig 3.1-2). In summary, then, the two flat and transparent materials used in this study showed a consistent difference in friction, on average 23% across participants.

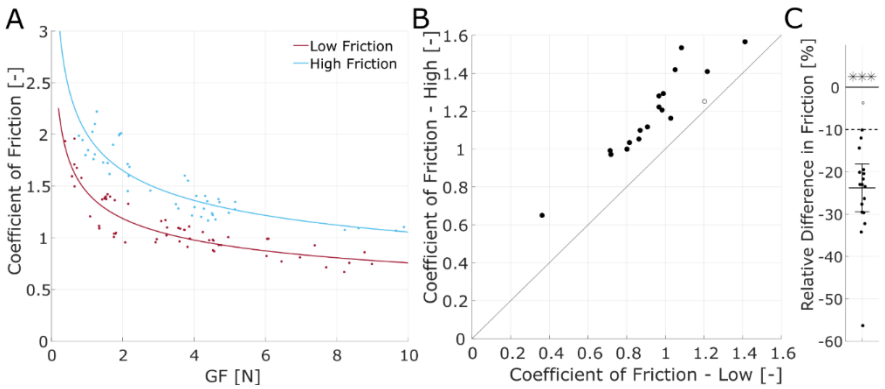


**Fig. 3.2. Consistent difference of friction. A|** Coefficient of friction of the index finger as a function of grip force for a typical participant obtained using the method described in (Barrea et al. 2016). **B|** Mean coefficient of friction of both materials over the observed manipulation range (1-5N) for each participant (n=18). **C|** Difference in friction of the materials over the manipulation interval (1-5N), relative to the mean of the values of the coefficient of friction of both materials. The brackets show the 95% confidence interval of the mean. The dashed line indicates the level of sufficient difference in friction between materials for a participant to be included in the study. In panels B| and C|, one point corresponds to one individual participant and the data were averaged across both fingers and the empty circle shows the participant that was removed from the following analysis because of a difference of friction smaller than 10%.

### 3.2.2. The grip force is adjusted to friction

Next, we sought to assess whether the different materials elicited different gripping behavior. First, we tested if participants could adapt to the difference in friction by using a consistently higher GF for the lower friction during the normal trials, i.e. those not following an unexpected change in friction. We found that indeed, most of the participants used a higher level of GF for the lower friction as averaged over the three static phases (Fig 3.3A), even though the level of GF varied widely across participants. Overall, the relative difference was statistically significant and close to 15 % (Fig 3.3B, mean 14.87±12.7%, paired t-test, $t(16)=4.8224$, $p<0.001$). Thus, participants spontaneously adjusted the GF level to the friction condition. Moreover, the relative GF difference was of the same order of magnitude as the relative friction difference. We observed that the participant that was removed from the analysis because of a lack of difference in friction showed no significant difference in behavior across the friction conditions (diff=2%, as measured by the average level of GF during the static phases of normal trials).

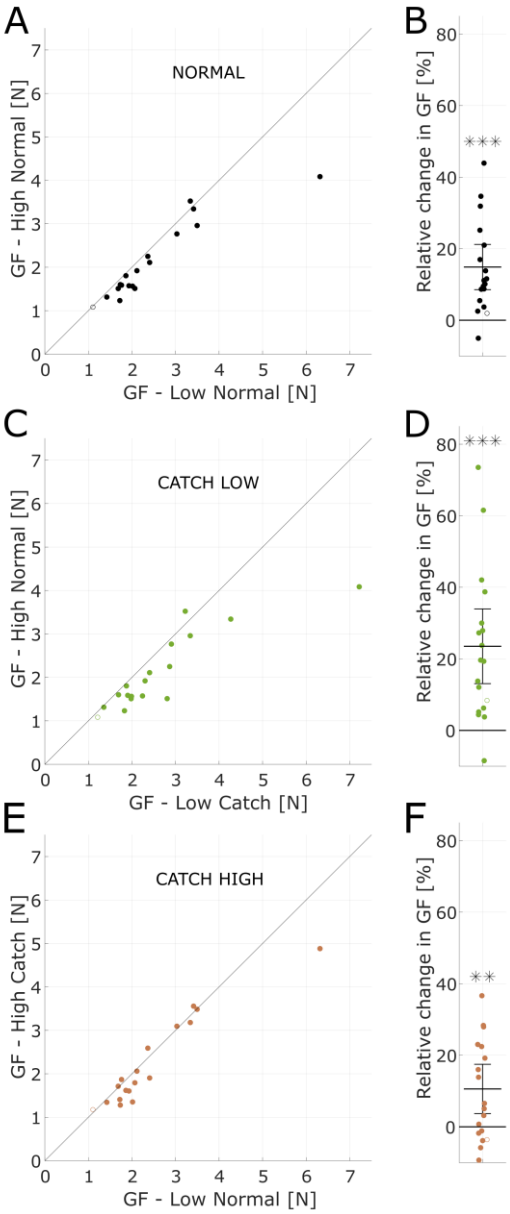


**Fig. 3.3. GF adaptation to friction during the static phases. A|** Mean value of the GF for each material during the static phases of normal trials for all participants (n=18). **B|** Change in the mean value of the GF from the high to low friction material during the static phases of normal trials, relative to the mean value of the GF in both friction conditions. The brackets show the 95% confidence interval of the mean. **C, D|** Same as A, B|, except the static phases of the high friction normal trials are compared to the first static phase of the low friction catch trials, which directly follow. The bar delimited with hashed lines indicates the catch trials. **E, F|** Same as C, D|, except the

static phases of the low friction normal trials are compared to the first static phases of the high friction catch trials, which directly follow. For D| and F|, the percentage of change is relative to the mean of the values of normal and catch trials. The participant that is removed from the study due to a low difference of friction is shown with an empty circle and is not included in the means and confidence intervals shown.

### 3.2.3. Catch trials show GF adjustment within the first movement

Having observed that there was indeed a GF adaptation to friction for normal trials, we then tested if a change in friction elicited a quick adjustment of the GF, as observed in the first static phase of the catch trials. To that end, we compared the static GF after the first movement (SP1, Fig 3.1D) of the catch trials to the static GF experienced and learned during the normal trials of the preceding block of trials associated with the material with different frictional properties. The catch trials could be of two types: (1) low friction catch trials, following an adapted exposure to high friction, were referred to as “catch-low”, and (2) high friction catch trials, following an adapted exposure to low friction, were referred to as “catch-high”. The difference or change between those two conditions really point out to the effect of a change in friction.

For the “catch-low” trials, which required an urgent increase in GF because the drop of friction increased the risk of slip and drop of the object, we found that the GF was already higher during the first static phase (Fig 3.3C-D, paired t-test, $t(16)=4.5486, p<0.001$). The adaptation was close to 20%, thus already of the same magnitude as the adaptation learned throughout many trials (Fig 3.3B). Then, we looked at the “catch-high” trials, for which the urgency was lower since the experienced surface friction increased and therefore the risk of slippage was lower than for the directly preceding trials. We also found that the GF changed after only one movement, although the relative difference of GF was about 10% on average, thus not as large as for the catch trials in the other direction. Although this difference was not observed for all participants, it was statistically significant (Fig 3.3E-F, paired t-test, $t(16)=3.1527, p<0.01$).

In brief, participants adapted the GF to the friction condition, and this adaptation was already present at the end of the first movement following catch trials, and for both directions of the changes in friction.

### 3.2.4. Grip force adjustments start close to the time of catch trials

Since we observed that the GF was already adjusted to the friction level after the first movement of catch trials, we investigated the temporal evolution of the GF during these catch trials to determine when the changes in GF evoked by the change in frictional properties arise (Figure 3.4). The participants produced movements with very similar kinematics across conditions, as shown by the height and LF curves, which could not be distinguished across conditions (Fig 3.4, top two rows of panels A and B). We observed that GF curves of the catch trials progressively diverged from those of the normal trials (Fig 3.4A-B, third row). In these graphs, the GF were normalized according to their average values during the first static phase for each subject (values reported in Supp Fig 3.3).

For the "catch-low" trials (Fig 3.4A), we found that the GF difference reached statistical significance very early, just after liftoff (114±23ms delay), or 50ms before the peak of LF (Fig 3.4A, bottom row). This timing corresponded to 308±80ms after initial contact. This difference was substantial, as it peaked on average at 40% with respect to GF during the first static phases of the normal trials.

For the "catch-high" trials (Fig 3.4B), the difference in GF reaches statistical significance later in the movement (540ms after the peak of LF, 709±20ms after liftoff, and about 902±74ms after initial contact) and is relatively smaller at the end of the first movement, as seen previously (Fig 3.3).

Importantly, note that participants tended to apply a slightly higher level of GF at the very beginning of the contact of catch trials no matter the sign of the friction change (i.e. catch-low or catch-high), which might be explained by the short break between blocks. This GF increase is better observed in Fig 3.5A. This increase is also very similar across the two conditions, as no significant difference were observed until 70ms after the peak of LF, when participants can start using tactile cues to adjust their GF (see next section). This systemic increase of the GF at the start of new blocks, similar regardless of the actual friction condition, suggests that participants did not anticipate the friction for the catch trials, and that the adjustment was purely made based on the sensory feedback.

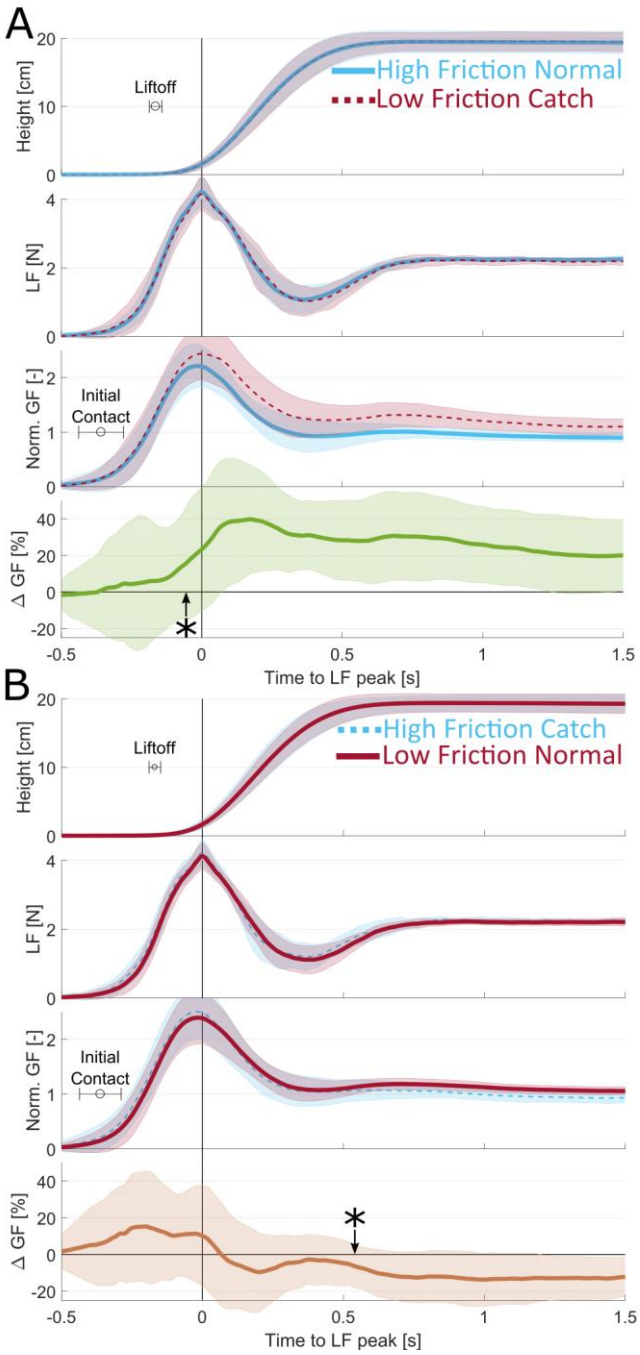


**Fig. 3.4. Adaptation to friction during the first movement of catch trials A|** Evolution of object height, LF, GF, and GF difference as a function of time for the first movement of catch-down trials for all participants (n=17). Trials are synchronized to the LF peak. Lines are averages across participants and shaded areas are the standard

deviation. 0s indicates the time of the maximum of Load Force. Blue is for high friction and red is for low friction. Thick continuous traces are normal trials and dashed lines are catch trials. GF normalization values are reported in Supp Fig 3.3. The star shows the time of the statistically significant difference between GF curves ($p<0.05$). The lower panel shows catch minus normal trials. **B|** Same as A for the catch-down trials.

In summary, we showed that GF reaches a level that is significantly different from the level of the normal trials during the first lift following a change in friction, around the time of liftoff for the "catch-low" and a bit more than half a second later for the "catch-high" trials.

### 3.2.5. Subtle contrast in skin strain rate before liftoff are cues for GF adjustments

Looking at the Δ GF traces (Figure 3.4A-B, bottom rows), we can observe an upward inflection for "catch-low" trials, and a downward inflection for "catch-high" trials, happening around the LF peak and suggesting that the corrective behavior kicks in around that time. To probe the timing of the reaction of the participants to the change in friction, we thus looked at the rate of change in GF (see Fig 3.5A).

In Fig 3.5A, we first show the catch-low and catch-high Δ GF traces zoomed in a 600ms time window centered on the LF peak, which appeared to be the instant of inflection of the curves. The time derivatives of those curves are also shown below in Fig 3.5A. Note that in this figure, in contrast to Fig 3.4, we excluded the data from two participants having consistently poor image quality and we also only included the trials in which the images reached high-quality standards (84% of trials among the remaining participants, see *Methods* for more details). As observed in Fig 3.5A, the two Δ GF traces followed very similar trends just after contact and started to diverge around the LF peak. We found that the Δ GF rates start to diverge significantly 10ms after the time of peak LF (or 370±76ms after initial contact or 176±21ms after liftoff), suggesting that online corrections to friction arise around this moment. Note that this is also approximately the time when the Δ GF rates become statistically significantly positive, or negative, for the "catch-low" trials, or the "catch-high" trials, both 20ms after the LF peak. The Δ GF traces diverged significantly only 70ms after the peak of LF, showing that participants did not anticipate a change in friction at the start of catch trials.

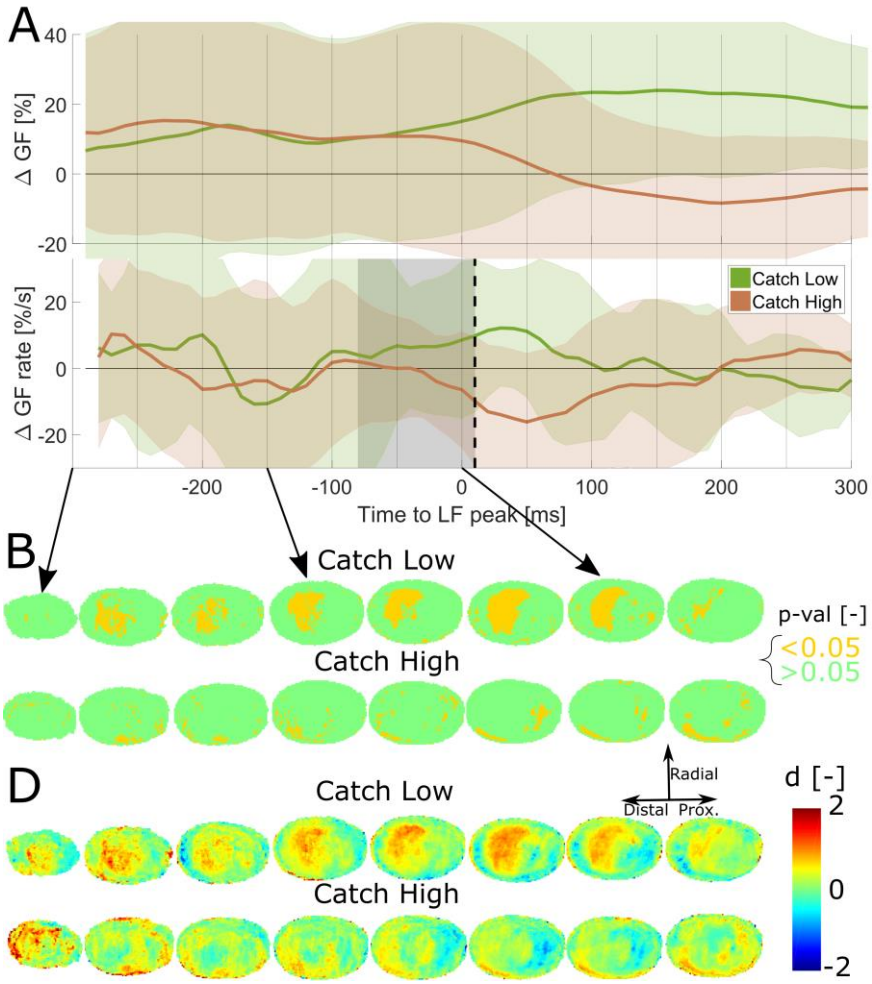


**Fig. 3.5. Differences in skin strains preceding the force adaptation A|** Mean difference of GF and mean difference of GF rate between catch and normal trials. Only participants for whom the images were of sufficient quality are included (n=15). 0ms indicates the time of the maximum Load Force. Shaded areas are the standard deviation. The vertical dashed line indicates the time when the differences of Grip Force rates are statistically significantly different from each other (10ms). The grey zone indicates the time during which tactile information was too close to the motor reaction to contribute to detecting the friction condition. **B|** Heat maps showing the areas where the deformations are statistically significantly different between conditions. A Student test with was used ($t(14) < 2.145$, alpha = 0.05). The first line compares normal high friction trials to catch-low friction trials and the second line compares catch-high friction trials and normal low friction trials. **C|** Heat maps of the effect-size of the differences in strains between catch and normal trials. The red color

indicates higher strains in the case of the catch trial and the blue color higher strains in the case of the normal trial.

The different responses of participants to catch-low and catch-high trials suggest that a sensory signal informative about the frictional properties of the material originated before this time. We further needed to take conduction delays into account, which for tactile-motor responses are close to 90ms on average. Accordingly, we drew a grey box that encompasses the 90ms before the instant of significant difference to indicate the minimal interval of time needed for the sensory feedback to reach the central nervous system and trigger a motor response (Pruszynski and Johansson, 2014; Pruszynski et al., 2016; Crevecoeur et al., 2017). Thus, to trigger a motor reaction observable just after the LF peak, a sensory signal must be readily observed before the beginning of this grey box (i.e. 80ms before LF peak).

Accordingly, we evaluated the skin strain associated with partial slip during a period encompassing 300ms before the LF peak until 100ms after (see Supp Fig 3.4). In the same manner, as for the GF, we report here the contrast between the catch and the normal trial, looking for a difference that might have triggered a corrective behavior. In Fig 3.5, we report the differences in strain rate norm between the different conditions (catch-low, top row and catch-high bottom row), as expressed in the form of a p-value, obtained from paired t-tests performed for each pixel over the whole fingertip contact area (see Methods). In Fig 3.5C, we report the differences in strain rate norm between the different conditions (catch-low, top row and catch-high bottom row), as expressed in the form of an effect size, obtained from paired t-tests performed for each pixel over the whole fingertip contact area (see Methods). Red zones show the parts of the fingertip where strain rates were significantly higher for the catch trials, i.e. where a significant excess of strain rate was observed, whereas blue zones show parts of the contact having a significantly lower strain rate for catch trials. Strains were first normalized according to their average value at the time of peak LF (see *methods* for more details and Supp Fig 3.3 for normalization values). This normalization procedure was performed because subjects showed markedly different average levels of strains.

For “catch-low” trials shown in the top row of Fig 3.5B, a zone of excess strain rate norm in the distal part of the center of the fingertip starts appearing 250ms before the maximum of LF and is consistently observed until the LF peaks. This excess disappears progressively when participants

start to adapt their GF to the level of friction and when the general level of strain rate becomes small. Conversely, some smaller zones in the periphery show lower levels of strain rates. Thus, surprising the participant with a material with friction lower than for the previous trials generates a consistently higher level of strain rates deeper inside the contact areas while leaving the periphery less strained at some places. This striking observation is valid over the span of several hundred milliseconds and can thus be taken into account by participants when adjusting their GF.

For the “catch-high” trials shown in the bottom row of Fig 3.5B, we do not observe any large zone of difference in strain rate norm. Some patches in the more central part tend to show lower levels of strains rate norm. The sensory signal is less contrasted in the case of “catch-high” trials suggesting that the GF decrease might be an automatic slow decrease following a light GF excess applied because of a new block. A typical “catch-high” and “catch-low” trials are provided in the supplementary video. These show that the strain rate reaches a higher level deeper in the surface of contact in the case of “catch-low” trials.

As the observed strain contrasts take place before the grey zone defined earlier, they can contribute to the information used by the participants to adapt their GF to the condition of friction.

In summary, we observed the onset of a motor response resulting from the friction change approximately at the moment of the LF peak and this online GF correction was consistent with a sensory signal resulting from an increase in the strains closer to the central parts for the contact area happening over 100ms before the motor response. This subtle but essential sensory signal, therefore, explains GF adaptation to changes in friction.

## 3.3. Discussion

This is, to our knowledge, the first study that quantifies how fast humans can adjust their GF to a change in friction in the case of flat transparent surfaces. We demonstrate that this adjustment can be based on a local strain pattern that takes place in the contact area with the manipulated object and signals an insecure grip. Specifically, we show that when confronted with lower friction than expected, skin strains advance deeper and faster in the contact area. The differences in skin strains with respect to a normal trial are already significant very early after the initial increase of the load force, and more than 100ms before the motor response, which is a reasonable delay to

explain it (Macefield and Johansson, 2003; Crevecoeur et al., 2017). These differences are present over a period of time of several hundred milliseconds and can thus constitute a warning signal that allows the central nervous system to adjust the GF to the friction condition.

We observed that the levels of skin strains varied greatly from participant to participant, as can be seen by the strain rates normalization values in Supp Fig 3.3. We have shown similar levels of variation of skin strains in a previous study where participants had to perform oscillations in a precision grip (Delhaye et al., 2021b). We can also observe in that study that a larger amount of skin strains is linked to a lower stick ratio and that the stick ratio also varied greatly between participants. The stick ratio was also measured in a study where participants had to perform a grip-lifting task (Tada et al., 2002). The authors hypothesized that humans control the level of GF to maintain a constant amount of partial slip (~40% of the contact area) when lifting objects of known friction and weight, but they mentioned in their paper that the validness of this hypothesis has to be verified, as only three participants were tested. It is worth noting that humans perceive slippage at very different levels of partial slip in a passive setting (Barrea et al., 2018). The variability in the levels of strains and stick ratio during manipulation and the variability in the partial slip between participants seem to point towards strategies of manipulation that vary from person to person. This requires further inquiring, by performing experiments with tasks of different nature, with varying friction and weight of the manipulated object. A characteristic of our results is the asymmetry of the participants' behavior between "catch-high" and "catch-low" trials (Fig 3.4). Although the motor reaction seemed to be triggered at the same time in both conditions (Fig 3.5A), it took more time to reach a level of GF that was adapted to friction in the catch-high condition. It is worth noting that a short reaction time in the catch-low condition is critical: it is urgent to increase GF since not correcting it could lead to a dramatic slip and drop of the object. In contrast, the excessive GF in the catch-high trials only results in a temporary slight excess of energy expenditure, which does not require to act quickly. The difference in urgency to adapt GF between conditions is observed in the differences of strains (Fig 3.5 B-C), where a surprisingly low level of friction caused significant differences in strains whereas a surprisingly high level of friction did not.

Although we characterized the friction between the fingers and the manipulated object by a constant scalar value per participant-condition pair (Fig 3.2B-C), this is clearly a gross approximation of a very complex

phenomenon. The tribology of the skin is complex and varies significantly at different temporal and spatial scales (Pataky et al., 2005; Adams et al., 2013; Van Kuilenburg et al., 2015). One aspect of this complexity is related to the complex geometry and mechanics of the finger: the fingertips are composed of several layers, from the bone in the interior of the fingertip to the epidermis in the exterior. The epidermis of the glabrous skin is characterized by the presence of ridges and furrows that form the fingerprints and present a complex topography (Choi et al., 2021). This complex geometry and mechanics is likely to impact the friction on a trial-to-trial basis, depending on how the finger contacts the object. Another aspect of the complex tribology of the skin is that it evolves over time: Sweat pores are present at the surface of the skin and produces humidity at the interface that heavily impacts the level of friction when gripping a material, which changes over the course of several seconds (André et al., 2010; Yum et al., 2020). The occlusion phenomenon defines humidity evolution and plasticization of the skin when in close contact with the material for a few seconds (Adams et al., 2013). The level of friction thus varies during a single trial as moisture varies due to occlusion. In our experiment, the moisture level is however probably partially maintained when trials are close enough to one another. Thus, in the context of this study, the differences in friction measured between materials, which could vary widely between participants, are to be considered as approximations of their actual values, which can vary during manipulation. However, it is clear that the difference in friction between materials was consistent and sufficient to generate coherent adaptation of GF during the overall experiment.

Several of our senses are used when performing a task as difficult as fine object manipulation. Our sense of touch in particular is very important. It sends critical information to the central nervous system to adjust GFs to various parameters of the manipulation such as friction. We have shown that when gripping and lifting small objects, the skin strains depended on the level of friction at the interface of the contact. The localized differences in skin strains between conditions during the loading phase were consistent with the timing of the first signs of adaptation of the GF and were sufficient to explain them. We have quantified and described those skin strains and measured the GF modulation, which started less than 500ms after the initial contact.

## 3.4. Supplementary figures

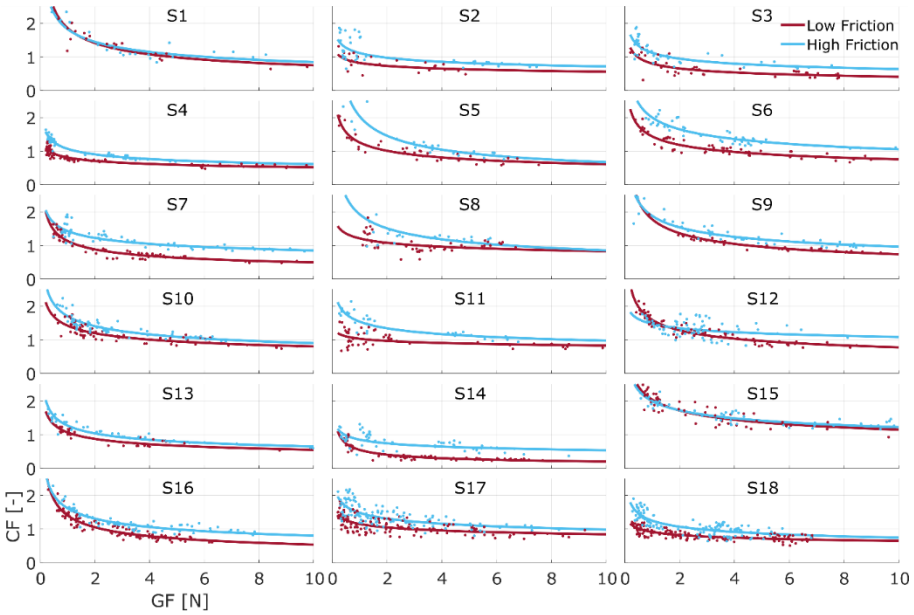


**Supp. Figure 3.1. Coefficient of friction of the index finger for all participants**

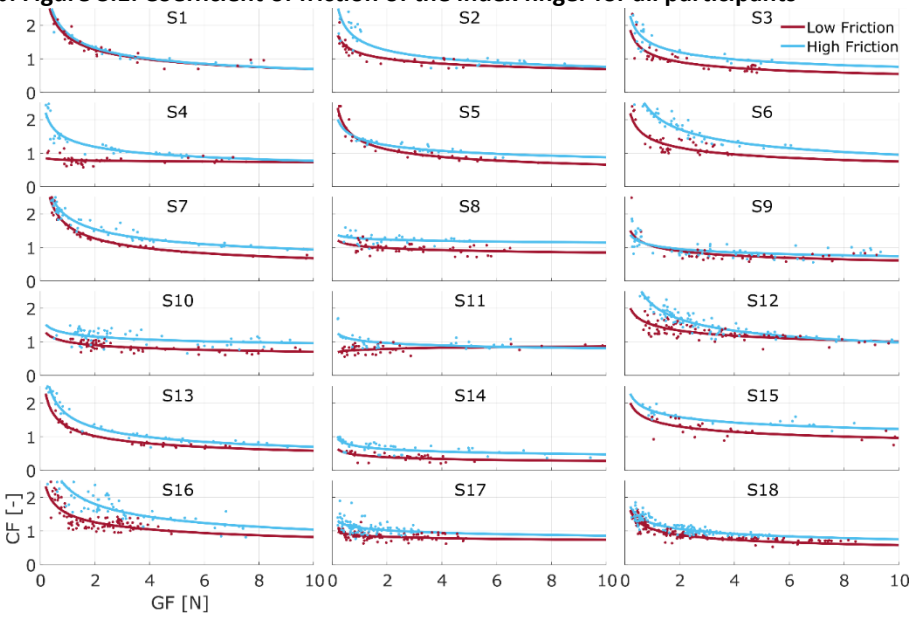


**Supp. Figure 3.2. Coefficient of friction of the thumb for all participants**

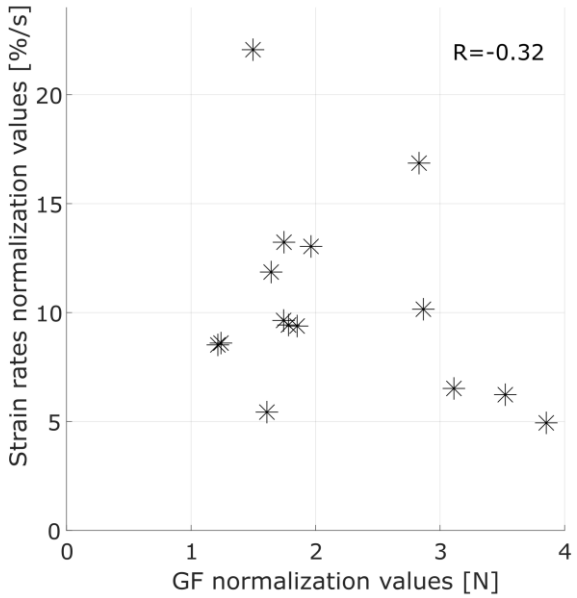


**Supp. Figure 3.3. Normalization values for the GF and strains**

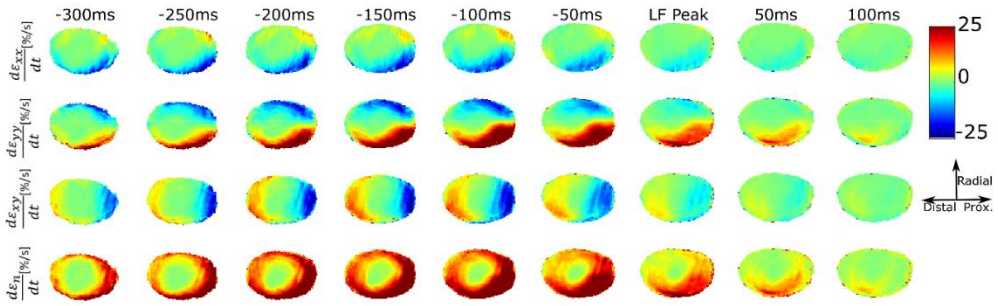


**Supp. Figure 3.4. Averaged strain rate data on the standard grid during the first movement for a typical participant.** Compression is shown in red and dilation in blue. The first row shows the horizontal strain rate, the second shows the vertical strain rate, the third shows the shear strain rate and the fourth shows the strain rate norm. The average was computed over all normal high friction trials (n=15) for a typical participant.

CHAPTER 4

# Grip Force is adjusted at a level that maintains an upper bound on partial slip across friction conditions during object manipulation

*"-You can't just turn on creativity like a faucet. You have to be in the right mood.*

*-What mood is that?*

*-Last minute panic."*

*Calvin & Hobbes – Bill Waterson*

Published as: Félicien Schiltz*, Benoît P. Delhaye*, Philippe Lefèvre and Jean-Louis Thonnard, "Grip Force is adjusted at a level that maintains an upper bound on partial slip across friction conditions during object manipulation", in IEEE Transactions on Haptics. (*) equal contribution.

Dexterous manipulation of objects heavily relies on the feedback provided by the tactile afferents innervating the fingertips. Previous studies have suggested that humans might take advantage of partial slip, localized loss of grip between the skin and the object, to gauge the stability of a

contact and react appropriately when it is compromised, that is, when slippage is about to happen. To test this hypothesis, we asked participants to perform point-to-point movements using a manipulandum. Through optical imaging, the device monitored partial slip at the contact interface, and at the same time, the forces exerted by the fingers. The level of friction of the contact material was changed every five trials. We found that the level of grip force was systematically adjusted to the level of friction, and thus partial slip was limited to an amount similar across friction conditions. We suggest that partial slip is a key signal for dexterous manipulation and that the grip force is regulated to continuously maintain an upper bound on partial slip across friction conditions.

## 4.1. Introduction

Dexterous manipulation requires to constantly adjust the grip force level to the object properties (e.g. weight, friction) and kinematics (e.g. inertial forces). In particular, the tactile system collects information about the object-skin frictional condition, such that the grip force is adequately scaled to this parameter. Indeed, a slippery surface is squeezed more firmly than a sticky surface (Johansson and Westling, 1984; Westling and Johansson, 1984; Cadoret and Smith, 1996). While tactile feedback is essential for a normal adjustment of the grip force (Augurelle et al., 2003; Witney et al., 2004), it remains unclear what is the nature of the sensory feedback responsible for the force adjustment to friction.

When passively loaded tangentially against a flat surface, the finger slips in a progressive manner, such that the periphery of contact first loses the grip and then partial slips propagate to the center until full slip is observed (Levesque and Hayward, 2003; Tada and Kanade, 2004; André et al., 2011; Delhaye et al., 2014). Partial slips are associated with substantial skin strains that are faithfully encoded by tactile afferents, suggesting that the central nervous system has access to at least some information about partial slip (Delhaye et al., 2016, 2021a). Partial slip can also be readily observed during active manipulation, and the resulting skin strains are directly related to the grip force level (Delhaye et al., 2021b). Given the stereotyped pattern of deformation associated with partial slip, it can be a very salient feedback signal for the central nervous system, since it provides a mean to continuously gauge the stability of the contact. That is, the further partial slip propagates inside the contact area, the closer to full slip is the contact, or said differently, the more insecure is the grip. Indeed, we have also recently

shown that following an unexpected reduction of friction, partial slip propagates further toward the center of contact and triggers quick grip adjustment (Schiltz et al., 2021).

Here, we asked whether grip force is continuously adjusted to maintain a similar upper bound on the level of partial slip. To that end, we asked healthy volunteers to perform point-to-point movements between targets while monitoring partial slip. Friction was changed every five trials. We found that while the amount of partial slip varied across participants, that is some participants manipulated the object with higher safety margin than others, most of them tended to manipulate the object to maintain a constant upper bound on the level of partial slip, thereby adjusting the grip force appropriately.

## 4.2. Material and methods

### 4.2.1. Experimental apparatus

We used a custom-made manipulandum with embedded optical imaging and intended to be held in a precision grip, i.e. between the thumb and the index fingers (Fig 4.1A). The device is described in detail in another publication (Delhaye et al., 2021b). Succinctly, the forces applied by the index and the thumb were measured using two force sensors (ATI Mini27 Ti, ATI-IA, Apex, NC, USA). From those measurements, the grip force (GF) and the load force (LF and LFv) were computed (see *Signals and Strains Measurements*). The mass of the device was 540g and it was partially compensated with a counterweight of 320g, resulting in a static load force around 2.2N (apparent weight). An optical distance sensor (DT20-P224B)

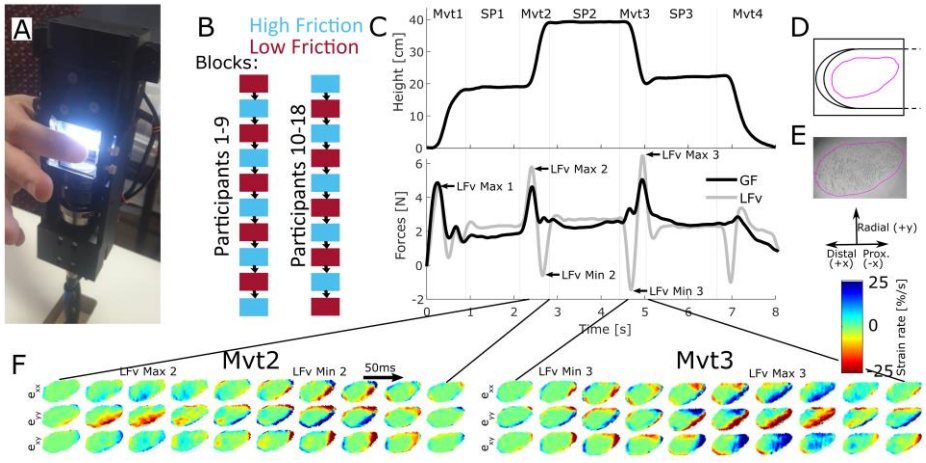

measured the vertical position of the manipulandum. The position and forces were sampled at 200Hz with a NI-DAQ card (NI3225, National Instruments).

**Fig. 4.1: Experimental setup, experimental procedure, and typical trial. A**| The manipulandum, held in a precision grip. **B|** The friction was alternated after every block of five trials. Half of the participants started with each friction condition. **C|** Position and forces during a typical high friction trial, which consisted of a grip-lifting task followed by three point-to-point movements. Note that the weight of the device was partially compensated with a system of pulleys. **D|** Schematics of the position of the index finger relative to the reader for strain rates heat maps. **E|** Typical image of the fingertip obtained with the device. The delimitation area of contact is shown in purple. **F|** Typical strain rates during movement 2 and 3, corresponding to the typical trial in C. Blue corresponds to dilation and red to compression. The time of min and max LFv are indicated above the corresponding strain rates maps.

The index fingerpad skin in contact with the glass was imaged using a custom optical system (Fig 4.1D-E). This system uses the principle of frustrated total internal reflection which results in a high contrast between the parts of the skin in contact with the glass and those that are not, thus giving a detailed image of the fingerprint ridges. Images are recorded at 100 fps with a high-resolution camera (GO-5000M-PMCL, JAI, monochrome, 2560 x 2048 full pixel resolution). Image size is 1696 x 1248 pixels, which corresponds to an area of 26.5 x 19.5mm, with a resolution of 4096 pixel/mm². Those images enabled to monitor the partial slips (see below).

Two kinds of glass plates with different levels of friction were used. One of them was optically flat glass, and the other had a treatment such that it displayed roughness at the nanoscale level, changing the real area of contact between skin and the glass plate and thus reducing the coefficient of friction (Derler et al., 2009; Skedung et al., 2011; Adams et al., 2013; Inamoto and Tomeno, 2019).

### 4.2.2. Experimental procedure

Eighteen participants (5 females, ages 20-65), took part in the experiment. They all provided written informed consent to the procedure and the study was approved by the ethics committee at the host institution (UCLouvain, Brussels, Belgium). They stood in front of the table on which the device was standing. Each trial consisted of a grip-lifting task followed by three vertical point-to-point movements (one up and two down, see Fig 4.1C), each of which had an amplitude of 20cm. The experimental procedures have already been described in greater details in a previous publication that

analyzed the grip-lift movement only (Schiltz et al., 2021). The procedures are therefore only summarized here. Auditory cues were used to pace each movement (0.8s) and pause between movements (1.5s). The glass plates of different friction were interchanged after each block of 5 trials (Fig 4.1B). Half of the participants started the experiment with the high friction condition and the other half with the low friction condition. Participants were instructed to apply a minimal level of GF while still avoiding slippage of the device. Ten blocks of five trials were performed, for a total of fifty trials.

Note that a part of the data, namely the first lift of the object, is described in a separate study (Schiltz et al., 2021).

At the end of the experiment, the coefficient of friction was measured by using the method described in (Barrea et al., 2016). Briefly, participants rubbed their index and thumb back and forth on the glass plates at different levels of normal forces. The ratio of tangential force over normal force at the moment of slippage was used as an estimation of the coefficient of friction as a function of the normal force. The average of this function over the interval of manipulation (1-5N) was used as a scalar coefficient of friction value for each individual subject, as in Fig 4.5. The measures of the coefficients of friction are provided in (Schiltz et al., 2021). The coefficients of friction were different for each material-participant pair, but were consistently higher for one of the two materials for each participant. However, one participant was removed from the analyses because the friction measurements showed no difference between the two materials and two others because the quality of the images obtained did not allow precise measurements of strains. In the context of this study, we omitted trials 1 to 10 because learning had a large influence during those. We also omitted the first trial of each block to diminish the influence of the previous block friction condition.

### 4.2.3. Signals and strains measurements

Force and position data were collected with a sampling rate of 200Hz and filtered with a fourth-order low-pass Butterworth filter with a cut-off frequency of 40Hz. The Grip Force (GF) is defined as the mean of the norm of the forces normal to the surface of the object exerted by each finger. The Load Force (LF) is defined as the norm of the sum of the forces applied tangentially to the surfaces by each finger. LFv is defined as the sum of the vertical component of the forces applied by the fingers tangentially to the surface of contact. As the levels of GF were markedly different across

participants, in some analyses, GF was normalized (i.e. Fig 4.2), by dividing it by the average value of GF during the first static phase across all trials for each participant. Normalization values are provided in (Schiltz et al., 2021).

The images were collected at 100 fps. A previously described pipeline was used to measure the skin strains from the images (Delhaye et al., 2014, 2016). Briefly, the area of contact was semi-automatically detected using a custom machine-learning algorithm. Then, feature points were detected at the beginning, middle, and end of each movement and tracked forward and backward in time using an optical flow algorithm (Lucas and Kanade, 1981; Shi and Tomasi, 1994). A Delaunay triangulation was then computed and the evolution of the shape of the triangles was used to compute the local strain rate tensors, containing the two axial strain rates on the diagonal (horizontal, $e_{xx}$, and vertical, $e_{yy}$) and the shear strain rate ($e_{xy}$) off the diagonal. The norm of the tensor ($e_n$) was also computed as a measure of the amplitude of the strain no matter the orientation or the sign. In order to be able to combine strain data across participants (as in Fig 4.4), we first projected the values of the strains from the triangulation on a standardized structured mesh common for all participants that took the form of an ellipse with a major to minor axis radii of 3/2. With all the data projected on a standard grid, we could then have an average of the strains rates norms for each participant in each condition and then compare those averages using t-tests (as in Fig 4.4).

The stick ratio (SR) is the proportion of the finger contact that is not slipping on the glass. The value of the 90$^{th}$ percentile of the strain rate norm used in Fig 4.2, 3 and 6 has been described in a previous publication (Delhaye et al., 2021b). Briefly, it is a measure of the strain rate norm of the parts of the finger that undergo the largest deformation. The greater the deformations, the greater the value.

## 4.3. Results

First, we describe typical strains rates patterns during point-to-point movements (Fig 4.1). Next, we describe how the kinematics and the dynamics changed according to the friction condition and observe that the grip force adapted to the friction condition during movements and static phases. We also describe the evolution of the stick ratio (SR) and the amplitude of strain rates (Fig 4.2). Next, we analyze the variables related to partial slip, such as the stick ratio and the amplitude of strain rates and we show that the grip force adjustment allowed to keep them unchanged

despite the change in friction at the times of max LFv 2 and 3 (Fig 4.3). After that, we compare the deformations according to the ratio of GF over LF and observe that when the ratio is lower, more deformation takes place (Fig 4.4). Moreover, we map those differences of deformations. Then, we observe that participants with lower levels of friction show stronger adaptation (Fig 4.5). Finally, we try to link the level of stick ratio to the adaptation of grip force from one movement to the next. No significant trend is observed (Fig 4.6).

### 4.3.1. Typical trial

The evolution of the device vertical position and forces applied by a participant during a typical trial are shown in Fig 4.1C. The trial is divided into four movements and three static phases according to the kinematics during the trial. Movements 1 and 2 are upwards movements of 20cm while movements 3 and 4 are downwards movements of 20cm. Each movement is characterized by a positive and a negative peak of LFv. The first peak is related to the acceleration of the object, and the second is due to the participants having to slow down the device at the end of the motion, partly because of the counterweight and the resulting high inertia of the system.

The skin strain rates associated with movements 2 and 3 and corresponding to the trial in Fig 4.1C are shown in Fig 4.1F. The first rows correspond to the strain rates in the horizontal direction (along x), the second to the strains in the vertical direction (along y) and thus aligned with the movement, and the third correspond to the shearing strain rates. When looking at the vertical strain rates, we see that maxima of LFv are associated with compressions of the bottom part of the fingerpad while minima of LFv are associated with compressions of the top part of the fingerpad and dilation from the bottom part. As a consequence of the elastic properties of the skin, horizontal compressions take place in the parts where vertical dilations take place and vice-versa. Positive LFv peaks are associated with a larger amount of strains that go further into the contact area because of the higher value of LFv.

### 4.3.2. Kinematics, dynamics and fingerpad mechanics during movements 2 and 3

We have already established in a previous study that the level of friction is indeed different between the two glass plates, with an average relative difference of friction between conditions across participants in the interval 1-5N of 24%. We also showed that participants start adapting their GF to the new friction condition during the first movement of the first trial of each

block (Schiltz et al., 2021). We start by describing the kinematics and dynamics of the second and third movements according to the friction condition (Fig 4.2). We can observe from the vertical position (Height) and LFv traces that participants performed very stereotyped movements and that the kinematics did not change across friction conditions. The Normalized GF and ΔGF curves show that participants squeezed the device harder in the low friction condition. This observation is valid for the static phases as well as during the movements. Note that those are expressed in terms of normalization values provided in (Schiltz et al., 2021). It is interesting to note that the ΔGF increases and decreases with LFv, thus showing that participants modulated their GF with the level of friction. The difference in GF according to the level of friction was the largest at the times of maxima of LFv and thus at the times when the risk of slippage is the highest. Looking at the stick ratio (SR), we see that slippage progresses during the movement and peaks at the time of max LFv 2 and 3. The values of SR are similar in both friction conditions and follow similar profiles. The 90$^{th}$ percentile of the strain rate norm follows a particular dynamic, where a double peak occurs for both movements 2 and 3. Again, the curves are very similar across friction conditions.

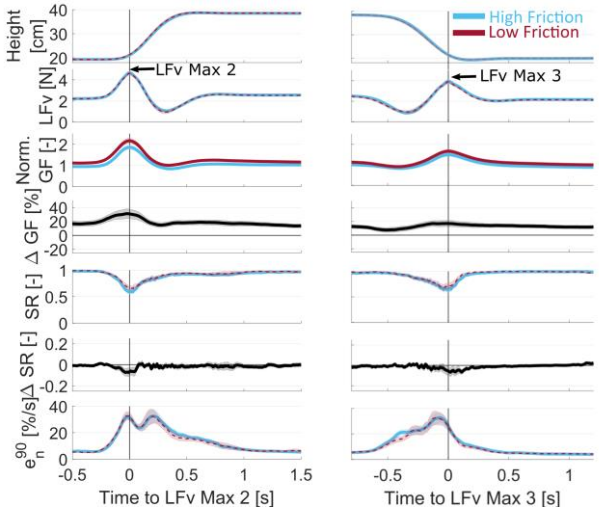


**Figure 4.2. Kinematics and dynamics during the second and third movements.** Evolution of the manipulandum position (height), LFv, Normalized GF, difference of Normalized GF, SR and 90$^{th}$ percentile of the strain rate norm during the second movement for all participants (n=15). Trials are synchronized at the time of LFv Max 2 and LFv Max 3. Shaded areas are standard errors of the mean.

### 4.3.3. Mechanical parameters remain stable across friction conditions thanks to Grip Force adaptation

Looking at Fig 4.2, we saw that participants adapt to friction by increasing their GF when it is more slippery, keep similar kinematics and that strains and SR levels remain very similar. In Fig 4.3A, we show the values of several variables of interest at the time of LFv Max 2 that describe the mechanics of the fingerpad as well as the forces applied. In the first row, each colored oblique line links the median value obtained for each participant across all trials. The second row is the difference of these median values between friction conditions for each participant. The colors of the individual points are each assigned to one participant and kept the same in all panels. They are classified from blue to red according to the ascending order of the values of ΔGF during movement 2. For movement 2 first, we observed that the GF differed across friction conditions (paired t-test, t(14)=-3.73.2, p=0.0022) even though the levels of GF varied across participants. The levels of LF also varied across participants, remained constant across conditions (paired t-test, t(14)=1.5, p=0.18). This shows that participants did not tend to change their kinematics according to the friction condition. Similarly, we did not observe any statistically significant difference across friction conditions for the strain rates ($e_n^{90}$, 90$^{th}$ percentile of the strain rate norm) (paired t-test, t(14)=-0.68, p=0.5) and for the Stick Ratio (paired t-test, t(14)=-0.32, p=0.75). As could be predicted, the GF/LF ratio differed across friction conditions (paired t-test, t(14)=-3.6, p=0.003). We can make similar observations for movement 3. Differences are observed for GF (paired t-test, t(14)=-4.36, p=0.0007) and GF/LF (paired t-test, t(14)=-3.48, p=0.004), but not for the LF (paired t-test, t(14)=-0.35,p=0.73), the strain rate norm ($e_n^{90}$, paired t-test,

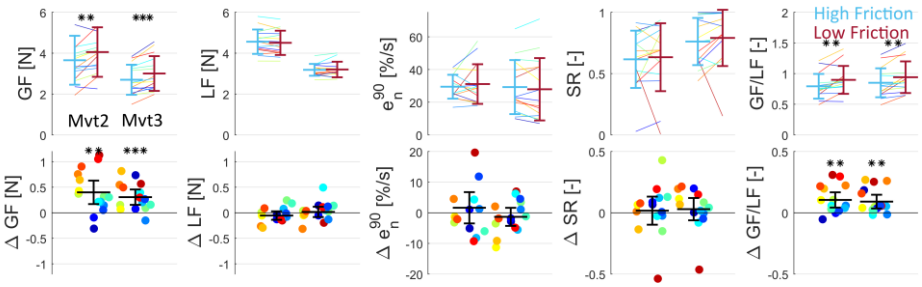


t(14)=0.97, p=0.35) and the stick ratio (paired t-test, t(14)=-0.69, p=0.5). We can thus observe that in both movements 2 and 3, when the friction changed, participants applied different levels of GF, which caused them to have similar levels of deformations and stick ratio while also keeping similar kinematics.

**Figure 4.3. Forces and mechanical parameters during the second and third movements.** Values of the GF, LF, 90 $^{th}$ percentile of strains rate norm, Stick Ratio, and GF/LF ratio at the time of the LFv max 2 and 3 (Mvt 2 and 3). In the first line, each point is the median value obtained for one participant across all trials of each friction condition. The error bars show the confidence intervals of the means. In the second line, each point is the paired difference of the Low Friction minus High Friction values of the first line. The colors of the points each correspond to one participant going from blue to red, from the lowest difference of GF to the highest at LFv Max 2. The error bars on the left and right of each panel correspond to movements 2 and 3 respectively.

### 4.3.4. Amount of strains increases when GF/LF is lower

Since we described the skin strain rates during movements 2 and 3 (Fig 4.1F) and we showed that the difference in GF between friction conditions caused the level of deformations to remain relatively similar in Fig 4.3, we investigated the effect of GF on the level of skin deformations. We compared the skin strains during movements 2 and 3, in Fig 4.4A and 4.4B, respectively. In the first row, we look at high friction trials and the second, at low friction trials. The values reported are the differences in strain rate norm between the trials with a value of GF/LF higher than the median and those with a value lower than the median, as expressed by the t-value obtained from t-tests performed for each point of the structured grid (see *Material and Methods)*. Intuitively, the blue patches show the parts where larger strains occur when GF/LF is lower, red patches where more strains occur when GF/LF is higher and green patches where the difference is not statistically significant.

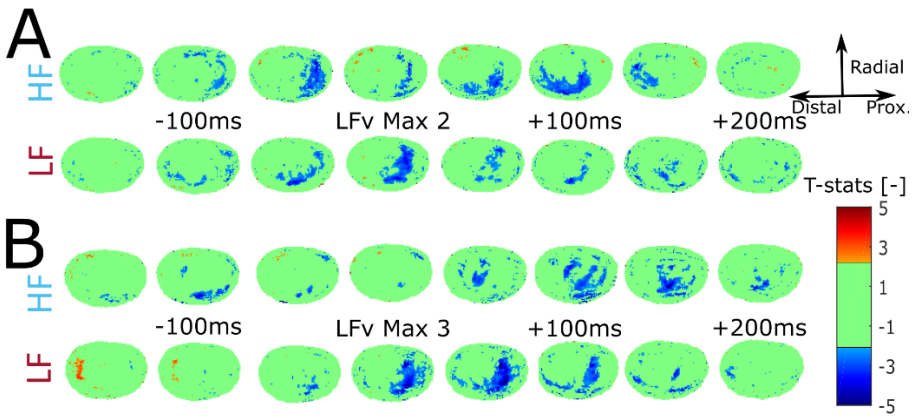


**Fig. 4.4. Differences in skin strain rates according to the GF/LF ratio A|** Heat maps of the t-statistics of the differences in strains rates between "high GF/LF" and "low GF/LF" trials during the second movement. The t-statistic is set to zero when the

difference is not statistically significant and the corresponding p-value is smaller than 0.05. The blue color indicates more deformations in the case of the "low GF/LF trials", the red color indicates more deformations in the case of the "high GF/LF trials" and the green no statistically significant difference. The first line is for the High Friction condition and the second for the Low Friction condition. **B|** Same as A, but for movement 3.

First, we can observe in Fig 4.4 that more strain takes place when GF/LF values are lower, as witnessed by the blue patches, which show the places where the finger deforms more in this case. Red patches are mostly absent, showing that when participants squeeze harder, there is almost no place in the fingerpad where more deformations take place. We can observe that the times when the largest differences in deformation take place are at the times of max LFv 2 and 3, as those are the times when there are the largest amounts of strains in general.

### 4.3.5. Participants with lower friction show more adaptation

Fig 4.5 shows for each participant the value of the coefficient of friction as a function of the Adaptation Index. The Adaptation Index is defined as the difference in the normalized GF from the low to the high friction condition. We can observe from this figure that participants who have lower coefficients of friction show larger adaptation (High Friction: $R^2$=0.27, p=0.03, Low Friction: $R^2$=0.3, p=0.02). This means that participants who have a higher risk of slippage overall tend to adapt to the friction condition more precisely.

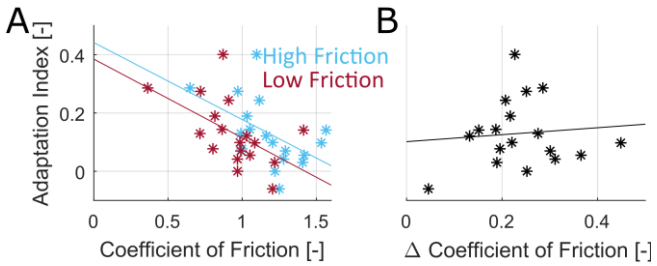


**Fig. 4.5. Coefficient of friction and Adaptation Index. A|** Values of the coefficient of friction in the high and low friction conditions as a function of the Adaptation Index. Values for the coefficient of friction are average values over the 1-5N interval of both fingers and the Adaptation Index is the difference in the normalized maxima of GF during movement 2. **B|** Same as A, but with the difference of coefficient of friction.

### 4.3.6. Level of SR is not linked to adaptation of GF/LF from one movement to the next

So far, we have found that GF/LF levels were different according to the friction condition while the amounts of strains and Stick Ratio remained similar during movement (sections B and C) and that lower levels of GF/LF caused higher levels of surface strains inside individual movements (section D). Next, we sought to determine whether the Stick Ratio or the amount of strain observed during one movement (in this case, the first movement) could cause a participant to increase or decrease their GF in the next movement. Thus, we asked if these sensory signals can be used by participants to adjust the level of GF between trials. We tested the hypothesis whether when the Stick Ratio falls at a very low level at movement 1, it causes the subject to increase GF or slow down their movement 2. To that end, we measured the difference in the GF/LF ratio from movement 1 to movement 2. The GF/LF ratio was computed at the instants of peak LFv for each movement (this instant was chosen because it corresponds to the time when the chance of slippage is the highest). Then, we looked if this change was correlated with the SR observed in the first movement (as measured by Pearson's linear correlation coefficient). Note that we used the GF/LF ratio instead of the GF alone to account for the variations of the kinematics across movements. We found that indeed for most participants, those values were negatively correlated, as witnessed by most of the colored stars of Fig 4.6 being below zero. Note that participants are ordered by ascending values of the coefficient of correlation in the left panel for clarity. This order is kept in the second panel so that the subjects can be identified across them. Most of the stars are below zero, suggesting that when SR was low during movement 1, participants tended to increase their GF/LF ratio for movement 2 and when SR was high, participants tended to decrease their GF/LF ratio for movement 2. However, for a given movement, GF and SR are also, by nature, correlated (lower GF is associated with lower SR). Therefore, our analysis is susceptible to spurious correlation. To test for such spurious effect, we shuffled the association between movement 1 and 2 across trials a thousand times, and recomputed the correlation (see shuffled data in Fig 4.6). It can be seen in Fig 4.6 that the error bars that result from the shuffling are generally also negative, showing similar levels of correlation, as indicated by the non-significant paired t-tests comparing the means of the shuffles and the actual data across participants (high friction, $t(16)=-0.59$, $p=0.56$, low friction, $t(16)=0.6$, $p=0.53$). Thus, the effect shown in Figure 4.6 might be due to spurious correlation and therefore

our analysis does not demonstrate any evidence that GF was adjusted according to the level of SR in the previous movement.

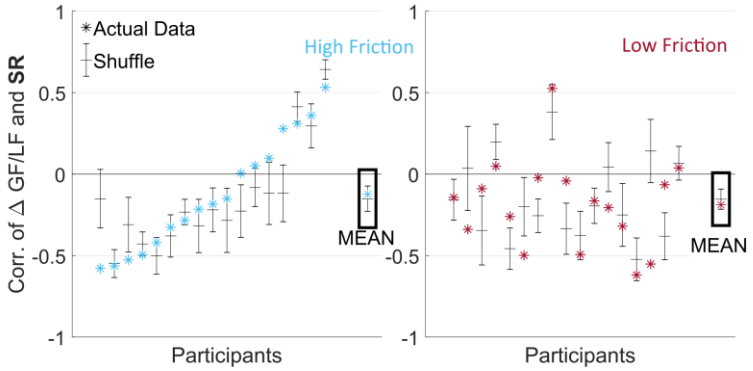


**Fig 4.6. Correlation between ΔGF/LF and SR.** The stars show the value of Pearson's linear correlation coefficient between ΔGF/LF and SR. ΔGF/LF is the difference between the values of GF/LF at LFvmax 2 and LFvmax 1. SR are taken at LFvmax 1. The boxes show the means across all participants. Error bars show the average and standard deviation for 1000 random permutations of the GF/LF of movement 2. For the means across participants, they show the standard error of the mean.

The same analysis was made with $e_n^{90}$ to see whether different levels of strain rates during movement 1 caused an adaptation of GF/LF between movement 1 and 2 (not shown here). These analyses yielded similar results. The correlations between $e_n^{90}$ and ΔGF/LF were generally positive, but not greater than when movements were shuffled (paired t-tests, high friction, t(16)=0.16, p=0.87, low friction, t(16)=-1.2, p=0.22).

## 4.4. Discussion

In this study, we have shown that, by adjusting their level of grip force, participants kept similar lower bounds on the levels of stick ratio and strain rates across friction conditions. This is consistent with the observation made in (Tada et al., 2002) that participants adjust their GF to keep similar lower bounds on the Stick Ratio when lifting objects. It is also consistent with the observation that humans detect slippage based on the level of partial slip (Barrea et al., 2018). Given that single tactile afferents signal localized strain rates during partial slip (Delhaye et al., 2021a), it is plausible that the stick ratio can be decoded at the population level (Khamis et al., 2014) during active manipulation and that the central nervous system adjusts the grip force to keep this parameter above a lower bound.

The observation that participants who have a lower coefficient of friction tend to show a better adaptation to the friction condition (Fig 4.5) might be anecdotic. However, it is not surprising since, given their low coefficient of friction, deformation of the skin will take place more easily, thus giving more information to the participant about the friction condition, as more afferents are activated. Moreover, the importance of adapting GF to the coefficient of friction will be higher for those participants, as the risk of slippage is also higher.

We have tried to assess whether the SR and the strains observed during a movement had an influence (corrective increase or decrease of GF) on the subsequent movement, but the data did not show any significant trend. The relationship between SR or the strain rates and the GF/LF ratio is not direct because several other factors, such as the position of the fingers on the glass, fingertip moisture that changes over time (Adams et al., 2007; André et al., 2011), non-linear behavior of the skin (Pailler-Mattei et al., 2008) also play an important role. The changes in SR and strain rates in the present study that allow the adjustment of GF are much more minute since they are far from causing a full slip as the safety margin is not compromised and thus more difficult to observe when compared to the differences that took place after a change in friction as in (Schiltz et al., 2021).

## 4.5. Conclusion

We have shown that GF adaptation across friction conditions allows maintaining similar lower bounds on the levels of Stick Ratio and upper bounds on skin strain rates during manipulation. Future experiments should be conducted to try to get insight into the mechanisms that lead to online corrective GF adjustments.

CHAPTER 5

# General discussion and future directions

*"There's never enough time to do all the nothing you want."*

*Calvin & Hobbes – Bill Waterson*

## 5.1. Summary of contributions

This thesis is a new element in a series of theses conducted at UCLouvain focused on touch, fingerpad deformations, and their influence on object manipulation. During what was arguably the first thesis of this series, Anne-Sophie Augurelle performed an experiment in which participants had to manipulate an object in a precision grip while their fingers were anesthetized. This experiment highlighted the importance of cutaneous feedback for dexterous manipulation, as participants were not able to adjust their grip force to the coefficient of friction (Augurelle et al., 2003). Then, in the next thesis, Thibaut André took a different approach to dexterous object manipulation. He studied how touch and deformations of the skin interact and described how the fingertip skin slips on a smooth material by visualizing it through a glass and how it is affected by the level of hydration (André et al., 2011). He developed a moisture evaluator to measure the fingertip skin hydration during object manipulation (André et al., 2008), used it to show that there is an optimal level of moisture to maximize the coefficient of friction (André et al., 2009) and that the level moisture is optimally modulated during object manipulation (André et al., 2010). Then, Benoît

Delhaye developed a custom robotic platform that allowed him to monitor fingerpad deformations while applying controlled levels of forces. He used it first to describe in more details how the stick ratio and the contact area evolved during tangential loading of the fingertip (Delhaye et al., 2014) and then to describe and quantify the surface strains in detail (Delhaye et al., 2016). Finally, Allan Barrea developed a method to measure the static coefficient of friction of the fingertips in a precision grip as a function of normal force (Barrea et al., 2016). He also used the robotic platform to investigate how humans detect partial slip (Barrea et al., 2018). Together with Benoît Delhaye, they combined this robotic platform with microneurography to describe how individual afferents respond to skin deformations (Delhaye et al., 2021a). Finally, he initiated the development of the Active Touch manipulandum, which allows measuring fingerpad deformations during object manipulation and is of crucial importance in the present thesis. All the above-mentionned works are essential in the context of this thesis, as they give insight into fingerpad deformations in a passive condition, fingerpad friction, how to measure it, and the factors that influence it (i.e., the normal force and the level of hydration in these studies).

In this thesis, we first completed the development of the Active Touch manipulandum and validated its function. We tested it on 18 participants in a vertical oscillation task (chapter 2). We described how the stick ratio and the strain rate evolved during the oscillations. That is, the stick ratio reached a minimum around the time of the maximum of load force and the strain rate approximately followed the load force rate, with a substantial level of strain rates (norm up to 100%/s). We also showed that participants had different strategies, with average levels of grip force going from 1 to 15N. We finally showed that this had an important effect, as participants with higher levels of grip force showed higher levels of stick ratio and lower levels of surface strain rates.

Then, we decided to investigate how humans adapt to friction when lifting objects (chapter 3). Using glass and a smooth material with a coefficient of friction lower than that of glass, we asked participants to perform grip-lifting tasks while monitoring the skin strains. We showed that when switching from the glass to the low friction material, participants quickly increased their Grip Force to avoid slip, within 370ms after contact with the surface. A strong increase of strain rate was observed in the central part of the fingertip before the transport phase and over 100ms before the

adjustment of Grip Force. This localized increase of strain rate is a good candidate for the sensory signal that allowed the Grip Force adaptation.

Finally, we described the differences in partial slip and skin deformations during point-to-point movements (chapter 4). We showed that, in fact, the levels of partial slip and skin strain rates remained approximately equivalent between the conditions thanks to the difference in Grip Force applied by the participants. We confirmed that, indeed, the level of Grip Force altered the fingerpad mechanics by showing that trials where participants applied lower levels of Grip Force resulted in larger surface skin strain rates. We also showed that participants with a smaller coefficient of friction showed a larger adaptation to the friction condition, as measured by the difference of grip force between the trials of different friction conditions.

Overall, in this work, we described fingerpad deformations during the manipulation of objects. On one side, we showed the influence of the grip force, load force, and coefficient of friction on the fingerpad skin deformations, and on the other side, how those deformations were, in turn, used to adjust the Grip Force during object manipulation. This contributes to understanding the extraordinary ability of humans to perform fine movements.

## 5.2. Limitations

This work inevitably presents limitations, most of them are linked to the Active Touch Device, which although ingenious cannot measure everything.

The first limitation is that, due to physical constraints of the device, only the index finger is imaged, leaving unobserved the skin deformations that take place on the thumb. The partial slip and skin strains probably do not progress in the same fashion on both fingers during all trials. It is thus possible that skin deformations taking place on the thumb could be the cause of Grip Force adjustments or changes in the kinematics of the movement. However, both fingers present a similar coefficient of friction (see Supp. Fig 3.1. and Supp. Fig 3.2). This leads us to think that both fingers present relatively similar skin deformations. They must thus have similar mechanics and transmit similar information used for fine object manipulation. Nonetheless, when searching for the cause of a change of grip force when a participant manipulates the active touch, we are only looking at the surface strains of one of the two fingers at a time. To remedy this problem, a solution would be to reproduce the same experiments by observing the thumb for

half of the trials and the index finger for the other half of the trials. Another better - yet more costly - solution would be to build a new version of the active touch in which both fingers are recorded at the same time.

Moreover, as we are using a standard camera, only 2-dimensional surface strains are measured. When the fingertip skin deforms during object manipulation, the deformations can propagate from the epidermis up to the bone, with vibrations detectable in the forearm. The mechanoreceptors are located inside the skin below the epidermis at different levels of depth according to the afferent type. It seems intuitive that they would be most sensitive to deformations and vibrations that propagate at those depths. Luckily, surface skin deformations are intrinsically linked to skin deformations under the surface. But the exact manner in which they are linked is not yet precisely described, despite multiple models with varying degrees of complexity (Dandekar et al., 2003; Tada et al., 2006b; Liu et al., 2017). However, precise surface strains have been linked to the activation of individual afferents (Delhaye et al., 2021a), proving that looking at surface strains as a tactile cue for fine object manipulation makes sense.

Another limitation of the device is its weight. The device was designed to be manipulated in the most natural manner possible. Nevertheless, as its weight is quite high (530g) and the surface of contact used (glass) is slippery, a counterweight and a system of pulleys have to be used so that participants can manipulate it without too many difficulties. This led to a considerable increase of the inertia of the system, making the experience of manipulating the device different than manipulating most objects on earth.

A final limitation comes from the fact that the optical technique used to image the fingerpad deformations requires close contact between the skin and the glass. This contact is dependent on the moisture content of the skin, which can start very low and increase for seconds when entering in contact with objects (Dzidek et al., 2017). Hence, for grip-lifting experiments, the first few images are usually unusable as moisture is entering in contact with the glass and the fingerprints are not immediately visible. It is therefore difficult to describe the surface strains during this period.

## 5.3. Open questions and future directions

Science wouldn't be science if all questions could be answered. This section identifies three questions that remain open and could be answered in future works.

### 5.3.1. What is the influence of skin hydration on fingerpad deformation and on the online control of the Grip Force during manipulation?

The coefficients of friction during the experiments conducted in this thesis were measured for each participant in all experiments. However, the coefficient of friction is a value highly impacted by the level of hydration of the skin (André et al., 2009). A fingertip that is too dry or too humid will tend to be more slippery than a fingertip with the right amount of moisture. Moreover, the moisture content tends to reach the optimal value to maximize the coefficient of friction when the skin is in contact with objects (André et al., 2010; Yum et al., 2020). Therefore, how the moisture content influences fingerpad deformations and the control of Grip Force inside a single trial remains to be elucidated. A transparent probe that can measure the moisture content of the fingertip during manipulation with the Active Touch is under development and will be used to answer this question. An additional question that can be answered using this device is the way how the real contact area between the fingerpad and the material $A_{real}$ is affected by the moisture content.

### 5.3.2. How do minute deformations affect the online control of Grip Force during object manipulation?

Although some level of online correction was present during individual trials between point-to-point movements (see chapter 4), we were unable to link them to the Stick Ratio or fingerpad strains. We assumed that the changes in this variable are too minute to be detected by our apparatus in the context of this experiment. This could be investigated by generating unexpected changes of weight or friction of varying degrees and linking them to corrective Grip Force changes.

### 5.3.3. What are the roles of cutaneous and proprioceptive afferents for weight and torque estimation during object manipulation?

As explained in chapter 1, proprioception and touch are both used during object manipulation. Although proprioception cannot be used to detect friction in the absence of a full slip, it can nevertheless give information about the weight of a manipulated object or the torque of an object whose center of mass is not located between the fingers because of the pressure that is exerted on the joints and muscle spindles. The mechanoreceptors of the skin can also transmit information about the weight and torque because they have an influence on fingerpad deformations. Performing experiments with the Active Touch device involving changes in weight and torque inevitably leads to the issue that it is impossible to know for certain the cause of online Grip Force correction, as they can be caused by sources located outside of the monitored contact area. Proprioception makes use of afferents with a higher conduction speed than skin mechanoreceptors. However, skin deformation could arguably give more precise information about the forces and torques applied on the fingertip. How the information of both systems is combined has been explored in a passive set-up (Crevecoeur et al., 2017) but remains to be further studied during active manipulation.

## 5.4. Potential applications

The science conducted in this thesis is fundamental at its core. The aim is eventually to understand how humans perform fine manipulation. However, several potential applications could one day make use of the work presented. We review two of them in the present section.

### 5.4.1. Biomimetism for friction sensors and slip detection in robots

For a long time, robots have been built to be specialized at performing just a few tasks each. With the advent of artificial intelligence, it is possible to create more versatile robots that could perform a broader range of tasks than ever before. If those robots are to manipulate previously unknown objects, they should be able to grasp those objects and squeeze them with the right force according to the coefficient of friction between the robot and the object. Thus, they need to be able to evaluate this coefficient of friction to manipulate the objects efficiently. Usually, friction sensors require rubbing of the contacted surfaces, which is not practical for dexterous object

manipulation. The absence of slippage can be detected by robots hands using the correlation between the signals of two force sensors situated at different places on the robotic hand, yet this only gives a lower bound on the coefficient of friction (Massalim et al., 2021).

According to Chen et al. (2018), tactile sensors that would allow robots to perform dexterous manipulation should be able to perform three tasks:

1. Detect *gross slip*[9], to adjust the grip force
2. Detect *incipient slip*[10], as an indication on the grip safety
3. Measure friction on contact with an object and/or following a gross or incipient slip event while manipulating an object

A whole range of friction sensors that are able to perform those tasks to varying degrees have been developed (Nakamura and Shinoda, 2001; Maeno et al., 2004; Chen et al., 2015, 2016; Heyneman and Cutkosky, 2016). However, all of them still present some limitations, such as requiring the manipulated object to have a planar surface, or the coefficient of friction to be included in a certain range, or requiring a long time to compute the coefficient of friction, etc. In the review by Chen et al. (2018), they mention in that the most promising solution to a sensor that would allow dexterous manipulation would include a visual detection of incipient slip of slip events. In this thesis, by describing how humans use slip events to adjust their grip force and by describing visually the specific deformations that lead to grip force correction, we participated in understanding nature's solution to this problem, which could potentially inspire future engineers.

[9] Gross slip has the same definition as full slip in the context of this thesis. It does not especially imply the object falling from the robot's hands.

[10] Incipient slip has the same definition as partial slip in the context of this thesis.

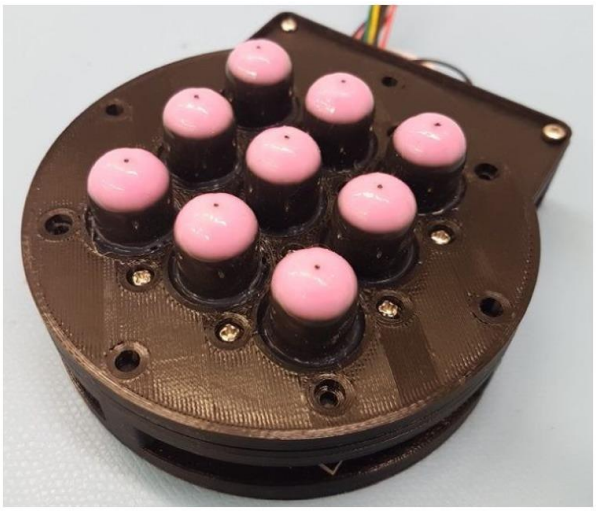

**Fig. 5.1. Example of a friction sensor, the "Papillaray".** The Papillarray consists of an array of silicone pillars with different heights, inspired by the skin of the human fingerpad. When a lateral force is applied, tracking the displacements of the pillars can be used to detect incipient slip. In conjunction with the measurements of the forces applied on the pillars, this can be used to estimate the coefficient of friction. Reproduced from (Khamis et al., 2019).

### 5.4.2. Somatosensory prosthesis

With two million amputees in the United States alone, the development of performant prosthetic limbs is important for the quality of life of many people around the world (Ziegler-Graham et al., 2008). In recent years, a lot of progress has been made in the development of prosthetic arms and hands for amputees and tetraplegics. The most recent ones allow voluntary movements controlled by thought and allow to feel through them. When possible, intended movements are inferred from activation patterns of residual muscles (Cipriani et al., 2011; Muceli et al., 2014; Sartori et al., 2018) and sensory feedback is delivered by stimulating the residual nerves in the stump (D'Anna et al., 2019; George et al., 2019; Vu et al., 2020). If not possible, as is the case with tetraplegic patients, intended movements can be inferred from activation patterns across populations of cortical neurons in the primary motor cortex and the posterior parietal cortex (Hochberg et al., 2006, 2012; Collinger et al., 2013) and sensory feedback can be delivered by stimulating neurons in the somatosensory cortex (Klaes et al., 2014). In all cases, the nature of the sensory signals sent by the prosthesis to the nerves or the brain is important. For now, those prostheses are a lot simpler than actual human hands and do not reach the same capabilities. In a recent review on the neural mechanisms of manual dexterity, the authors explain

that the brain-controlled bionic hands are limited by an insufficient understanding of the neural mechanisms underlying manual control (Sobinov and Bensmaia, 2021). In the context of this thesis, although we did not look at the neural mechanisms directly, we improved the understanding of manual control. This better understanding could be of use when designing prosthetic limbs.

**Fig. 5.2. A patient picking grapes with the DEKA LUKE arm.** The DEKA Luke arm is a six-DOF bidirectional neuromyoelectric prosthetic hand and wrist that conveys biomimetic sensory feedback and is activated using electromyographic recordings from residual arm muscles. Adapted from (George et al., 2019).

## 5.5. Concluding words

In this thesis, we made progress in understanding how the fingerpad skin deforms during fine object manipulation and how those deformations impact the control of the forces applied by human participants. Using a novel custom-made device called the Active Touch, we conducted experiments that allowed us to describe how the forces applied during object manipulation and fingerpad deformations interact. We showed that the deformations are influenced by the Grip Force and that they were used to adjust the level of Grip Force to the friction themselves. At the end of the day, we can be impressed by how our skin, the mechanoreceptors, the central nervous system, the brain and muscles all work together to give humans the amazing ability to perform fine manipulation of objects. The next

time you use your fingers to cut an onion or bring a glass of Belgian beer to your lips, I suggest that you have a small thought about the complexity of our body and the impressive tasks that this mysterious choreography of organs working together allows you to accomplish in everyday life…

# Bibliography


Adams MJ, Briscoe BJ, Johnson S a. 2007. Friction and lubrication of human skin. *Tribol Lett* **26**:239–253. doi:10.1007/s11249-007-9206-0

Adams MJ, Johnson SA, Lefèvre P, Lévesque V, Hayward V, André T, Thonnard J. 2013. Finger pad friction and its role in grip and touch. *J R Soc Interface* **10**:20120467. doi:10.1098/rsif.2012.0467

Adams MJ, McKeown R, Whall A. 1997. A micromechanical model for the confined uni-axial compression of an assembly of elastically deforming spherical particles. *J Phys D Appl Phys* **30**:912–920. doi:10.1088/0022-3727/30/5/025

André T, De Wan M, Lefèvre P, Thonnard J-L. 2008. Moisture Evaluator: a direct measure of fingertip skin hydration during object manipulation. *Skin Res Technol* **14**:385–389. doi:10.1111/j.1600-0846.2008.00314.x

André T, Lefèvre P, Thonnard J-L. 2009. A continuous measure of fingertip friction during precision grip. *J Neurosci Methods* **179**:224–229. doi:10.1016/j.jneumeth.2009.01.031

André T, Lefèvre P, Thonnard J. 2010. Fingertip moisture is optimally modulated during object manipulation. *J Neurophysiol* **103**:402–408. doi:10.1152/jn.00901.2009

André T, Lévesque V, Hayward V, Lefèvre P, Thonnard J. 2011. Effect of skin hydration on the dynamics of fingertip gripping contact. *J R Soc Interface* **8**:1574–1583. doi:10.1098/rsif.2011.0086

Augurelle A-S, Smith AM, Lejeune T, Thonnard J. 2003. Importance of cutaneous feedback in maintaining a secure grip during manipulation of hand-held objects. *J Neurophysiol* **89**:665–671. doi:10.1152/jn.00249.2002

Baker LB. 2019. Physiology of sweat gland function: The roles of sweating and sweat composition in human health. *Temperature* **6**:211–259.

doi:10.1080/23328940.2019.1632145

Barrea A. 2017. Finger pad mechanics, tactile signals and dexterous manipulation. UCLouvain.

Barrea A, Cordova Bulens D, Lefevre P, Thonnard J-L. 2016. Simple and Reliable Method to Estimate the Fingertip Static Coefficient of Friction in Precision Grip. *IEEE Trans Haptics* **9**:492–498. doi:10.1109/TOH.2016.2609921

Barrea A, Delhaye BP, Lefèvre P, Thonnard J-L. 2018. Perception of partial slips under tangential loading of the fingertip. *Sci Rep* **8**:7032. doi:10.1038/s41598-018-25226-w

Bau O, Poupyrev I, Israr A, Harrison C. 2010. TeslaTouch: Electrovibration for Touch Surfaces. *Proc UIST 2010* 283–292. doi:10.1145/1866029.1866074

Bell J, Bolanowski S, Holmes MH. 1994. The structure and function of pacinian corpuscles: A review. *Prog Neurobiol* **42**:79–128. doi:10.1016/0301-0082(94)90022-1

Betts JG, Desaix P, Johnson E, Johnson JE, Korol O, Kruse D, Brandon P, Wise JA, Womble M, Young KA. 2013. Anatomy and Physiology. Openstax.

Birznieks I, Burstedt MK, Edin BB, Johansson RS. 1998. Mechanisms for force adjustments to unpredictable frictional changes at individual digits during two-fingered manipulation. *J Neurophysiol* **80**:1989–2002.

Blouin J, Bard C, Teasdale N, Paillard J, Fleury M, Forget R, Lamarre Y. 1993. Reference systems for coding spatial information in normal subjects and a deafferented patient. *Exp Brain Res* **93**. doi:10.1007/BF00228401

Bochereau S, Dzidek B, Adams M, Hayward V. 2017. Characterizing and Imaging Gross and Real Finger Contacts under Dynamic Loading. *IEEE Trans Haptics* **10**:456–465. doi:10.1109/TOH.2017.2686849

Bowden FP, Tabor D. 1954. The friction and lubrication of solids. Clarendon Press.

Bradski G. 2008. The OpenCV Library. *Dr Dobb's J Softw Tools*.

Brisben AJ, Hsiao SS, Johnson KO. 1999. Detection of vibration transmitted through an object grasped in the hand. *J Neurophysiol* **81**:1548–1558.

Buchholz B, Frederick LJ, Armstrong TJ. 1988. An investigation of human palmar skin friction and the effects of materials, pinch force and

moisture. *Ergonomics* **31**:317–325. doi:10.1080/00140138808966676

Buckingham G, Goodale MA. 2010. The influence of competing perceptual and motor priors in the context of the size-weight illusion. *Exp Brain Res* **205**:283–288. doi:10.1007/s00221-010-2353-9

Burke D, Gandevia SC, Macefield G. 1988. Responses to passive movement of receptors in joint, skin and muscle of the human hand. *J Physiol* **402**:347–361. doi:10.1113/jphysiol.1988.sp017208

Cadoret G, Smith AM. 1996. Friction, not texture, dictates grip forces used during object manipulation. *J Neurophysiol* **75**:1963–9.

Chambers MR, Andres KH, von Duering M, Iggo A. 1972. The structure and function of the slowly adapting type II mechanoreceptor in hairy skin. *Q J Exp Physiol Cogn Med Sci* **57**:417–445. doi:10.1113/expphysiol.1972.sp002177

Chen W, Khamis H, Birznieks I, Lepora NF, Redmond SJ. 2018. Tactile Sensors for Friction Estimation and Incipient Slip Detection - Toward Dexterous Robotic Manipulation: A Review. *IEEE Sens J* **18**:9049–9064. doi:10.1109/JSEN.2018.2868340

Chen W, Rodpongpun S, Luo W, Isaacson N, Kark L, Khamis H, Redmond SJ. 2015. An eight-legged tactile sensor to estimate coefficient of static friction2015 37th Annual International Conference of the IEEE Engineering in Medicine and Biology Society (EMBC). IEEE. pp. 4407–4410. doi:10.1109/EMBC.2015.7319372

Chen W, Wen H, Khamis H, Redmond SJ. 2016. An Eight-Legged Tactile Sensor to Estimate Coefficient of Static Friction: Improvements in Design and Evaluation. pp. 493–502. doi:10.1007/978-3-319-42321-0_46

Childs THC, Henson B. 2007. Human tactile perception of screen-printed surfaces: Self-report and contact mechanics experiments. *Proc Inst Mech Eng Part J J Eng Tribol* **221**:427–441. doi:10.1243/13506501JET217

Choi C, Ma Y, Li X, Ma X, Hipwell MC. 2021. Finger Pad Topography beyond Fingerprints: Understanding the Heterogeneity Effect of Finger Topography for Human-Machine Interface Modeling. *ACS Appl Mater Interfaces* **13**:3303–3310. doi:10.1021/acsami.0c15827

Cipriani C, Antfolk C, Controzzi M, Lundborg G, Rosen B, Carrozza MC, Sebelius F. 2011. Online myoelectric control of a dexterous hand prosthesis by transradial amputees. *IEEE Trans Neural Syst Rehabil Eng*

**19**:260–270. doi:10.1109/TNSRE.2011.2108667

Collinger JL, Wodlinger B, Downey JE, Wang W, Tyler-Kabara EC, Weber DJ, McMorland AJC, Velliste M, Boninger ML, Schwartz AB. 2013. High-performance neuroprosthetic control by an individual with tetraplegia. *Lancet* **381**:557–564. doi:10.1016/S0140-6736(12)61816-9

Comaish S, Bottoms E. 1971. The skin and friction: deviations from Amonton's laws, and the effects of hydration and lubrication. *Br J Dermatol* **84**:37–43. doi:10.1111/j.1365-2133.1971.tb14194.x

Cornuault P, Carpentier L, Bueno M, Cote J, Monteil G. 2015. Influence of physico-chemical, mechanical and morphological fingerpad properties on the frictional distinction of sticky/slippery surfaces. *J R Soc Interface* **12**:20150495. doi:10.1098/rsif.2015.0495

Crevecoeur F, Barrea A, Libouton X, Thonnard J-L, Lefèvre P. 2017. Multisensory components of rapid motor responses to fingertip loading. *J Neurophysiol* **118**:331–343. doi:10.1152/jn.00091.2017

Crevecoeur F, Giard T, Thonnard J-LJ-L, Lefèvre P, Lefevre P. 2011. Adaptive control of grip force to compensate for static and dynamic torques during object manipulation. *J Neurophysiol* **106**:2973–2981. doi:10.1152/jn.00367.2011

Crevecoeur F, McIntyre J, Thonnard J-L, Lefèvre P. 2010. Movement stability under uncertain internal models of dynamics. *J Neurophysiol* **104**:1301–1313. doi:10.1152/jn.00315.2010

D'Anna E, Valle G, Mazzoni A, Strauss I, Iberite F, Patton J, Petrini FM, Raspopovic S, Granata G, Iorio R Di, Controzzi M, Cipriani C, Stieglitz T, Rossini PM, Micera S. 2019. A closed-loop hand prosthesis with simultaneous intraneural tactile and position feedback. *Sci Robot* **4**. doi:10.1126/scirobotics.aau8892

Dale Wilson B, Moon S, Armstrong F. 2012. Comprehensive review of ultraviolet radiation and the current status on sunscreens. *J Clin Aesthet Dermatol* **5**:18–23.

Dandekar K, Raju BI, Srinivasan M a. 2003. 3-D Finite-Element Models of Human and Monkey Fingertips to Investigate the Mechanics of Tactile Sense. *J Biomech Eng* **125**:682. doi:10.1115/1.1613673

Delhaye BP, Barrea A, Edin BB, Lefèvre P, Thonnard J-L. 2016. Surface strain measurements of fingertip skin under shearing. *J R Soc Interface* **13**:20150874. doi:10.1098/rsif.2015.0874

Delhaye BP, Jarocka E, Barrea A, Thonnard J-L, Edin BB, Lefèvre P. 2021a. High-resolution imaging of skin deformation shows that afferents from human fingertips signal slip onset. *Elife*.

Delhaye BP, Lefèvre P, Thonnard J-L. 2014. Dynamics of fingertip contact during the onset of tangential slip. *J R Soc Interface* **11**:20140698. doi:10.1098/rsif.2014.0698

Delhaye BP, Long KH, Bensmaia SJ. 2018. Neural Basis of Touch and Proprioception in Primate Cortex. *Compr Physiol*. doi:10.1002/cphy.c170033

Delhaye BP, Schiltz F, Barrea A, Thonnard J-L, Lefèvre P. 2021b. Measuring fingerpad deformation during active object manipulation. *J Neurophysiol* 2021.07.20.453037. doi:10.1152/jn.00358.2021

Derler S, Gerhardt L-C, Lenz A, Bertaux E, Hadad M. 2009. Friction of human skin against smooth and rough glass as a function of the contact pressure. *Tribol Int* **42**:1565–1574. doi:10.1016/j.triboint.2008.11.009

Derler S, Schrade U, Gerhardt L-C. 2007. Tribology of human skin and mechanical skin equivalents in contact with textiles. *Wear* **263**:1112–1116. doi:10.1016/j.wear.2006.11.031

Dzidek B, Bochereau S, Johnson SA, Hayward V, Adams MJ. 2017. Why pens have rubbery grips. *Proc Natl Acad Sci* 201706233. doi:10.1073/pnas.1706233114

Dzidek BM, Adams MJ, Andrews JW, Zhang Z, Johnson SA. 2017. Contact mechanics of the human finger pad under compressive loads. *J R Soc Interface* **14**:20160935. doi:10.1098/rsif.2016.0935

Edin BB. 1992. Quantitative analysis of static strain sensitivity in human mechanoreceptors from hairy skin. *J Neurophysiol* **67**:1105–1113. doi:10.1152/jn.00628.2004

Ellis RR, Lederman SJ. 1993. The role of haptic versus visual volume cues in the size-weight illusion. *Percept Psychophys* **53**:315–324. doi:10.3758/BF03205186

Farajian M, Leib R, Kossowsky H, Zaidenberg T, Mussa-Ivaldi FA, Nisky I, Vaadia E. 2020. Stretching the skin immediately enhances perceived stiffness and gradually enhances the predictive control of grip force. *Elife* **9**:1–38. doi:10.7554/eLife.52653

Flanagan JR, Wing AM. 1997. The role of internal models in motion planning and control: evidence from grip force adjustments during movements

of hand-held loads. *J Neurosci* **17**:1519–28.

Flanagan JR, Wing AM. 1995. The stability of precision grip forces during cyclic arm movements with a hand-held load. *Exp Brain Res* **105**:455–464. doi:10.1007/BF00233045

Flanagan JR, Wing AM. 1993. Modulation of grip force with load force during point-to-point arm movements. *Exp Brain Res* **95**:131–143. doi:10.1007/BF00229662

Fleming MS, Luo W. 2013. The anatomy, function, and development of mammalian A$β$ low-threshold mechanoreceptors. *Front Biol (Beijing)* **8**:408–420. doi:10.1007/s11515-013-1271-1

Gasser HS. 1941. THE CLASSIFICATION OF NERVE FIBERS HERBERT. *Ohio J Sci* **41**:145–159.

George JA, Kluger DT, Davis TS, Wendelken SM, Okorokova E V., He Q, Duncan CC, Hutchinson DT, Thumser ZC, Beckler DT, Marasco PD, Bensmaia SJ, Clark GA. 2019. Biomimetic sensory feedback through peripheral nerve stimulation improves dexterous use of a bionic hand. *Sci Robot* **4**:1–12. doi:10.1126/scirobotics.aax2352

Giard T, Crevecoeur F, McIntyre J, Thonnard J-L, Lefèvre P. 2015. Inertial torque during reaching directly impacts grip-force adaptation to weightless objects. *Exp Brain Res* **233**:3323–3332. doi:10.1007/s00221-015-4400-z

Goldsmith LA. 1990. My organ is bigger than your organ. *Arch Dermatol* **126(3)**:301–302.

Goodwin AW, Wheat HE. 2004. Sensory signals in neural populations underlying tactile perception and manipulation. *Annu Rev Neurosci* **27**:53–77. doi:10.1146/annurev.neuro.26.041002.131032

Gould J. 2018. Superpowered skin. *Nature* **563**:S84–S85. doi:10.1038/d41586-018-07429-3

Gueorguiev D, Bochereau S, Mouraux A, Hayward V, Thonnard J-L. 2016. Touch uses frictional cues to discriminate flat materials. *Sci Rep* **6**:25553. doi:10.1038/srep25553

Guillery E, Mouraux A, Thonnard J-L. 2013. Cognitive-Motor Interference While Grasping, Lifting and Holding Objects. *PLoS One* **8**:e80125. doi:10.1371/journal.pone.0080125

Guillery E, Mouraux A, Thonnard JL, Legrain V. 2017. Mind your grip: Even

usual dexterous manipulation requires high level cognition. *Front Behav Neurosci* **11**. doi:10.3389/fnbeh.2017.00220

Hadjiosif AM, Smith MA. 2015. Flexible Control of Safety Margins for Action Based on Environmental Variability. *J Neurosci* **35**:9106–9121. doi:10.1523/JNEUROSCI.1883-14.2015

Handler A, Ginty DD. 2021. The mechanosensory neurons of touch and their mechanisms of activation. *Nat Rev Neurosci* **22**:521–537. doi:10.1038/s41583-021-00489-x

Harrington T, Merzenich MM. 1970. Neural coding in the sense of touch: Human sensations of skin indentation compared with the responses of slowly adapting mechanoreceptive afferents innervating the hairy skin of monkeys. *Exp Brain Res* **10**:251–264. doi:10.1007/BF00235049

Hertenstein MJ, Weiss SJ. 2011. The handbook of touch. Springer.

Heyneman B, Cutkosky MR. 2016. Slip classification for dynamic tactile array sensors. *Int J Rob Res* **35**:404–421. doi:10.1177/0278364914564703

Hochberg LR, Bacher D, Jarosiewicz B, Masse NY, Simeral JD, Vogel J, Haddadin S, Liu J, Cash SS, Van Der Smagt P, Donoghue JP. 2012. Reach and grasp by people with tetraplegia using a neurally controlled robotic arm. *Nature* **485**:372–375. doi:10.1038/nature11076

Hochberg LR, Serruya MD, Friehs GM, Mukand JA, Saleh M, Caplan AH, Branner A, Chen D, Penn RD, Donoghue JP. 2006. Neuronal ensemble control of prosthetic devices by a human with tetraplegia. *Nature* **442**:164–171. doi:10.1038/nature04970

Inamoto M, Tomeno S. 2019. Tactile feel designed glassIEEE World Haptics Conference.

Jarocka E, Pruszynski JA, Johansson RS. 2021. Human touch receptors are sensitive to spatial details on the scale of single fingerprint ridges. *J Neurosci* JN-RM-1716-20. doi:10.1523/jneurosci.1716-20.2021

Jenmalm P, Birznieks I, Goodwin AW, Johansson RS. 2003. Influence of object shape on responses of human tactile afferents under conditions characteristic of manipulation. *Eur J Neurosci* **18**:164–176. doi:10.1046/j.1460-9568.2003.02721.x

Johansson RS, Flanagan JR. 2009. Coding and use of tactile signals from the fingertips in object manipulation tasks. *Nat Rev Neurosci* **10**:345–359. doi:10.1038/nrn2621

Johansson RS, Flanagan JR. 2009. Sensorimotor Control of Manipulation. *Encycl Neurosci*.

Johansson Roland S., Flanagan JR. 2009. Coding and use of tactile signals from the fingertips in object manipulation tasks. *Nat Rev Neurosci* **10**:345–359. doi:10.1038/nrn2621

Johansson RS, Flanagan JR. 2008. Tactile Sensory Control of Object Manipulation in HumansThe Senses: A Comprehensive Reference, Vol 6, Somatosensation. pp. 67–86.

Johansson RS, Vallbo ÅB, Westling G. 1980. Thresholds of mechanosensitive afferents in the human hand as measured with von Frey hairs. *Brain Res* **184**:343–351. doi:10.1016/0006-8993(80)90803-3

Johansson RS, Westling G. 1988. Coordinated isometric muscle commands adequately and erroneously programmed for the weight during lifting task with precision grip. *Exp Brain Res* **71**:59–71.

Johansson RS, Westling G. 1984. Roles of glabrous skin receptors and sensorimotor memory in automatic control of precision grip when lifting rougher or more slippery objects. *Exp Brain Res* **56**:550–564. doi:10.1007/BF00237997

Johnson KL. 1985. Contact mechanics. Cambridge University Press.

Johnson KO. 2001. The roles and functions of cutaneous mechanoreceptors. *Curr Opin Neurobiol* **11**:455–461.

Johnson KO, Yoshioka T, Vega Bermudez F. 2000. Tactile functions of mechanoreceptive afferents innervating the hand. *J Clin Neurophysiol* **17**:539–558. doi:10.1097/00004691-200011000-00002

Johnson SA, Gorman DM, Adams MJ, Briscoe BJ. 1993. The friction and lubrication of human stratum corneum. *Tribol Ser* **25**:663–672. doi:10.1016/S0167-8922(08)70419-X

Khamis H, Redmond SJ, Macefield V, Birznieks I. 2014. Classification of Texture and Frictional Condition at Initial Contact by Tactile Afferent ResponsesHaptics: Neuroscience, Devices, Modeling, and Applications. pp. 460–468. doi:10.1007/978-3-662-44193-0_58

Khamis H, Xia B, Redmond SJ. 2019. A novel optical 3D force and displacement sensor – Towards instrumenting the PapillArray tactile sensor. *Sensors Actuators, A Phys* **291**:174–187. doi:10.1016/j.sna.2019.03.051

Khamis HA, Redmond SJ, Macefield VG, Birznieks I. 2014. Tactile afferents encode grip safety before slip for different frictions.36th Annual International Conference of the IEEE Engineering in Medicine and Biology Society. IEEE. pp. 4123–4126. doi:10.1109/EMBC.2014.6944531

Kinoshita H, Bäckström L, Flanagan JR, Johansson RS. 1997. Tangential torque effects on the control of grip forces when holding objects with a precision grip. *J Neurophysiol* **78**:1619–1630. doi:10.1152/jn.1997.78.3.1619

Klaes C, Shi Y, Kellis S, Minxha J, Revechkis B, Andersen RA. 2014. A cognitive neuroprosthetic that uses cortical stimulation for somatosensory feedback. *J Neural Eng* **11**:056024. doi:10.1088/1741-2560/11/5/056024

Knibestöl M. 1975. Stimulus-response functions of slowly adapting mechanoreceptors in the human glabrous skin area. *J Physiol* 63–80.

Knibestöl M. 1973. Stimulus-response functions of rapidly adapting mechanoreceptors in the human glabrous skin area. *J Physiol* 427–452.

Kobayashi K, Maeno T. 1998. Relationship between the Structure of Finger Tissue and the Location of Tactile Receptors (2nd Report, Method of Dynamic Contact Analysis and Results for contact between the Finger and Plane Plate). *Nihon Kikai Gakkai Ronbunshu, C Hen/Transactions Japan Soc Mech Eng Part C* **64**:4798–4805. doi:10.1299/kikaic.64.4798

Körding KP, Wolpert DM. 2004. Bayesian integration in sensorimotor learning. *Nature* **427**:244–247. doi:10.1038/nature02169

Levesque V. 2002. Measurement of skin deformation using fingerprint feature tracking.

Levesque V, Hayward V. 2003. Experimental evidence of lateral skin strain during tactile exploration. *Proc Eurohaptics*.

Liu X, Lu Z, Lewis R, Carré MJ, Matcher SJ. 2013. Feasibility of using optical coherence tomography to study the influence of skin structure on finger friction. *Tribol Int* **63**:34–44. doi:10.1016/j.triboint.2012.08.020

Liu X, Maiti R, Lu ZH, Carré MJ, Matcher SJ, Lewis R. 2017. New Non-invasive Techniques to Quantify Skin Surface Strain and Sub-surface Layer Deformation of Finger-pad during Sliding. *Biotribology* **12**:52–58. doi:10.1016/j.biotri.2017.07.001

Lucas B, Kanade T. 1981. An iterative image registration technique with an

application to stereo vision. *IJCAI* **130**:121–130.

Macefield VG, Häger-Ross C, Johansson RS. 1996. Control of grip force during restraint of an object held between finger and thumb: responses of cutaneous afferents from the digits. *Exp Brain Res* **108**:155–171.

Macefield VG, Johansson RS. 2003. Loads applied tangential to a fingertip during an object restraint task can trigger short-latency as well as long-latency EMG responses in hand muscles. *Exp brain Res* **152**:143–9. doi:10.1007/s00221-003-1421-9

Macefield VG, Johansson RS. 1996. Control of grip force during restraint of an object held between finger and thumb: responses of muscle and joint afferents from the digits. *Exp Brain Res* **108**:172–184.

Maeno T, Kawamura T, Cheng S-C. 2004. Friction Estimation by Pressing an Elastic Finger-Shaped Sensor Against a Surface. *IEEE Trans Robot Autom* **20**:222–228. doi:10.1109/TRA.2003.820850

Mancini F, Bauleo A, Cole J, Lui F, Porro CA, Haggard P, Iannetti GD. 2014. Whole-body mapping of spatial acuity for pain and touch. *Ann Neurol* **75**:917–924. doi:10.1002/ana.24179

Massalim Y, Kappassov Z, Varol HA, Hayward V. 2021. Robust detection of absence of slip in robot hands and feet. *IEEE Sens J* 1–1. doi:10.1109/jsen.2021.3127501

Miall RC, Rosenthal O, Ørstavik K, Cole JD, Sarlegna FR. 2019. Loss of haptic feedback impairs control of hand posture: a study in chronically deafferented individuals when grasping and lifting objects. *Exp Brain Res* **237**:2167–2184. doi:10.1007/s00221-019-05583-2

Monnoyer J, Diaz E, Bourdin C, Wiertlewski M. 2018. Perception of Ultrasonic Switches Involves Large Discontinuity of the Mechanical Impedance. *IEEE Trans Haptics* **11**:579–589. doi:10.1109/TOH.2018.2844186

Muceli S, Jiang N, Farina D. 2014. Extracting signals robust to electrode number and shift for online simultaneous and proportional myoelectric control by factorization algorithms. *IEEE Trans Neural Syst Rehabil Eng* **22**:623–633. doi:10.1109/TNSRE.2013.2282898

Nakamura K, Shinoda H. 2001. Tactile Sensing Device Instantaneously Evaluating Friction Coefficients. *Tech Dig Sens Symp* **18**:151–154.

Nowak DA, Hermsdörfer J, Glasauer S, Philipp J, Meyer L, Mai N. 2001. The effects of digital anaesthesia on predictive grip force adjustments during vertical movements of a grasped object. *Eur J Neurosci* **14**:756–

762. doi:10.1046/j.0953-816X.2001.01697.x

O'Neill GC, Watkins RH, Ackerley R, Barratt EL, Sengupta A, Asghar M, Sanchez Panchuelo RM, Brookes MJ, Glover PM, Wessberg J, Francis ST. 2019. Imaging human cortical responses to intraneural microstimulation using magnetoencephalography. *Neuroimage* **189**:329–340. doi:10.1016/j.neuroimage.2019.01.017

Opsomer L, Crevecoeur F, Thonnard J-L, McIntyre J, Lefèvre P. 2021. Distinct adaptation patterns between grip dynamics and arm kinematics when the body is upside-down. *J Neurophysiol* **125**:862–874. doi:10.1152/jn.00357.2020

Opsomer L, Théate V, Lefèvre P, Thonnard JL. 2018. Dexterous manipulation during rhythmic arm movements in Mars, Moon, and micro-gravity. *Front Physiol* **9**:1–10. doi:10.3389/fphys.2018.00938

Pailler-Mattei C, Bec S, Zahouani H. 2008. In vivo measurements of the elastic mechanical properties of human skin by indentation tests. *Med Eng Phys* **30**:599–606. doi:10.1016/j.medengphy.2007.06.011

Paré M, Behets C, Cornu O. 2003. Paucity of presumptive ruffini corpuscles in the index finger pad of humans. *J Comp Neurol* **456**:260–266. doi:10.1002/cne.10519

Pasumarty SM, Johnson SA, Watson SA, Adams MJ. 2011. Friction of the human finger pad: Influence of moisture, occlusion and velocity. *Tribol Lett* **44**:117–137. doi:10.1007/s11249-011-9828-0

Pataky TC, Latash ML, Zatsiorsky VM. 2005. Viscoelastic response of the finger pad to incremental tangential displacements. *J Biomech* **38**:1441–9. doi:10.1016/j.jbiomech.2004.07.004

Peckham M, Knibbs A, Paxton S. 2017. The Histology Guide (online).

Peters RM, Hackeman E, Goldreich D. 2009. Diminutive digits discern delicate details: fingertip size and the sex difference in tactile spatial acuity. *J Neurosci* **29**:15756–15761. doi:10.1523/JNEUROSCI.3684-09.2009

Phillips JR, Johnson KO. 1981. Tactile spatial resolution. II. Neural representation of Bars, edges, and gratings in monkey primary afferents. *J Neurophysiol* **46**:1192–1203.

Plaisier MA, Smeets JBJ. 2012. Mass is all that matters in the size-weight illusion. *PLoS One* **7**:1–6. doi:10.1371/journal.pone.0042518

Pruszynski JA, Johansson RS. 2014. Edge-orientation processing in first-order

tactile neurons. *Nat Neurosci* **17**:1404–1409. doi:10.1038/nn.3804

Pruszynski JA, Johansson RS, Flanagan JR, Pruszynski JA, Johansson RS, Flanagan JR. 2016. Report A Rapid Tactile-Motor Reflex Automatically Guides Reaching toward Handheld Objects Report A Rapid Tactile-Motor Reflex Automatically Guides Reaching toward Handheld Objects. *Curr Biol* **26**:788–792. doi:10.1016/j.cub.2016.01.027

Quaresma JAS. 2019. Organization of the skin immune system and compartmentalized immune responses in infectious diseases. *Clin Microbiol Rev* **32**. doi:10.1128/CMR.00034-18

Quek ZF, Schorr SB, Nisky I, Okamura AM, Provancher WR. 2014. Augmentation of stiffness perception with a 1- Degree-of-Freedom skin stretch device. *IEEE Trans Human-Machine Syst* **44**:731–742. doi:10.1109/THMS.2014.2348865

Romanovsky AA. 2014. Skin temperature: its role in thermoregulation. *Acta Physiol* **210**:498–507. doi:10.1111/apha.12231

Rothwell JC, Traub MM, Day BL, Obeso JA, Thomas PK, Marsden CD. 1982. Manual motor performance in a deafferented man. *Brain* **105**:515–542. doi:10.1093/brain/105.3.515

Sainburg RL, Poizner H, Ghez C. 1993. Loss of proprioception produces deficits in interjoint coordination. *J Neurophysiol* **70**:2136–2147. doi:10.1152/jn.1993.70.5.2136

Sankaran A, Jain A, Vashisth T, Vatsa M, Singh R. 2017. Adaptive latent fingerprint segmentation using feature selection and random decision forest classification. *Inf Fusion* **34**:1–15. doi:10.1016/j.inffus.2016.05.002

Sarlegna FR, Gauthier GM, Bourdin C, Vercher JL, Blouin J. 2006. Internally driven control of reaching movements: A study on a proprioceptively deafferented subject. *Brain Res Bull* **69**:404–415. doi:10.1016/j.brainresbull.2006.02.005

Sartori M, Durandau G, Došen S, Farina D. 2018. Robust simultaneous myoelectric control of multiple degrees of freedom in wrist-hand prostheses by real-time neuromusculoskeletal modeling. *J Neural Eng* **15**:066026. doi:10.1088/1741-2552/aae26b

Sarwak J. 2010. Essentials of Muscuskeletal Care, 4th ed. Rosemont, IL: American Academy of Orthopaedic Surgeons.

Schallamach A. 1952. The Load Dependence of Rubber Friction. *Proc Phys Soc*

*Sect B* **65**:657–661. doi:10.1088/0370-1301/65/9/301

Schiltz F, Delhaye BP, Crevecoeur F, Thonnard J-L, Lefèvre P. 2021. Fast Grip Force Adaptation To Friction Relies On Localized Fingerpad Strains. *bioRxiv* 2021.07.20.452911.

Shi J, Tomasi C. 1994. Good features to trackProceedings of IEEE Conference on Computer Vision and Pattern Recognition CVPR-94. IEEE Comput. Soc. Press. pp. 593–600. doi:10.1109/CVPR.1994.323794

Skedung L, Danerlöv K, Olofsson U, Aikala M, Niemi K, Kettle J, Rutland MW. 2010. Finger Friction Measurements on Coated and Uncoated Printing Papers. *Tribol Lett* **37**:389–399. doi:10.1007/s11249-009-9538-z

Skedung L, Danerlöv K, Olofsson U, Michael Johannesson C, Aikala M, Kettle J, Arvidsson M, Berglund B, Rutland MW. 2011. Tactile perception: Finger friction, surface roughness and perceived coarseness. *Tribol Int* **44**:505–512. doi:10.1016/j.triboint.2010.04.010

Sobinov AR, Bensmaia SJ. 2021. The neural mechanisms of manual dexterity. *Nat Rev Neurosci* **22**:741–757. doi:10.1038/s41583-021-00528-7

Soneda T, Nakano K. 2010. Investigation of vibrotactile sensation of human fingerpads by observation of contact zones. *Tribol Int* **43**:210–217. doi:10.1016/j.triboint.2009.05.016

Srinivasan M a, Dandekar K. 1996. An investigation of the mechanics of tactile sense using two-dimensional models of the primate fingertip. *J Biomech Eng* **118**:48–55.

Tada M, Kanade T. 2004. An imaging system of incipient slip for modelling how human perceives slip of a fingertip. *26th Annu Int Conf IEEE Eng Med Biol Soc* **3**:2045–2048. doi:10.1109/IEMBS.2004.1403601

Tada M, Mochimaru M, Kanade T. 2006a. How does a fingertip slip? - Visualizing partial slippage for modeling of contact mechanics. *Eurohaptics 2006* 2–7.

Tada M, Pai DK. 2008. Finger Shell: Predicting Finger Pad Deformation under Line Loading. *2008 Symp Haptic Interfaces Virtual Environ Teleoperator Syst* 107–112. doi:10.1109/HAPTICS.2008.4479924

Tada M, Shibata T, Ogasawara T. 2002. Investigation of the touch processing model in human grasping based on the stick ratio within a fingertip contact interface. *IEEE Int Conf Syst Man Cybern* **vol.5**:6. doi:10.1109/ICSMC.2002.1176358

Tada M, Yoshida H, Mochimaru M, Kanade T. 2006b. Generating subject-specific FE models of fingertip with the use of MR volume registrationEuroHaptics 2006. pp. 99–104.

Tomimoto M. 2011. The frictional pattern of tactile sensations in anthropomorphic fingertip. *Tribol Int* **44**:1340–1347. doi:10.1016/j.triboint.2010.12.004

Torebjörk HE, Ochoa JL. 1980. Specific sensations evoked by activity in single identified sensory units in man. *Acta Physiol Scand* **110**:445–447. doi:10.1111/j.1748-1716.1980.tb06695.x

Tuthill JC, Azim E. 2018. Proprioception. *Curr Biol* **28**:R194–R203. doi:10.1016/j.cub.2018.01.064

Vallbo ÅB, Hagbarth K-E. 1968. Activity from skin mechanoreceptors recorded percutaneously in awake human subjects. *Exp Neurol* **21**:270–289. doi:10.1016/0014-4886(68)90041-1

van Kuilenburg J, Masen M a., van der Heide E. 2013. A review of fingerpad contact mechanics and friction and how this affects tactile perception. *Proc Inst Mech Eng Part J J Eng Tribol*. doi:10.1177/1350650113504908

van Kuilenburg J, Masen M a., van der Heide E. 2012. Contact modelling of human skin: What value to use for the modulus of elasticity? *Proc Inst Mech Eng Part J J Eng Tribol* **227**:349–361. doi:10.1177/1350650112463307

Van Kuilenburg J, Masen MA, Van Der Heide E. 2015. A review of fingerpad contact mechanics and friction and how this affects tactile perception. *Proc Inst Mech Eng Part J J Eng Tribol*. doi:10.1177/1350650113504908

van Polanen V, Davare M. 2015. Sensorimotor memory biases weight perception during object lifting. *Front Hum Neurosci* **9**. doi:10.3389/fnhum.2015.00700

Vardar Y, Guclu B, Basdogan C. 2017. Effect of Waveform on Tactile Perception by Electrovibration Displayed on Touch Screens. *IEEE Trans Haptics* **1412**:1. doi:10.1109/TOH.2017.2704603

Vu PP, Vaskov AK, Irwin ZT, Henning PT, Lueders DR, Laidlaw AT, Davis AJ, Nu CS, Gates DH, Gillespie RB, Kemp SWP, Kung TA, Chestek CA, Cederna PS. 2020. A regenerative peripheral nerve interface allows real-time control of an artificial hand in upper limb amputees. *Sci Transl Med* **12**:1–12. doi:10.1126/scitranslmed.aay2857

Wang Q, Hayward V. 2007. In vivo biomechanics of the fingerpad skin under

local tangential traction. *J Biomech* **40**:851–860. doi:10.1016/j.jbiomech.2006.03.004

Warman PH, Ennos a R. 2009. Fingerprints are unlikely to increase the friction of primate fingerpads. *J Exp Biol* **212**:2016–2022. doi:10.1242/jeb.028977

Westling G, Johansson RS. 1987. Responses in glabrous skin mechanoreceptors during precision grip in humans. *Exp Brain Res* **66**:128–140. doi:10.1007/BF00236209

Westling G, Johansson RS. 1984. Factors influencing the force control during precision grip. *Exp brain Res* **53**:277–84.

White O, McIntyre J, Augurelle A-S, Thonnard J-L. 2005. Do novel gravitational environments alter the grip-force/load-force coupling at the fingertips? *Exp Brain Res* **163**:324–334. doi:10.1007/s00221-004-2175-8

White O, Thonnard J-L, Wing AM, Bracewell RM, Diedrichsen J, Lefèvre P. 2011. Grip force regulates hand impedance to optimize object stability in high impact loads. *Neuroscience* **189**:269–276. doi:10.1016/j.neuroscience.2011.04.055

Wiertlewski M, Fenton Friesen R, Colgate JE. 2016. Partial squeeze film levitation modulates fingertip friction. *Proc Natl Acad Sci* 201603908. doi:10.1073/pnas.1603908113

Wiertlewski M, Hayward V. 2012. Mechanical behavior of the fingertip in the range of frequencies and displacements relevant to touch. *J Biomech* **45**:1869–1874. doi:10.1016/j.jbiomech.2012.05.045

Witney AG, Wing A, Thonnard J-L, Smith AM. 2004. The cutaneous contribution to adaptive precision grip. *Trends Neurosci* **27**:637–643. doi:10.1016/j.tins.2004.08.006

Wu JZ, Welcome DE, Dong RG. 2006. Three-dimensional finite element simulations of the mechanical response of the fingertip to static and dynamic compressions. *Comput Methods Biomech Biomed Engin* **9**:55–63. doi:10.1080/10255840600603641

Yam M, Loh Y, Tan C, Khadijah Adam S, Abdul Manan N, Basir R. 2018. General Pathways of Pain Sensation and the Major Neurotransmitters Involved in Pain Regulation. *Int J Mol Sci* **19**:2164. doi:10.3390/ijms19082164

Yum S-M, Baek I-K, Hong D, Kim J, Jung K, Kim Seontae, Eom K, Jang J, Kim

Seonmyeong, Sattorov M, Lee M-G, Kim Sungwan, Adams MJ, Park G-S. 2020. Fingerprint ridges allow primates to regulate grip. *Proc Natl Acad Sci* **117**:31665–31673. doi:10.1073/pnas.2001055117

Ziegler-Graham K, MacKenzie EJ, Ephraim PL, Travison TG, Brookmeyer R. 2008. Estimating the Prevalence of Limb Loss in the United States: 2005 to 2050. *Arch Phys Med Rehabil* **89**:422–429. doi:10.1016/j.apmr.2007.11.005